Electronic Theses and Dissertations   Theses, Dissertations, and Major Papers

5-16-2018

Development and Integration of Stretchable Electronic Components into Light-Emitting Devices.pdf

Yiting Chen
University of Windsor

Development and Integration of Stretchable Electronic Components into Light-Emitting Devices

By

Yiting Chen

A Dissertation

Submitted to the Faculty of Graduate Studies

through the Department of **Chemistry and Biochemistry**

in Partial Fulfillment of the Requirements for

the Degree of **Doctor of Philosophy**

at the University of Windsor

Windsor, Ontario, Canada

2018

Development and Integration of Stretchable Electronic Components into Light-Emitting Devices

by

Yiting Chen

APPROVED BY:

—————————————————
J. Yang, External Examiner
Western University

—————————————————
X. Nie
Materials and Mechanical Engineering

—————————————————
J.R. Green
Department of Chemistry and Biochemistry

—————————————————
J. Rawson
Department of Chemistry and Biochemistry

—————————————————
T. Carmichael, Advisor
Department of Chemistry and Biochemistry

May 10, 2018

Declaration of Co-Authorship / Previous Publications

I.   Co-Authorship Declaration

I hereby declare that this thesis incorporates material that is result of joint research, as follows: This thesis incorporates the outcome of the research undertaken in Professor Tricia Carmichael's research group. In all cases, the key ideas, primary contributions, experimental designs, data analysis, interpretation, and writing were performed by the author. Chapter 2 and 3 of the thesis was co-authored with R. Stephen Carmichael under the supervision of Professor Tricia Carmichael. R. Stephen Carmichael contributed to providing feedback on experimental designs in Chapter 2 and 3 as well as assisting data analysis of light-emitting devices and acquisition of photograph in Chapter 2. Chapter 4 contains joint research with Danny Mansour, R. Stephen Carmichael under the supervision of Professor Tricia Carmichael and is the outcome of a collaboration with Dr. John Trant, Dr. Elizabeth R. Gillies of University of Western. Danny Mansour contributed to conducting the optoelectronic tests for LEECs fabricated from pristine iridium complex. R. Stephen Carmichael assisted data analysis of light-emitting devices. Dr. John Trant and Dr. Elizabeth R. Gillies synthesized the RgP graft copolymer. Chapter 5 of the thesis was co-authored with Yunyun Wu and Sara Mechael under the supervision of Professor Tricia Carmichael. Both Yunyun Wu and Sara Mechael contributed to editing of the manuscript. Sara Mechael also contributed to designing the Figure 3 in Chapter 5.

I am aware of the University of Windsor Senate Policy on Authorship and I certify that I have properly acknowledged the contribution of other researchers to my dissertation and have obtained written permission from each of the co-author(s) to include the above material(s) in my dissertation. I certify that, with the above qualification, this thesis, and the research to which it refers, is the product of my own work.

II.   Declaration of Previous Publication

This thesis includes 4 original papers that will be published/submitted for publication in peer reviewed journals, as follows:

Dissertation Chapter	Publication title/full citation	Publication status
Chapter 2	Yiting Chen, R. Stephen Carmichael, Tricia Breen Carmichael, *"Patterned and Compliant Transparent Conductive Electrodes Based on Silver Nanowires"*	In preparation
Chapter 3	Yiting Chen, R. Stephen Carmichael, Tricia Breen Carmichael, *"Stretchable and Durable AgNW Composites on Transparent Butyl Rubber"*	In preparation
Chapter 4	Yiting Chen, Danny Mansour, R. Stephen Carmichael, John Trant, Elizabeth R. Gillies, and Tricia Breen Carmichael, *"Stretchable Light-Emitting Electrochemical Cells Incorporating Butyl Rubber-Poly(ethylene oxide) Graft Copolymers"*	In preparation
Chapter 5	Yiting Chen, Yunyun Wu, Sara Mechael, Tricia Breen Carmichael, *"Exploiting the Formation of Nanocracks in Solution-Deposited Gold Films on PDMS for Stretchable Electronics"*	In preparation

I certify that I have obtained a written permission from the copyright owner(s) to include the above published material(s) in my thesis. I certify that the above material describes work completed during my registration as a graduate student at the University of Windsor.

III. General

I declare that, to the best of my knowledge, my thesis does not infringe upon anyone's copyright nor violate any proprietary rights and that any ideas, techniques, quotations, or any other material from the work of other people included in my thesis, published or otherwise, are fully acknowledged in accordance with the standard referencing practices. Furthermore, to the extent that I have included copyrighted material that surpasses the bounds of fair dealing within the meaning of the Canada Copyright Act, I certify that I have obtained a written permission from the copyright owner(s) to include such material(s) in my thesis.

I declare that this is a true copy of my thesis, including any final revisions, as approved by my thesis committee and the Graduate Studies office, and that this thesis has not been submitted for a higher degree to any other University or Institution.

Abstract

Flexible and stretchable electronics are the new format of electronics that remain functional with mechanical bending, twisting, and stretching. These new kinds of devices are expected to open up new opportunities and uses by reforming the way we interact with electronics and fundamentally change our life. To reach these goals, we must move beyond conventional hard, inorganic materials such as glass and silicon and find ways to incorporate electrical function into soft materials that are flexible or even stretchable. This thesis focuses on the development of compliant electronic components including transparent conductive electrodes, light-emitting materials, and metallic electrodes, and their integration into soft light-emitting devices.

Chapter 2 reports a new and simple method using shadow masks to produce flexible and stretchable patterned silver nanowire (AgNW) coatings. We easily obtain a variety of geometries and resolutions of the patterns using different shadow masks. These coatings are highly conductive and transparent and exhibit high flexibility, stretchability, and mechanical robustness. We demonstrate their use as electrodes in light-emitting electrochemical cells (LEECs) and show that these devices function during bending.

However, due to the high permeability of PDMS substrate, water and air in ambient condition easily penetrate through the substrate and corrode AgNW network to form less conductive particles or rods, making it not suitable for long-term stable applications. To solve this challenge, Chapter 3 reported the fabrication of a chemical stable AgNW composite by simply replacing the highly permeable PDMS substrate with

a new airtight material—transparent butyl rubber. The resulting coatings very well maintain their optical, electrical, and mechanical properties when exposing to extremely harsh conditions such as underwater or acidic vapor.

Chapter 4 investigates a feasible method to fabricate a stretchable light-emitting material with an improved optical performance by mixing an ionic transition metal complex with an elastic graft copolymer and an ionic conductor. The graft copolymer not only provides the stretchability by its elastic backbone but also acts as ion hosting materials due to its ion trapping side chains. We demonstrate that devices made from this material emit bright yellow light and keep emitting light under repetitive strain cycles.

Chapter 5 describes a new, simple, low-cost solution-based scalable method to produce patterned gold film with microcontact printing on elastomeric polydimethylsiloxane (PDMS). This solution-based method enables the metal deposition on not only flat surfaces but also any other irregular shapes. Additionally, the patterning method is also compatible with uneven surface due to the high comfortability of PDMS. Unlike traditional physical vapor deposited gold films that experience electrical failure at very low strain (~1%), our gold films still remain highly conductive at 90% elongations.

Dedication

This dissertation is dedicated to my parents, Jiang Chen and Cuiping Lu

Acknowledgements

First and the most, I would like to thank my parents, Jian Chen and Cuiping Lu for their moral support in all my decisions and pursuits. I cannot become the person who I am now without their love, encouragement, and guidance. When I go through any rough situations, no matter the research obstacles or homesick, they are always there willing to listen to me and relieve my stress. I also would like to thank my boyfriend, Hongjun Luo, for releasing my stress anytime I need.

I would like to thank my advisor, Prof. Tricia Carmichael, for offering me the chance to join her research group. I cannot embark on my wonderful journey of graduate study without her help. I also need to thank her for her patient guidance, numerous encouragement, and unflagging support for the past, nearly six, years. Prof. Carmichael's passion for research, rigorous work attitude, and the constant quest for excellence have had a great influence on me now and in the future. Additionally, she not only trained my skills on designing and conducting a research project but also taught me so much on how to write scientifically in English and how to present results in an effective way. All these experiences will be the wealth of my whole life.

I would also like to thank Steve Carmichael for the work to improve my oral communication skills, the technical discussions to make me think out of the box, the willingness to share his life experiences with me, and the selfless care of me over the past few years. I cannot enjoy my experience in Canada so much without his delicious food in all the memorable group parties.

to thank all my friends in the department who created all my best memories in the last few years.

I would like to thank all the support staffs who have helped me in countless situations in Chemistry and Biochemistry Department. Thank you to Marlene Bezaire, Catherine Wilson, and Elizabeth Kickham for the sincere help and support. Thank you to Joe Lichaa for being dedicated to fixing our instruments and my computer. Thank you to Sharon Leckie at GLIER for SEM and EDX analysis. Thank you to the staff at Surface Science Western and the Nanofab at the University of Western Ontario (Dr. Mark Biesinger, Dr. Todd Simpson, and Tim Goldhawk) for SEM and XPS analysis and the training on photolithography.

Finally, I would like to thank my committee members: Prof. James Green, Prof. Jeremy Rawson, Prof. Xueyuan Nie for their feedback at my committee meetings and for the guidance over the course of my graduate study. I would also like to thank Dr. Jun Yang for agreeing to be my external examiner. I appreciate all the critiques and suggestions you will provide that will improve this dissertation.

Table of Contents

List of Tables

List of Schemes

List of Figures

List of Abbreviations / Symbols

3D	three-dimensional
%T	percent transmittance
°	degree
AC	alternating current
ACEL	alternating-current electroluminescence
AFM	atomic force microscopy
AgNW	silver nanowire
APTES	3- aminopropyltriehthoxysilane
bpy	bipyridine
cc-mm/m^2-day	cubic centimeter-millimeter/meter squared-per-day
CNT	carbon nanotube
DC	direct current
dtb	di-tert butyl
ε	mechanical strain
ELD	electroless deposition
e-beam	electron beam
ECD	electrochemical doping
ED	electrodynamic
EDL	electric double layer
EGaIn	eutectic gallium-indium
EL	electroluminescence
EQE	external quantum efficiency
PF$_6$	hexafluorophosphate
IIR	isobutylene-co-isoprene rubber
iTMC	ionic transitional metal complex

ITO	indium tin oxide
Ir	iridium
$t_{1/2}$	lifetime of device
LEEC	light-emitting electrochemical cell
MACP	matrix-assisted catalytic printing
R_{max}	maximum radiance
μCP	micro contact printing
n-doped	negatively doped
OLED	organic light-emitting diode
p-doped	positively doped
PDMS	poly(dimethylsiloxane)
PEG	poly(ethylene glycol)
PEO	poly(ethylene oxide)
PET	poly(ethylene terephthalate)
PI	polyimide
PLEC	polymer light-emitting electrochemical cell
PMMA	poly(methyl methacrylate)
PMETAC	poly[2-(methacryloyloxy)ethyl-trimethylammonium chloride]
PEDOT:PSS	poly(3,4-polyethylenedioxythiophene)-poly(styrenesulfonate)
ppy	phenylpyridine
MEH-PPV	poly[5-(2'-ethylhexyloxy)-2-methoxy-1,4-phenylene vinylene]
Psig	pounds per square inch
PVD	physical vapor deposition
R	resistance
R/R_0	change in resistance
R_0	initial resistance

RH	relative humidity
RMS	root-mean-squared
R_{RMS}	root-mean-square roughness
rpm	rotations per minute
R_s	sheet resistance
SAM	self-assembled monolayer
SEM	scanning electron microscopy
t_{on}	turn-on time
TCE	transparent conductive electrode
T-IIR	transparent poly(isobutylene-co-isoprene) rubber
UV	ultraviolet
UV-Vis	ultraviolet visible
XPS	X-ray photoelectron spectroscopy
XRD	X-ray diffraction

1. Chapter 1

Introduction

1.1. Compliant Electronics

The global market for compliant electronics has had tremendous growth and is expected to reach > $800 million USD dollars by 2023 from ~$28 million in 2017.[1] Unlike traditional electronics that are made from rigid and bulky components, these flexible and stretchable electronics are a new format of devices fabricated from materials that retain their functionality even during mechanical deformation such as bending, twisting, and stretching. These fully deformable devices open up new applications that were previously impossible to achieve using conventional rigid materials such as compliant energy harvesting systems,[2] optoelectronics,[3,4] sensors,[5] actuators,[6] artificial skins,[7] smart clothing,[8] soft robots,[9] and bioelectronics.[10] This dissertation focuses on the development of deformable, low-cost, electroluminescent (EL) devices.

1.2. EL Devices

Compliant lighting devices are expected to bring new possibilities that inspire people's imagination for a display-centric world in the future. With these technologies, we could unfold and then hang a large-area screen on the wall to use, and then fold it into our pockets when we are done. We could directly laminate light therapy devices made completely from conformable materials to our human body and conduct the treatment while we can still move freely. We could continuously monitor our health using a suite of truly conformable health monitors distributed across the body without noticing their existence. The advance of flexible and stretchable optoelectronics brings these types of products closer to reality. One principle consideration for fabricating these compliant optoelectronics is the device structure. It is difficult to incorporate stretchability into each

layer in a multilayer stack such as the typical conventional organic light-emitting diodes (OLEDs) consisting of eight individual layers responsible for charge injection, transport, and emissive recombination (Figure 1.1a).[11] Thus, new types of light-emitting devices with a simple structure need to be designed.
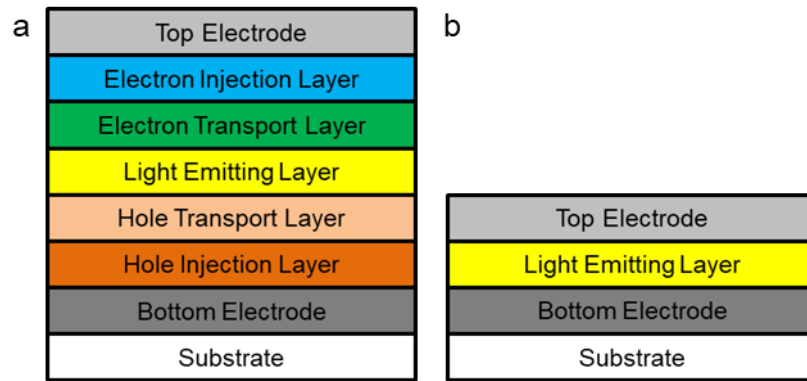
Figure 1.1. *(a) Structure of a typical OLED that contains eight layers of active materials. (b) Structure of a typical ACEL device and LEEC. Adapted with permission from reference 11.*

Fortunately, researchers have developed two very promising light emitting alternatives suitable for stretchability: Alternating-current electroluminescent (ACEL) devices and light-emitting electrochemical cells (LEECs). These types of EL devices sandwich a single layer of EL material that combines charge injection and transport together between two electrodes (Figure 1.1b),[12,13] and possess much simpler structures compared to conventional OLEDs. Thus, it is easier to impart compliance into all three layers and integrate these three components into one single stretchable EL device. Another interesting note is that the emissive materials used in these devices are solution-

3

processable, which lowers the fabrication cost. In the following sections, we will discuss ACEL devices and LEECs in greater detail.

1.2.1. ACEL Devices

ACEL devices have been explored for display and lighting applications for almost three decades.[14] It sandwiches a layer of EL material between two electrodes, and is driven by alternating voltage. The emissive material consists of two materials: an organic or inorganic phosphor, the luminescent center that dominates the optoelectronic properties of the emissive material, and an insulator, the host material that dominates the electrical properties of the emissive material.[15] The commonly used phosphor is inorganic ZnS doped with different impurities such as Cu, Mn, and Al to achieve various emission colors including red, blue, green, and white.[16]

In these devices, the light originates from field-induced luminescence in the following sequence: charge injection into the phosphor layer upon the application of AC voltage beyond threshold, typically from 150 V to 250 V,[14] acceleration of the electrons to high energies under high electrical field and then excite luminescent centers to form excitons, and radiative relaxation of the luminescent center.[17] The high operating voltage, however, likely stunts their applications in portable and wearable electronics.

1.2.2. Light Emitting Electrochemical Cells (LEECs)

The concept of the LEEC was first introduced by Pei and coworkers in 1995.[18] LEECs possess a similar device structure to ACEL devices with an emissive layer sandwiched between two electrodes. The emissive material consists of an ionic EL material in an ionic environment and is processed from solution.[12,19]

4

1.2.2.1. Working Mechanism of LEECs under DC Voltage

Studies have revealed two working mechanisms for LEECs: electrodynamic (ED) model[20-23] (Figure 1.2a) and electrochemical doping (ECD) model (Figure 1.2b).[18,24-27] Both models agree that separating the cations and anions in the EL layer upon application of a voltage reduces the electron and hole injection barrier.

The ED model assumes that upon the application of a voltage above the threshold, charged ions begin to migrate and are redistributed at the respective electrode interfaces to form electric double layers (EDLs). The EDLs induce a sharp drop of the electric potential near the electrode interfaces and lower the charge injections barrier. Once the injection barrier is reduced, significant numbers of electrons and holes are injected into the emissive material leading to the oxidation and reduction of the emissive material in the bulk of the material. The oxidized and reduced species are then recombined together, emitting light in a field-free region.

The ECD model also assumes that the accumulation of ions at anodes and cathodes leads to the formation of EDLs at the electrodes. The injection of electrons and holes at the cathode and anode respectively also causes the development of positively doped (p-doped) and negatively doped (n-doped) regions in the bulk. The counter ions migrate to neutralize the charge. The doped regions expand over time until a negative doped-intrinsic undoped-positive doped junction between them forms. Across the intrinsically undoped region, the applied potential drops substantially and charges recombine and emit light.

A recent study, however, shows that both the ECD and the ED model are valid descriptions of the doping action in LEECs where the ED model predominates when only

limited electrons inject into the EL material, and then the ECD model prevails when substantial electron injection occurs.[28]   The doped region continuously grows toward each other at the expense of the undoped area, which causes the quenching of excitons and leads to a decline in EL intensity and efficiency.[29]   The speed of forming the EDL determines the turn-on time of LEECs, and the growing rate of the doped zone is directly related to the lifetime of LEECs. Both speeds are determined by the electronic and ionic mobility, the applied voltage and the thickness of the emissive layer.[30]
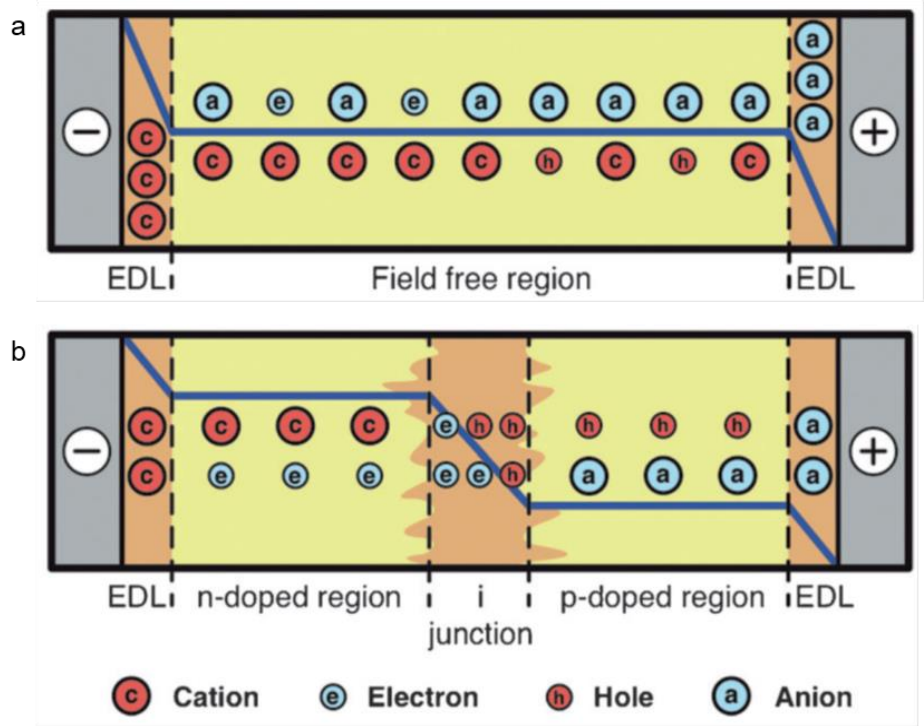
Figure 1.2. Illustration of potential profile and electronic along with ionic charge distribution in a LEEC during steady-state operation for the (a) ED model and (b) ECD model. Adapted with permission from reference 11.

1.2.2.2. Figures of Merit

A set of figures of merit are used in order to quantify the performance of LEECs with different EL materials. The commonly used figures of merit include:

1. Maximum radiance (R_{max}): Maximum flux of light emitted by LEECs, measured in Watts.

2. Turn-on time (t_{on}): Time it takes for the device to emit light above a particular threshold. While some researchers define this as the time for the onset of light emission[31] or the time it takes to reach the R_{max},[12] we define this as the time it takes for the device to reach ~10 nW radiance.

3. t_{max}: Time it takes for the device to reach the R_{max}.

3. External quantum efficiency (EQE): The ratio of emitted photons to the total amount of injected electrons.

4. Lifetime ($t_{1/2}$): The time it takes for the device radiance to decay to one half of its maximum value.

1.2.2.3. Classification of LEECs

LEECs are classified into two categories according to the difference in the composition of light-emitting material: polymer LEECs (PLECs) and ionic transition metal complex LEECs (iTMC-LEECs).[12,19]

The active layer of a PLEC is a mixture of electronic and ionic conductors. The conjugated polymer, such as poly[5-(2'-ethylhexyloxy)-2-methoxy-1, 4-phenylene vinylene) (MEH-PPV)[18] or poly(phenylene vinylene),[32] acts as the electronic conductor,

and the solid-state electrolyte, typically consisting of an ion-solvating polymer such as poly(ethylene oxide) (PEO) and a lithium salt, acts as the ionic conductor to provide mobile ions (Figure 1.3a).[33] By changing the active conjugated polymer, PLECs emitting red, blue, green, yellow, and even white light have been reported.[18,34-36]
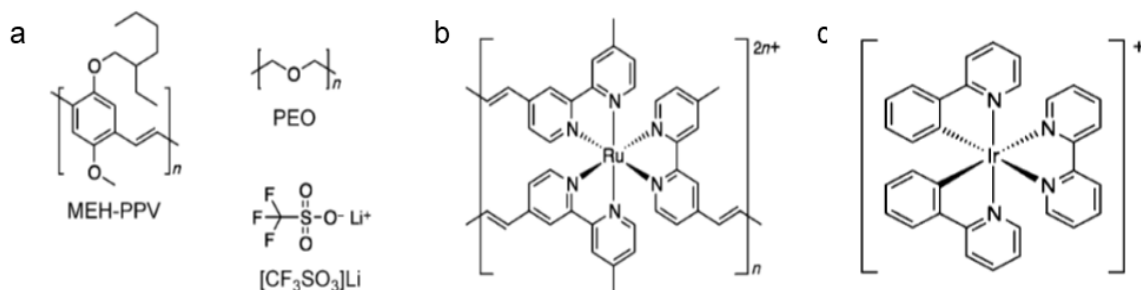
Figure 1.3. (a) Materials used in the first PLEC: conjugated polymer of MEH-PPV, ionic conductors of PEO and lithium trifluoromethanesulfonate salt. (b) The first [Ru(vbpy)$_3$](PF$_6$)$_2$ Ru^{II}-iTMC used for LEECs. (c) Structure of [Ir(bpy)$_3$]$^+$ (bpy = bipyridine), a sample of the largest class of Ir^{III}-iTMCs used in LEECs. Adapted with permission from reference 11.

iTMC-LEECs require a single iTMC as the emissive material since the ionic nature of iTMC allows it to act as both ionic and electronic conductors. The light emission occurs by phosphorescence, originating from long live-triplet excitons, and can be quenched by electrochemical doping. In 1996, Maness et al.[37] and Lee et al.[38] report the first iTMC-LEECs made from [Ru(vbpy)$_3$](PF$_6$)^2 (vbpy = 4-vinyl-4'-methyl-2,2'-bipyridine) that emitted orange light (Figure 1.3b). Nowadays, research on iTMC-LEECs is mostly based on luminescent ionic biscyclometalated Ir^{III} complexes[39] since they can emit various colors due to the easily tunable band gap of these molecules.[40] Figure 1.3c shows a sample of the Ir^{III} complex.

1.2.2.4. Challenge of LEECs

As discussed in Section 1.2.2.1, the ion conductivity in the emissive material strongly influences the optoelectrical performance of LEECs. Mobile ion is essential for the redistribution of ions to form EDLs to promote the electron injection. The turn-on time of LEECs is directly determined by the speed of the formation of EDLs; the lifetime of LEECs is dominated by the growing speed of the doped regions, both of which are influenced by the ion conductivity. However, the low ion conductivity in the solid state compared to that in the liquid state results in a delay period (few seconds to several hours) for LEECs to become operative, which is an obstacle for most practical applications that require instant response. Several strategies have been reported to overcome this drawback. The first approach directly adds ionic conductors to the light-emitting material to increase the ion conductivity. Costa et al. and Parker et al. mixed iridium iTMCs with an ionic liquid and demonstrated that the t_{max} or t_{on} of LEECs fabricated from these iTMCs/ionic liquid composites were decreased by one order of magnitude.[31,41] Lyons et al. and Pei et al. blended poly(ethylene oxide)/lithium trifluoromethanesulfonate (PEO/LiCF$_3$SO$_3$), a known solid electrolyte, into either ruthenium iTMC or conjugated polymer to enhance the ion conductivity. The t_{on} was within a few seconds after incorporating the solid electrolyte into the emissive material.[18,40] The second strategy is to increase the device driving voltage.[37,42,43] The high driving voltage reduces the charge injection barriers as well as increases the ion movement speed, resulting in a faster build-up of the EDLs and thus lowering the t_{on}.

Although increasing ion conductivity can reduce the t_{on}, it also reduces the device lifetime. The faster ion movement increases the speed to produce doped regions, which

causes a quicker exciton quenching and a faster degradation of the emissive materials. Thus, there is a trade-off between the turn-on time and the lifetime. It is crucial to adjust the ion conductivity of the light-emitting materials in order to balance the trade-off effect.

To prepare compliant EL devices, each layer in the device needs to remain soft and functional with deformation. In the following sections, we will explore methods to incorporate compliance into each layer of ACEL devices and LEECs.

1.3. Strategies to Incorporate Compliance in Transparent Conductive Electrode (TCE)

The transparent conductive electrode (TCE) is a crucial component of compliant optoelectronics and largely dictates their mechanical deformability and electrical performance. It not only acts as a window for light to enter or leave in devices but also remains conductive under mechanical stress. Several figures of merit are employed to judge the performance of TCEs made from different materials, which include:

1. Transmittance (T%): Transparency of the material over the visible wavelengths. It is used to characterize the optical property of the TCE. In general, high T% is desired for TCE applications. Typically, researchers report the transmittance at a wavelength of 550 nm since it is in the middle of the visible-light wavelength.

2. Sheet resistance (R_s): A measurement of the resistance of a thin uniform sheet, analogous to density, that is invariable under scaling of the sheet size, and is used to compare how conductive a material is regardless of size. Material with a lower R_s value is more ideal for application as conductive thin films.

3. Surface roughness: A measurement that quantifies the deviations in the surface smoothness of a film and is often expressed as root-mean-square roughness (R_{RMS}) which is an averaging method. R_{RMS} plays an important role in thin-film devices by affecting both the film quality and the device performance. In TCEs, specifically, R_{RMS} can influence the optical and electrical properties: Rougher surface results in more light scattering and thus lower the transparency of TCE; it also leads to potential electrical shorts if the protruding part of the electrode penetrates through the functional layer and makes contact with the other electrode. Thus, a low R_{RMS} is preferred in thin TCEs.

Other features that are important for the development of compliant TCEs include good conductivity at high bending and stretching strains; durability to repetitive strains; high throughput patterning methods; and inexpensive fabrication.

Indium tin oxide (ITO) is universally employed in rigid optoelectronic devices due to its excellent transparency ($\geq$ 80%), low R_s (10 ~40 Ω/sq), and low surface roughness ($<$ 10 nm).[44-47] However, its brittle nature limits its application as a TCE in flexible or stretchable electronics.[48] Although depositing ITO on a flexible substrate such as polyethylene terephthalate (PET) slightly increases its flexibility from $<$ 1% to $<$ 5% before electrical failure, the low processing temperature of PET substrate results in insufficient conductivity of the resulting ITO film.[49] In addition, the slow sputtering process (linear coating rate of ~0.01 m/s) decreases the throughput rate and thus, raising the fabrication cost.[50]

Extensive research has been devoted to replacing the ITO based TCE with one that can deliver the same high conductivity and transparency, combined with the ability to tolerate mechanical bending and stretching. Current significant materials for

substitution include carbon nanotubes,[51,52] graphene,[53] conductive polymers,[54] metal grids,[55] and random meshes of nanowires.[56,57] Silver nanowires (AgNWs) are considered to be a very promising replacement for ITO due to intrinsically low R_s (as low as <1 Ω/sq) and high transparency (as high as > 90%).[58] Randomly arranged AgNWs form an interconnected percolation network, creating pathways for electrons to migrate and thus result in a conductive network (Figure 1.4a). The gaps among AgNWs allow light to pass through and thus make the network transparent. We can easily alter the transparency and conductivity of AgNWs with a certain diameter and length by controlling the density of AgNWs deposited on the substrate.[58] Additionally, the AgNWs dispersed in a solvent such as water and ethanol can be used as an ink for low-cost and high throughput processing such as roll-to-roll (R2R) techniques,[59,60] making it a practical printable conductor. The contact resistance between individual AgNWs increases the overall R_s of the AgNW network and is undesirable for TCEs.[61] To lower the contact resistance between AgNWs, annealing is used to fuse the AgNW-AgNW junctions.[57,62,63] Thermal annealing of AgNW networks at a temperature of 200 ºC results in the reduction of R_s by several orders of magnitude (Figure 1.4b).[62,63] Moreover, this annealing temperature is compatible with both plastic substrates, such as PET, polyimide, and poly(ethylene naphthalate) (PEN), and elastic substrates such as poly(dimethylsiloxane) (PDMS), making AgNWs suitable for the fabrication of flexible and stretchable TCEs.
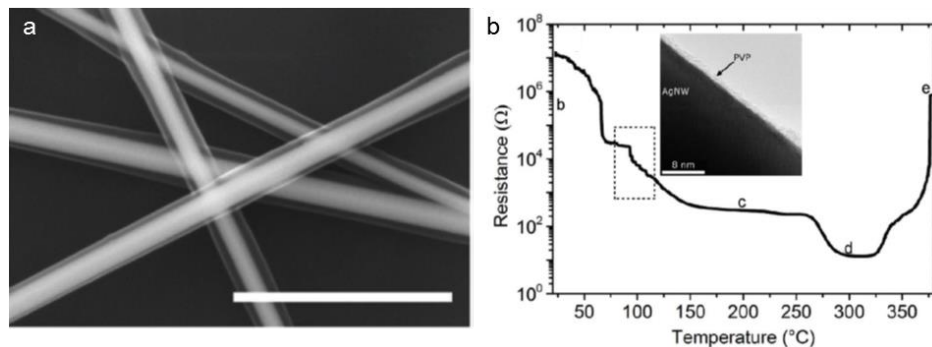
Figure 1.4. *(a) SEM image of AgNW network. Scale bar = 1 μm (b) Change in resistance as a function of thermal annealing temperature. The concentration of AgNW dispersion is 0.75 mg/mL and the deposited density is 105 mg/m². Adapted with permission from reference 62.*

1.3.1. Strategies to Prepare Flexible AgNW-TCEs

The inherently high aspect ratio of AgNWs makes them intrinsically flexible and enables the feasible fabrication of flexible TCEs by depositing AgNW dispersion on a flexible substrate such as PET[64-67] or PEN.[68] The good dispersity of AgNWs in solvents such as water and ethanol allows the fabrication of AgNW films using various solution-based deposition methods including drop casting,[57,69] spin coating,[70,71] spray coating,[72,73] vacuum filtration,[74] and Meyer-rod coating.[75] As the demand for low-cost fabrication methods keeps increasing, the R2R process attracts researchers' attention. The production cost can be reduced to a fraction of the cost of traditional semiconductor manufacturing methods due to its high throughput.[59,60,76]

Unfortunately, AgNW films produced by many of these techniques have two main issues: poor adhesion to the underlying substrate[77] and high surface roughness due to irregular piles of AgNWs with individual AgNWs protruding > 100 nm from the surface (Figure 1.5a, b).[74,78] The poor adhesion causes AgNWs to be easily removed

13

from the surface by touching or scratching. The high surface roughness not only lowers the efficiency of optoelectronics but also increases the risk of potential short circuits by causing contacts between two electrodes, or damaging layers with localized high electric fields.
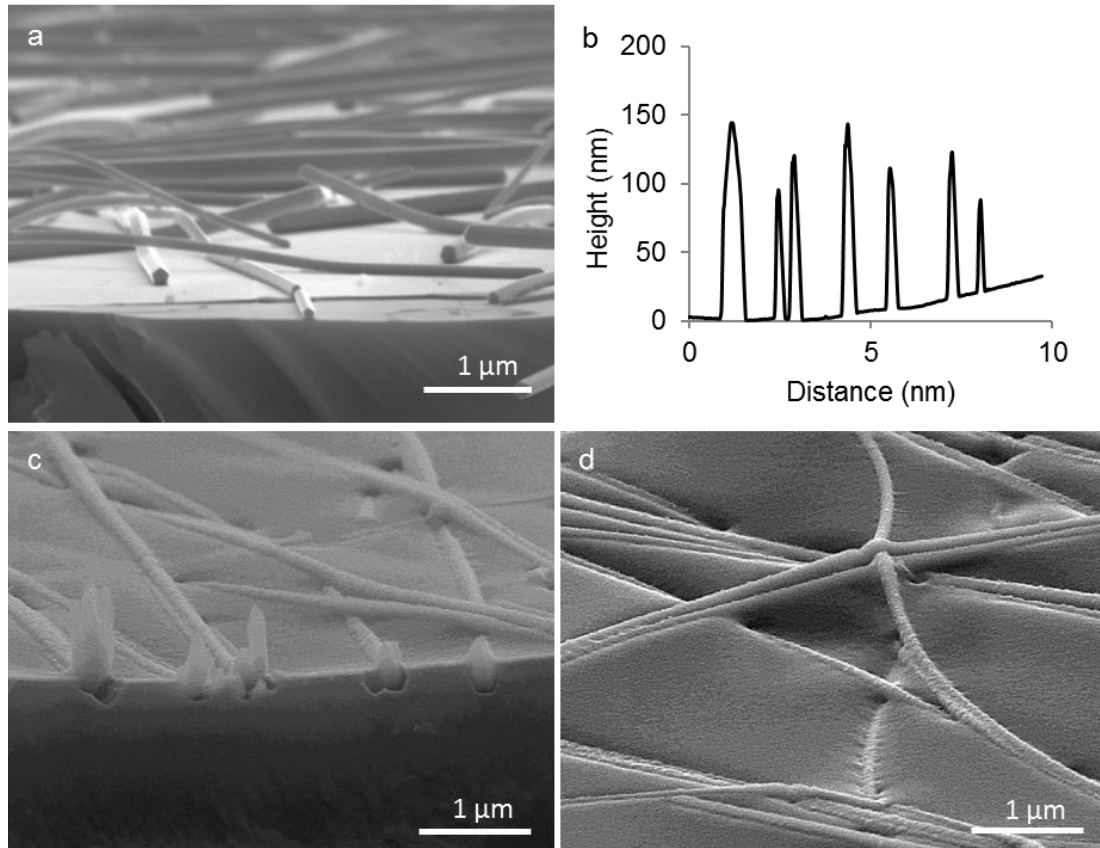
Figure 1.5. (a) Cross-sectional SEM image of AgNWs protrusion from the surface of a substrate. (b) AFM profile measurement of a AgNW film on a silicon wafer. (c) Cross-sectional SEM image of AgNW-OA coating on a glass substrate. (d) Top view SEM image of a AgNW-OA coating surface. Adapted with permission from reference 78 (a) and 74 (b-d).

One widely used solution to decrease the surface roughness is to embed AgNWs in a polymer matrix such as polyurethane,[74] polycarbonate,[79] and polyvinyl alcohol[77]

14

followed by transfer of the AgNW/polymer composite to the target substrate. The polymer fills in the voids among AgNWs and results in a smooth surface. Additionally, the polymer adheres to the AgNW network, enhancing the mechanical flexibility. For example, Miller et al. produced a uniform AgNW network by vacuum filtering and embedded it in a transparent polyurethane optical adhesive (OA).[74] The AgNW composite adheres strongly to the underlying substrate and is durable, resisting marring, scratching and solvent exposure. Similarly, Liang et al. used Meyer rod or airbrush to produce AgNW network on a glass substrate followed by transferring it into a polyurethane acrylate matrix.[80] Kim et al. embedded AgNW network in the polyurethane urea matrix to decrease the surface roughness of the AgNW composite.[81] The resulting AgNW composites with uniform and smooth surfaces were embedded in, and not protruding from the surface of polymer matrix (Figure 1.5c, d).

1.3.2. Strategies to Prepare Stretchable AgNW-TCEs

One major strategy to improve the stretchability of AgNWs based TCEs is to embed AgNWs into a stretchable polymer matrix such as polyacrylate,[82] polyurethane,[83] and poly(urethane acrylate).[80] This polymer matrix functions the same as the polymer matrix in the flexible AgNW-TCEs while significantly increasing the stretchability of the resulting AgNW-polymer network. Yu et al. embedded AgNWs in a polyacrylate matrix to prepare an elastic TCE with a transmission of 45% at 550 nm and a stretchability of 16% strain at room temperature.[84] Hu et al. further improved the optical, electrical and mechanical properties of the AgNW/polyacrylate composite by incorporating an aromatic monoacrylate (Sartomer CN131) and acrylic acid to the polyacrylate matrix.[82] The

resulting composite showed a transmission of 79.6% with a R_s of 7.5 Ω/sq and remained conductive up to 80% elongations.

1.3.3. Strategies to Prepare Patterned AgNW-TCEs

Applications such as displays and touch screens require patterned electrodes. Thus, to realize the practical use of AgNW-TCEs in a compliant display, we need to develop patterned and soft AgNW films with various feature sizes.

Various patterning techniques have been demonstrated to produce patterned AgNW films. Madaria et al. used a dry transfer technique to produce patterned AgNW-TCE. They first fabricated a PDMS stamp with repeating 1-mm-length square patterns, and then used this stamp to selectively pick up AgNWs on an aluminum oxide membrane and pressing them to the target PET or glass substrate.[85] The patterned AgNWs exhibited the same features as the PDMS stamp, and the minimum dimension was defined by the dimension of the PDMS stamp. Ko et al. employed a photolithographic method to produce AgNWs with circle and line patterns on a glass substrate.[86] Drop casting a poly(ethylene glycol) (PEG) precursor on top of a deposited AgNW network and then selectively gelating the PEG through a photomask under UV light enables the transfer of the cured PEG gel along with the underlying AgNWs to a target substrate, leaving the uncured PEG on the carrier substrate. The generated patterns had a minimum dimension of 200 μm. Liang et al. screen printed a layer of AgNWs from a dispersion in methanol through a shadow mask on a glass substrate to obtain patterned AgNW lines with a dimension of 100 μm x 5000 μm.[87] Tybrandt et al. filtered an AgNW dispersion through a patterned photoresist layer on top of a PVDF membrane.[88] After removing the

photoresist, patterned AgNWs with dimension as small as 10 μm were left on the PVDF membrane, which was then transferred to a PDMS substrate. Song et al. produced patterned AgNW grids on plastic substrate such as PET, PEN, and colorless-polyimide (cPI) utilizing a two-step intense-pulsed-light (IPL) irradiation: first, irradiation of the AgNW network with IPL through a photomask using a high voltage (2.5 kV for PET and PEN, 3.0 kV for cPI); and second, removal of the nonradiated AgNWs using either ultrasonication or a commercial tape.[89] The appropriate IPL irradiation time caused the welding of AgNWs while too long IPL irradiation time damaged the AgNW network.

1.3.4. Challenge of AgNW-TCEs: Degradation of AgNWs

When the scale reduces to the nanometer, the high aspect ratio of AgNWs provides a significantly large surface area to react with oxygen and sulfur, thus accelerating the silver corrosion process.[90,91] Previous studies have shown that AgNWs break into small rods or particles after reacting with oxygen and sulfur-containing gases (Figure 1.6a, b) and undergo electrical failure in only a month when storing in atmosphere and even shorter lifetime when exposed to harsh environments.[90,92-94] This poor stability makes it challenging to employ bare AgNWs for any realistic applications.

A barrier layer has been employed to coat individual AgNW or fully overcoat the entire AgNW network to delay the degradation process of AgNWs. Coating the surface of each individual AgNW with a protective material such as metal,[95,96] metal oxide,[97] and photoresist[98] forms a core-shell structure (Figure 1.6c). The outer shell shields the inner AgNW core from interacting with the destructive environment and therefore protects it from corrosion. Eom et al. electrodeposited a nickel shell on the exposed surface of AgNWs for 20 s to produce a Au/Ni core-shell structure on PDMS substrate with a

transmittance of 75% and a R_s of 26.03 Ω/sq. The R_s increased 1.35x after exposing to 80 °C and 85% relative humidity (RH) for 14 days.[96] Wang et al. deposited a patterned barrier of positive photoresist (OFPR-800 LB) in situ on the surface of AgNW on glass to realize the stability improvement.[98] The resistance of the resulting AgNW films increased to 1.7x after storing 30 days in 85 °C/85% RH environment. Although this method could preserve the conductivity of AgNW network in hot and humid conditions, the change in transparency and mechanical deformability has not been systematically studied yet.
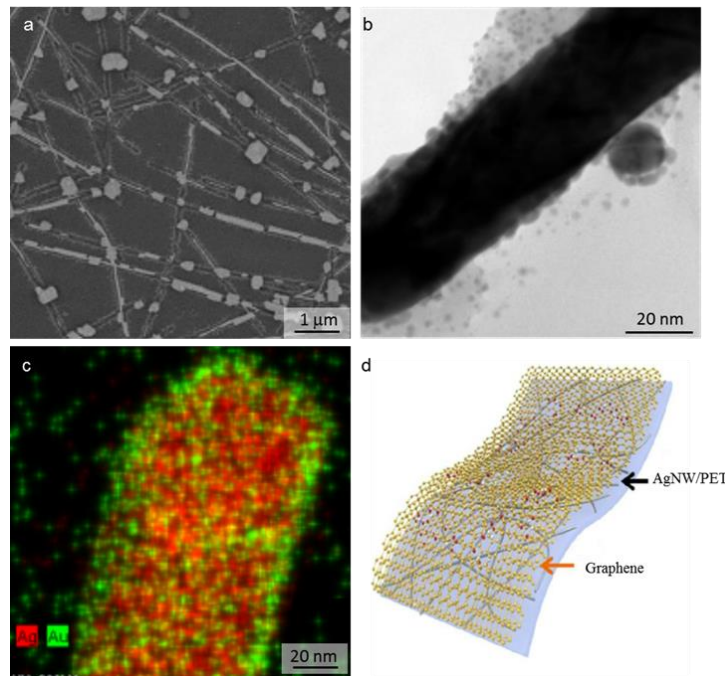
Figure 1.6. *(a) SEM and (b) TEM images of corroded AgNW network after storing in ambient conditions for 30 days. (c) Illustration of core-shell structure that protects AgNW from interacting with corrosive environments. The green shell represents the gold shell and red core represents the silver core. (d) Schematic structure of the graphene barrier on top of AgNW network on PET substrate. Adapted with permission from reference 92 (a), 90 (b), 95 (c), and 101 (d).*

Coating or encapsulating the whole AgNW network using chemical inert material is another option. Graphene is an attractive over-coating material due to its high chemical and thermal stability, high mechanical property, and high optical transparency.[99,100] Additionally, the graphene sheet also provides extra electron pathway, increasing the conductivity of the resulting AgNW-graphene hybrid film. Dong et al. fabricated graphene coated AgNW network on flexible PET or PEN substrate by first spin-coating AgNW dispersion onto a chemical vapor deposited monolayer graphene and then transferring this AgNW-graphene structure to the target flexible substrate.[101] The resulting graphene/AgNW/polymer composites display a transmittance of 88.3%, a R_s of 8.06 Ω/sq, and a repetitive bendability (250 cycles of bending the composite to a radius of 2.0 mm). The conductivity of this structure changes negligibly within one-month storage in ambient conditions. Butyl rubber (poly(isobutylene-co-isoprene), IIR) is another promising protective material. It is known for its elasticity, chemical inertness, and high impermeability and has been widely used in applications in the automotive industry as inner liners of tires, in the pharmaceutical industry as impermeable stoppers, in laboratory products such as gloves, and so on. Vohra et al. developed a new method to produce transparent IIR (T-IIR) sheets with a high transmittance of 75% at a wavelength of 550 nm.[102] The elastic, inert, and impermeable properties combined with the high transparency now make it suitable as a barrier material to protect AgNWs. Vohra et al. also showed that laminating a T-IIR sheet as over the AgNW network on glass successfully protect the AgNW percolation network and preserved its conductivity and transparency even after exposing to concentrated nitric acid vapor for 24 h.[102]

1.4. Strategies to Incorporate Compliance into Emissive Materials

The emissive layer is one of the most crucial components in LEECs and ACEL devices. This layer needs to maintain its performance under reversible deformation in order to be used in compliant EL devices. There are two strategies to impart compliance to the emissive material. The first approach transfers the entire ultrathin device onto a pre-stretched elastomeric substrate. The substrate is first stretched to a desired high strain followed by transferring the already-fabricated ultrathin device onto the substrate. Upon relaxing to its initial state (0% strain), the substrate along with the device buckles to accommodate the compression strain. When the devices are subjected to stretching, the buckles are flattened and converting the stretching strain to bending strain, and thus enables a high stretchability. White et al. employed this method to prepare elastic polymer-based organic light-emitting diodes (PLEDs) on 1.4 μm ultrathin VHB substrates.[103] With 100% prestrain of the substrate, the PLED remains functional up to 100% tensile strain and many times of repeated stretching cycles.

The second strategy is to develop intrinsically stretchable light-emitting material. In 2011, Yu et al. demonstrated the first elastic PLEC by utilizing a mixture of fluorescent polymer super yellow (SY), an ionic conductor PEO-dimethacrylate ether, and a lithium salt as the emissive material and two single-walled carbon nanotube (SWNT)-polymer composite as both electrodes.[52] This PLEC retained light emission with stretching up to 45% elongation when heated to 70 °C. In 2013, Liang et al. further improved the stretchability of PLECs by using the same emissive material but replacing the electrodes with two AgNW-polyurethane acrylate (PUA) composite electrodes.[80] The resulting PLEC continued to emit yellow light even when subjected to elongations as

large as 120% (Figure 1.7a). However, the EL performance trailed off quickly at strains above 40% elongation due to damage to the SY.
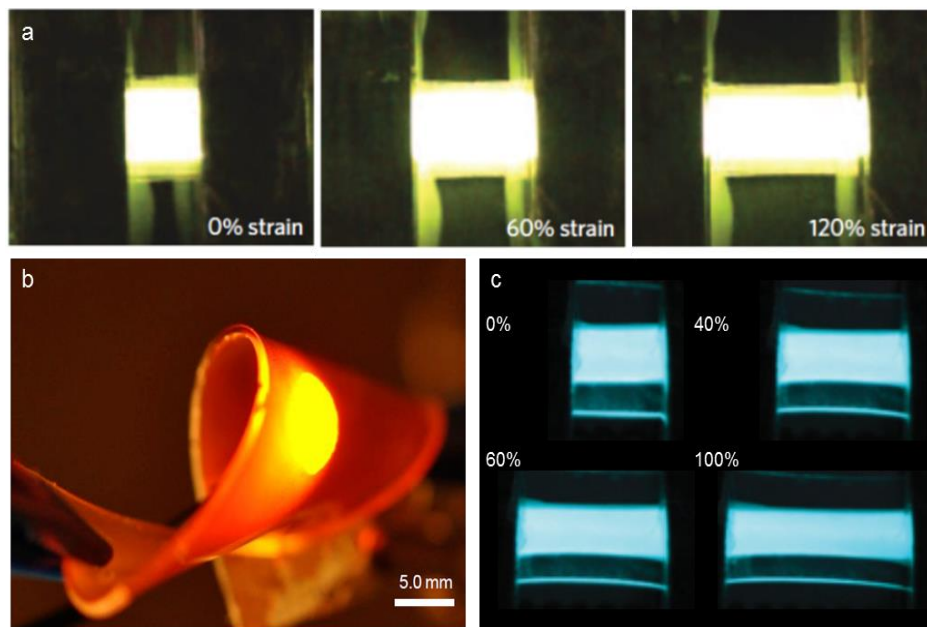
Figure 1.7. *Examples of intrinsically stretchable light-emitting devices: (a) stretchable PLEC, (b) stretchable iTMC-LEEC, and (c) stretchable ACEL devices. Adapted with permission from reference 80 (a), 104 (b), and 105 (c).*

Filiatrault et al. realized the first stretchable iTMC-LEEC in 2012.[104] They dispersed Ru(dtb-bpy)$_3$(PF$_6$)$_2$ (dtb-bpy = 4,4'-di-tert-butyl-2,2'-dipyridyl) in an elastomeric matrix of PDMS as the emissive material, a semi-transparent thin gold film on PDMS substrate as the top electrode, and a drop of deformable liquid metal, eutectic indium gallium (EGaIn) as the bottom electrode. The resulting device emitted bright orange light with bending, twisting (Figure 1.7b), stretching up to 27% strain, and after 50 cycles of 15% stretching strain.

21

In 2015, Wang et al. developed highly stretchable ACEL devices using copper doped ZnS powder as the phosphor and PDMS as the insulator.[105] PDMS also provides stretchability to the emissive layer. To complete the device, they used AgNWs on PDMS substrates as both electrodes. The resulting ACEL device exhibited a stretchability of 100% while still emitting bright blue light (Figure 1.7c). Later in 2016, they replaced the PDMS matrix to a more stretchable silicone rubber, EcoFlex, with an elongation at break of 980% to improve the stretchability of both electrodes and emissive materials.[106] ACEL devices fabricated with ionic conductor-EcoFlex composite as both electrodes and ZnS: Cu-EcoFlex composite as the emissive material remained to emit bright blue light up to 700% elongation.

1.5. Strategies to Incorporate Stretchability to Metallic Electrode

The last layer in ACEL devices and LEECs is the bottom electrode which is a conductive layer that does not require transparency. Metal is the material of choice due to their low electrical resistivity ($> 10^{-8}$ Ω·m).[107] In particular, gold attracts researchers' attention due to its chemical inertness and biocompatibility besides the high conductivity. These properties enable the application of gold in bioimplantable electronics,[108] health monitors,[109] and wearable devices.[110] However, freestanding metal films fracture at low strains (< 1 %) since the strain localization at the defect sites causes the metal to neck and generating a crack (Figure 1.8a).[111] The single crack will propagate through the film and breaks the electrical pathway, resulting in a limited stretchability.[112] Hence, it is challenging to directly adapt metals to bottom electrodes in stretchable EL devices.

Many studies have shown that adhering the metal thin film onto a compliant substrate can delocalize the strain over the entire metal film to enable an improved stretchability. Stretching causes the well-adhered metal film to elongate with the compliant substrate and forming multiple cracks instead of a single rupture (Figure 1.8b).[111,113-115] These cracks increase the resistance of the metal film with stretching. Further elongation causes the cracks to propagate to form channel cracks (Figure 1.8c). Eventually, the channel cracks propagate through the whole width of the metal film, resulting in the cease of conductivity at ~20% strain. Lacour et al. showed that 100-nm-thick gold films on top of a 5-nm-thick adhesion interlayer of chromium bonded to PDMS substrate can remain electrically conductive to 22% tensile strain.[114] Further elongation causes the break of conductive pathways and the cease of conductivity (Figure 1.8d).
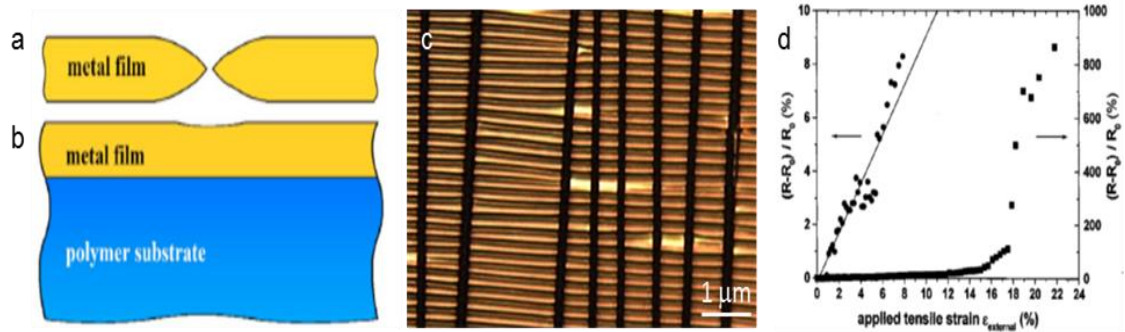
Figure 1.8. Illustrative scheme of (a) fracture of freestanding metal film and (b) the local elongation in the film suppressed by the substrate when the film well adheres to a substrate. (c) Optical micrograph of the gold film on PDMS substrate at 20% strain. (d) Normalized change in resistance as a function of applied tensile strain. Adapted with permission from reference 111 (a, b) and 123(c) and 114(d).

Compliant optoelectronics need to remain operative to strains higher than 22%. Thus, we need to develop new methods to impart higher stretchability into metal films. The following sections will discuss the strategies employed to achieve these goals.

1.5.1. Stretchable Configurations

One of the most common methods to improve the stretchability of metal films is to configure them into stretchable structures such as wavy,[116,117] pop-up,[118] or serpentine designs[119,120] that convert the applied stretching strain to less destructive bending strain (Figure 1.9a-c). A pre-stretch method is used to generate a wavy ribbon design. Specifically, the flat metal film is adhered to the pre-stretched elastic substrate (Figure 1.9a). Upon releasing the pre-strain, compression force in the system causes nonplanar buckling of the metal film and generates a wavy structure. The amplitudes and periods of the waves change to accommodate the mechanical deformation when stretching the wavy ribbons. Jones et al. fabricated stretchable gold films that retain electrical conductivity up to 100% strain by evaporating 5 nm of chromium and 20 nm of gold on 25% uniaxially prestretched PDMS substrate followed by relaxing to 0% strain.[117] In a pop-up structure, the out-of-plane interconnects flatten to accommodate the deformation when subjected to mechanical strains (Figure 1.9b). Kim et al. exploited this method to prepare gold circuits that remained conductive up to 100% tensile strain.[118] In-plane metal serpentines rotate in plane and twist out of plane at the peaks to accommodate the applied stretching strain, leading to reduced intrinsic strains in metal (Figure 1.9c). Gray et al. showed that the serpentine gold wires remained conductive up to 14.2 ± 0.5% elongation while straight wires lost conductivity at 2.4 ± 0.5% strain.[119]
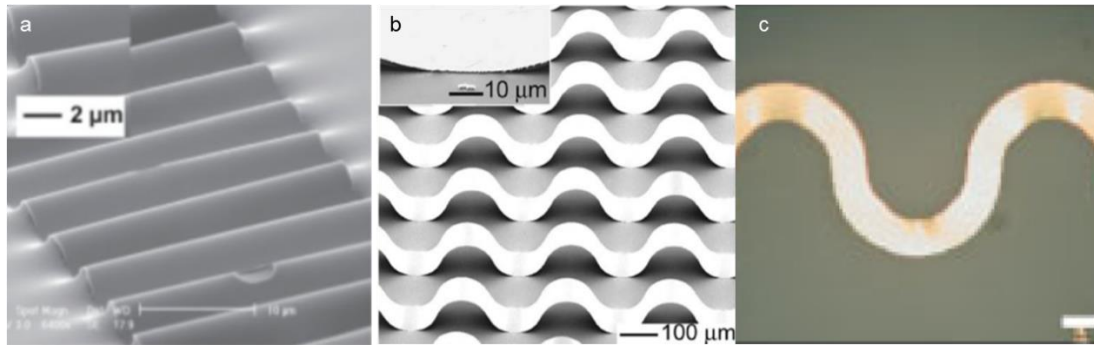
Figure 1.9. *SEM images of (a) stretchable wavy ribbons, (b) popup structure, and (c) coplanar serpentine designs. Adapted with permission from reference 117 (a), 118 (b) and 119 (c).*

These methods allow for the fabrication of conductors that will experience very low resistance changes up to a limit after which the tensile strain can no longer be converted to bending strain. Tensile strain beyond the prestretch or the critical point results in crack formation to accommodate the elongation. Thus, these conductors are only suitable for applications with a limited stretching range. Although the stretchable metal films fabricated with pop-up configurations can be used as interconnects or strain sensors, their uneven surfaces could cause a heterogeneous distribution of the electric field, resulting in non-uniform charge injection and consequently affecting the EL performance. Therefore, metal films with out-of-plane configurations are not suitable to act as electrodes in thin film devices. Also, the high-profile surface has the potential to cause electrical shorts between the top and bottom electrodes, which is undesirable for electronics. Although the low-profile in-plane serpentine structures can reduce the chance of a short circuit, the conductive areas are limited (typically micrometer scale), making these films not suitable for the fabrication of large-area stretchable electronics.

1.5.2. Morphology-Induced Cracking

Another promising method to enhance stretchability of metal films is to control the propagation of cracks with morphology-induced cracks. These topographies, such as nano-scale pyramids,[121] micron-scale circular pillars,[122] or random microstructures,[123,124] act as defect sites to localize strain and initiate small cracks that relieve strain in the film when stretching (Figure 1.10). When larger strains are applied, these small cracks propagate and intercept with each other, limiting the formation of long channel cracks and preserving the conductive pathway. Mandlik et al. fabricated a two-dimensional array of nano-scaled pyramids with a height of 250 nm and a period of 1 μm on PDMS surface followed by depositing a gold film on top (Figure 1.10a).[121] The electrical resistance of the obtained films increased by 4.5 x at an elongation of 25%. Tilting the nanopatterns 30° further decreased the change in resistance to 1.5 x at 25% strain. Filiatrault et al. imparted random organized microstructured features to the PDMS surface followed by coating the surface with gold to generate highly stretchable and conductive metal films (Figure 1.10b, c).[123] The microstructured features were fabricated by spin-coating a commercially available white poly(vinyl acetate) glue onto PDMS surface. The resulting PDMS/glue/gold structures maintain conducting up to 65% elongation, much beyond the typical fractures strain of gold on PDMS (~20%).
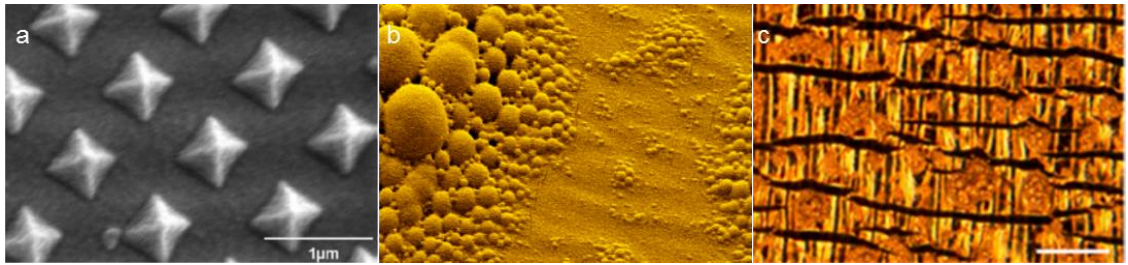
Figure 1.10. *(a) SEM micrograph of gold film on nanopatterned pyramids with 30° tilt. (b) SEM of gold film on random features at 0% strain. (c) Optical micrograph of gold film on random features at 60% strain. Adapted with permission from reference 121 (a), and 123 (b, c).*

1.5.3. Deposition of Thin Metal Films Using Electroless Deposition (ELD)

To date, electron-beam (e-beam) evaporation, one type of physical vapor deposition (PVD), has been widely employed in the deposition of metal thin films due to its variable deposition rate and the precise control of film thickness, structure, and morphology. However, PVD must operate under vacuum conditions which increases the deposition cost. Furthermore, PVD is only compatible with planar surfaces, which limits its application in the coating of three-dimensional objects and the inner surface of complex geometries. Photolithography is the dominant technology to generate patterned electronic circuits. However, it generally requires multiple processing steps, and cannot be easily applied to nonplanar surfaces, further increasing the fabrication cost and procedure complexity. Thus, we need a low-cost deposition method to generate stretchable metal films for applications in compliant electronics.

The solution-based electroless deposition (ELD) process is a very promising alternative. ELD is a solution-based redox reaction that has been widely used to fabricate microelectronics such as printed circuit boards.[125] It can be used to deposit metals such

as silver, copper, nickel, gold, and cobalt onto either metallic or insulating substrates.[125] Compared to PVD, ELD does not require expensive instrumentation and is high throughput, make it cost-effective. Furthermore, the solution-based process enables the metal layer to coat irregularly-shaped surfaces. It is also a bottom-up process with no material deposited in undesired regions, utilizing materials efficiently.

The ELD process involves two steps: first, activation of the substrate by immobilization of the catalyst on its surface, and second, ELD of metal on the activated surface.[125] Pd/Sn colloids are one of the most commonly used catalysts in ELD.[126-131] The colloids consist of a Pd rich core and are protected from oxidation by a hydrolyzed Sn shell. The chloride ions associated with this shell give the colloids a negative charge to inhibit aggregation and allow the colloids to be electrostatically bound to cationic functional groups on a substrate. After etching away the Sn shell, the Pd catalyst initiates metallization in the ELD plating bath, in which metal cation in the plating bath is reduced chemically to metal atoms at the Pd catalytic surface (Figure 1.11), and the initial layer of deposited metal autocatalyzes further metal deposition.
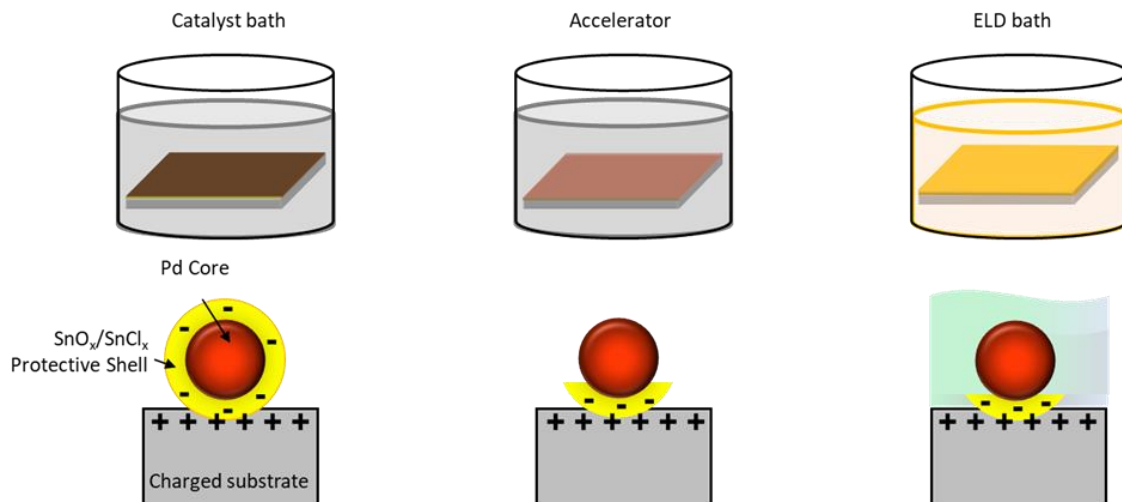
Figure 1. 11. *Schematic illustration of ELD process. After deposition of the catalyst, the substance is first immersed into a typical Pd/Sn colloidal catalyst bath. In the following accelerator step, the Sn shell is etched away, exposing the inner Pd core. In the last ELD bath, the metallic ions are deposited on a catalyzed surface. The initial layer of metal further initiates the metal deposition with the presence of reducing agent and eventually results in a continuous metal thin film.*

It is important to pattern the metal films since most real applications require a patterned circuit. One method to pattern the metal film uses microcontact printing (μCP) of chemical resist to selectively deactivate a reactive surface (subtractive method)[132] or chemical binder to the catalyst to selectively activate a nonreactive surface (additive approach).[133] μCP is a non-photolithographic microfabrication method and is able to construct features on the micrometer to nanometer scale.[134] Additionally, this technique provides access to nonplanar surface since the stamp is fabricated with an elastomer as well as remains inexpensive and experimentally convenient. It uses a patterned PDMS stamp to directly print the desired features to the surface of the target substrate by contact. Printing the "ink" on to the target substrate generates self-assembled monolayers (SAMs). After printing, the surface of the substrate contains regions with and without

SAMs, and thus produces areas with different surface chemistry that directs the deposition of metal in the ELD process. Miller et al. prepared stretchable copper films that remained conductive up to 52% elongation using the subtractive patterning method. They first used μCP technique to transfer a polymer resist, poly(octadecenyl-alt-maleic anhydride) (POMA) to the positively charged PDMS surface (Figure 1.12a).[132] POMA prevented the underlying surface from binding to the negatively charged Pd/Sn catalyst and thus deactivated the ELD process in these regions. After metallization in the copper ELD bath, they formed patterned copper wires that only deposited into the regions without POMA. Later in 2010, they used the additive patterning approach to prepare patterned copper films.[133] They used μCP to selectively transfer a catalyst binder (tetraphenlyporphyrinato) aluminum (III) methoxide ((TPP) Al-OMe) to the surface of oxidized polymer substrates. The regions with (TPP) Al-OMe SAMs adsorbed the Pd/Sn colloidal catalyst, in which copper was deposited in the following ELD process.

The second patterning method is called matrix-assisted catalytic printing (MACP). It first polymerizes a receiving matrix polymer on the substrate surface, followed by patterning an inorganic catalytic salt in a delivering matrix polymer using dip-pen nanolithography, inject printing, or screen printing.[135] After contact, the catalytic salt transfers from the delivering matrix polymer to the receiving matrix polymer on PDMS and forms patterned catalyst area where metal deposits in the following ELD process. Guo *et al*. exploited polyethylene glycol (PEG) as the delivering matrix polymer, poly[2-(methacryloyloxy)ethyl-trimethylammonium chloride] (PMETAC) as the receiving matrix polymer, and $(NH_4)_2PdCl_4$ as the catalytic salt to prepare copper patterns such as stripes, squares, and serpentines on various substrates (PET, PI, cellulose

paper, cotton fabrics, and PDMS) using this MACP method (Figure 1.12b).[136] The resistance of serpentine metal film increased 1.1 x at 6% strain.
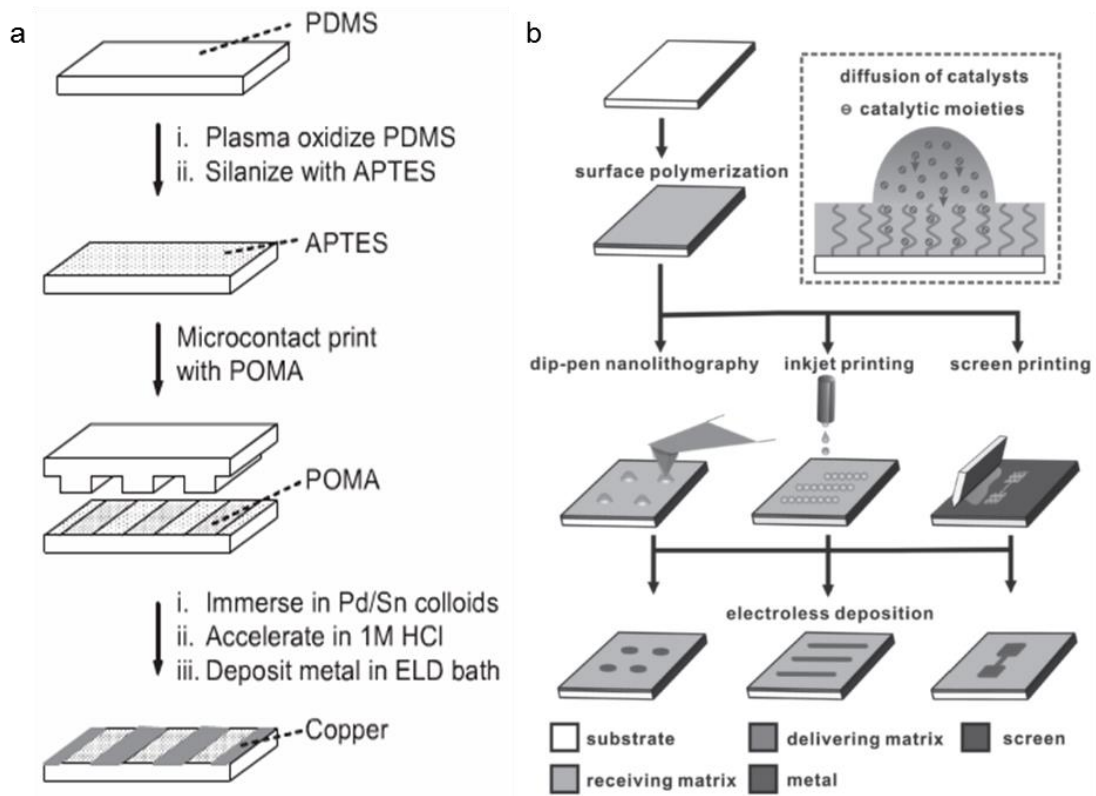
***Figure 1.12.** Schematic illustration of patterning copper films using (a) μCP and (b) MACP process. Adapted with permission from reference 132 (a) and 136 (b).*

1.6. Dissertation Objectives

The overall goal of this dissertation is to develop new materials and simple, low-cost methods for compliant electronic components and integrate them into EL devices. This dissertation reports the fabrication of compliant top transparent electrode, emissive materials, and bottom metallic electrode.

1.6.1. Fabrication of Patterned and Durable AgNW Composites on Elastomer

The first section of the thesis investigates a new method to prepare AgNW-based TCEs. We first present a new solution-based wetting/dewetting approach to selectively deposit AgNW dispersions onto a PDMS substrate. Wetting/dewetting is an inexpensive, fast, and high throughput method that exploits the difference in surface free energy to direct the deposition of AgNW dispersion in ethanol. We create patterned AgNW-polymer coatings with smooth surfaces and high bendability and stretchability by embedding AgNWs into a polymer matrix (either flexible urethane OA or stretchable urethane CF). We examine the surface morphological, optical, electrical, and mechanical properties of the obtained AgNW patterns and demonstrate the use of AgNW TCEs in flexible ACEL devices. This research is presented in Chapter 2.

Second, we generate stretchable and durable AgNW-CF coatings on a gas-impermeable and watertight T-IIR substrate and on PDMS. We compare the change in the optical, electrical, and mechanical performance of the AgNW-CF coatings after exposure to humidity, storage under water, and corrosive acid vapor. This study provides a new solution to prolong the lifetime of functional AgNW-based electronics. This work is reported in Chapter 3.

1.6.2. Development of Elastomeric Emissive Materials for Light-Emitting Devices

The second section of the thesis presents the design of new stretchable emissive materials and their use in LEECs. The low ion conductivity in solid-state emissive material results in a delayed response for LEECs. Increasing the ion conductivity reduces

the onset time of LEECs, however, decreasing the device lifetime at the same time. Optimized ion conductivity is required to achieve fast response and long lifetime. In addition, the emissive materials used for iTMC-LEECs are brittle, not suitable for the fabrication of stretchable LEECs. Although mixing iTMCs with elastomers imparts stretchability to the emissive materials, this thermodynamically unfavorable mixing process leads to significant phase separation in the emissive materials, which adversely influences the optoelectronic performance of the iTMC-LEECs. To address all the challenges, we blended an amphiphilic graft copolymer with the iridium iTMC. The graft copolymer consists of IIR backbone and poly(ethylene oxide) (PEO) side chains with various PEO content (IIR-g-PEO, RgP). The PEO side chains assist in mixing with the iridium iTMC as well as form solid electrolyte with $LiCF_3SO_3$ to improve the ion conductivity. The soft RgP copolymer imparts elasticity in the emissive material. By varying the molecular weight of the PEO graft, we demonstrate the effect of PEO content on phase separation, device turn-on time and lifetime in rigid LEECs. We also establish that RgP copolymer supports mechanical stretchability of LEECs fabricated in stretchable device architecture. This work is presented in Chapter 4.

1.6.3. Fabrication of Stretchable Gold Films on PDMS Substrate

Last, we present the use of a low-cost solution-based method to selectively deposit gold films onto elastomeric PDMS substrates that retain high conductivity to high elongations due to the unusual formation of distributed nanocracks on the surface. We use a combination of electroless nickel/immersion gold (ENIG) deposition and soft lithographic patterning using a polymeric resist as the ink to prepare the patterned gold films. The solution-based ENIG process generates polycrystalline gold films that form

numerous cracks with stretching, which is likely attributed to that the heterogeneous crystallite orientations of the ENIG films impede the crack propagation. We demonstrate the use of these films as the bottom electrode in stretchable ACEL devices. This work is presented in Chapter 5.

1.7. References

(1)   *Stretchable and Conformal Electroncis 2018-2028*; Ghaffarzadeh, K.; Hayward, J.; He, X.; IDTechEx, 2018.

(2)   Wu, H.; Huang, Y. A.; Xu, F.; Duan, Y. Q.; Yin, Z. P. *Adv. Mater.* **2016**, *28*, 9881.

(3)   Wang, J.; Lee, P. S. *Nanophotonics* **2016**, *5*, 81.

(4)   Lipomi, D. J.; Tee, B. C. K.; Vosgueritchian, M.; Bao, Z. N. *Adv. Mater.* **2011**, *23*, 1771.

(5)   Amjadi, M.; Kyung, K.-U.; Park, I.; Sitti, M. *Adv. Funct. Mater.* **2016**, *26*, 1678.

(6)   Chen, D.; Pei, Q. *Chem. Rev.* **2017**, *117*, 11239.

(7)   Wang, X.; Dong, L.; Zhang, H.; Yu, R.; Pan, C.; Wang, Z. L. *Adv. Sci.* **2015**, *2*, 1500169.

(8)   Stoppa, M.; Chiolerio, A. *Sensors* **2014**, *14*, 11957.

(9)   Rus, D.; Tolley, M. T. *Nature* **2015**, *521*, 467.

(10)   Choi, S.; Lee, H.; Ghaffari, R.; Hyeon, T.; Kim, D.-H. *Adv. Mater.* **2016**, *28*, 4203.

(11)   Reineke, S.; Lindner, F.; Schwartz, G.; Seidler, N.; Walzer, K.; Lüssem, B.; Leo, K. *Nature* **2009**, *459*, 234.

(12)   Costa, R. D.; Ortí, E.; Bolink, H. J.; Monti, F.; Accorsi, G.; Armaroli, N. *Angew. Chem. Int. Ed.* **2012**, *51*, 8178.

(13)   Wang, J. X.; Yan, C. Y.; Chee, K. J.; Lee, P. S. *Adv. Mater.* **2015**, *27*, 2876.

(14)   Rack, P. D.; Holloway, P. H. *Mater. Sci. Eng. R Rep.* **1998**, *8*, 171.

(15)   Rack, P.; Naman, A.; Holloway, P.; Sun, S.; Tuenge, R. T. *MRS Bull.* **1996**, *21*, 49.

(16)   *Handbook of Electroluminescent Materials*; Vij, D. R., Ed.; Institue of Physics: Bristol, U. K., 2004.

(17)   Fischer, A. G. *J. Electrochem. Soc.* **1963** *110*, 733.

(18)   Pei, Q. B.; Yu, G.; Zhang, C.; Yang, Y.; Heeger, A. J. *Science* **1995**, *269*, 1086.

(19)   Sun, Q.; Li, Y.; Pei, Q. *J. Display Technol.* **2007**, *3*, 211.

(20)   deMello, J. C.; Tessler, N.; Graham, S. C.; Friend, R. H. *Phys. Rev. B* **1998**, *57*, 12951.

(21)   deMello, J. C. *Phys. Rev. B* **2002**, *66*.

(22)   Malliaras, G. G.; Slinker, J. D.; DeFranco, J. A.; Jaquith, M. J.; Silveira, W. R.; Zhong, Y. W.; Moran-Mirabal, J. M.; Craighead, H. G.; Abruna, H. D.; Marohn, J. A. *Nat. Mater.* **2008**, *7*, 168.

(23)   Slinker, J. D.; DeFranco, J. A.; Jaquith, M. J.; Silveira, W. R.; Zhong, Y. W.; Moran-Mirabal, J. M.; Craighead, H. G.; Abruna, H. D.; Marohn, J. A.; Malliaras, G. G. *Nat. Mater.* **2007**, *6*, 894.

(24)   Pei, Q. B.; Yang, Y.; Yu, G.; Zhang, C.; Heeger, A. J. *J. Am. Chem. Soc.* **1996**, *118*, 3922.

(25)   Smith, D. L. *J. Appl. Phys.* **1997**, *81*, 2869.

(26)   Matyba, P.; Maturova, K.; Kemerink, M.; Robinson, N. D.; Edman, L. *Nat. Mater.* **2009**, *8*, 672.

(27)   Hu, Y. F.; Gao, J. *J. Am. Chem. Soc.* **2011**, *133*, 2227.

(28)   van Reenen, S.; Matyba, P.; Dzwilewski, A.; Janssen, R. A. J.; Edman, L.; Kemerink, M. *J. Am. Chem. Soc.* **2010**, *132*, 13776.

(29)   Pachler, P.; Wenzl, F. P.; Scherf, U.; Leising, G. *J. Phys. Chem. B* **2005**, *109*, 6020.

(30)   van Reenen, S.; Janssen, R. A. J.; Kemerink, M. *Org. Electron.* **2011**, *12*, 1746.

(31)   Parker, S. T.; Slinker, J. D.; Lowry, M. S.; Cox, M. P.; Bernhard, S.; Malliaras, G. G. *Chem. Mater.* **2005**, *17*, 3187.

(32)   Pei, Q.; Yang, Y. *Synth. Met.* **1996**, *80*, 131.

(33)   Yu, Z.; Li, L.; Gao, H.; Pei, Q. *Sci.China Chem.* **2013**, *56*, 1075.

(34)   Pei, Q. I.; Yang, Y. *Adv. Mater.* **1995**, *7*, 559.

(35)   Yang, Y.; Pei, Q. *J. Appl. Phys.* **1997**, *81*, 3294.

(36)   Tang, S.; Buchholz, H. A.; Edman, L. *ACS Appl. Mater. Interfaces* **2015**, *7*, 25955.

(37)   Maness, K. M.; Terrill, R. H.; Meyer, T. J.; Murray, R. W.; Wightman, R. M. *J. Am. Chem. Soc.* **1996**, *118*, 10609.

(38)   Lee, J. K.; Yoo, D. S.; Handy, E. S.; Rubner, M. F. *Appl. Phys. Lett.* **1996**, *69*, 1686.

(39)   Flamigni, L.; Barbieri, A.; Sabatini, C.; Ventura, B.; Barigelletti, F. *Top Curr. Chem.* **2007**, *281*, 143.

(40)   Lowry, M. S.; Bernhard, S. *Chem. Eur. J.* **2006**, *12*, 7970.

(41)   Slinker, J. D.; Koh, C. Y.; Malliaras, G. G.; Lowry, M. S.; Bernhard, S. *Appl. Phys. Lett.* **2005**, *86*, 173506.

(42)   Handy, E. S.; Pal, A. J.; Rubner, M. F. *J. Am. Chem. Soc.* **1999**, *121*, 3525.

(43)   Bernhard, S.; Barron, J. A.; Houston, P. L.; Abruna, H. D.; Ruglovksy, J. L.; Gao, X. C.; Malliaras, G. G. *J. Am. Chem. Soc.* **2002**, *124*, 13624.

(44)   Granqvist, C. G. *Solar Energy Mater. Solar Cells* **2007**, *91*, 1529.

(45)   De, S.; Coleman, J. N. *MRS Bull.* **2011**, *36*, 774.

(46)   Kim, K.-B.; Tak, Y.-H.; Han, Y.-S.; Baik, K.-H.; Yoon, M.-H.; Lee, M.-H. *Jpn. J. Appl. Phys.* **2003**, *42*, L438.

(47)   Thirumoorthi, M.; Thomas Joseph Prakash, J. *J. Am. Ceram. Soc.* **2016**, *4*, 124.

(48)   Madaria, A. R.; Kumar, A.; Ishikawa, F. N.; Zhou, C. W. *Nano Res.* **2010**, *3*, 564.

(49)   Boehme, M.; Charton, C. *Surf. Coat. Technol.* **2005**, *200*, 932.

(50)   Ye, S.; Rathmell, A. R.; Chen, Z.; Stewart, I. E.; Wiley, B. J. *Adv. Mater.* **2014**. *26*, 6670

(51)   Hecht, D. S.; Hu, L.; Irvin, G. *Adv. Mater.* **2011**, *23*, 1482.

(52)   Yu, Z.; Niu, X.; Liu, Z.; Pei, Q. *Adv. Mater.* **2011**, *23*, 3989.

(53)   Kim, K. S.; Zhao, Y.; Jang, H.; Lee, S. Y.; Kim, J. M.; Kim, K. S.; Ahn, J. H.; Kim, P.; Choi, J. Y.; Hong, B. H. *Nature* **2009**, *457*, 706.

(54)   Elschner, A.; Lövenich, W. *MRS Bull.* **2011**, *36*, 794.

(55)   Hong, S.; Yeo, J.; Kim, G.; Kim, D.; Lee, H.; Kwon, J.; Lee, H.; Lee, P.; Ko, S. H. *ACS Nano* **2013**, *7*, 5024.

(56)   Hwang, C.; An, J.; Choi, B. D.; Kim, K.; Jung, S. W.; Baeg, K. J.; Kim, M. G.; Ok, K. M.; Hong, J. *J. Mater. Chem. C* **2016**, *4*, 1441.

(57)   Lee, J. Y.; Connor, S. T.; Cui, Y.; Peumans, P. *Nano Lett.* **2008**, *8*, 689.

(58)   De, S.; Higgins, T. M.; Lyons, P. E.; Doherty, E. M.; Nirmalraj, P. N.; Blau, W. J.; Boland, J. J.; Coleman, J. N. *ACS Nano* **2009**, *3*, 1767.

(59)   dos Reis Benatto, G. A.; Roth, B.; Corazza, M.; Søndergaard, R. R.; Gevorgyan, S. A.; Jørgensen, M.; Krebs, F. C. *Nanoscale* **2016**, *8*, 318.

(60)   Angmo, D.; Andersen, T. R.; Bentzen, J. J.; Helgesen, M.; Søndergaard, R. R.; Jørgensen, M.; Carlé, J. E.; Bundgaard, E.; Krebs, F. C. *Adv. Funct. Mater.* **2015**, *25*, 4539.

(61)   Mutiso, R. M.; Sherrott, M. C.; Rathmell, A. R.; Wiley, B. J.; Winey, K. I. *ACS Nano* **2013**, *7*, 7654.

(62)   Langley, D. P.; Lagrange, M.; Giusti, G.; Jiménez, C.; Bréchet, Y.; Nguyen, N. D.; Bellet, D. *Nanoscale* **2014**, *6*, 13535.

(63)   Lagrange, M.; Langley, D. P.; Giusti, G.; Jiménez, C.; Bréchet, Y.; Bellet, D. *Nanoscale* **2015**, *7*, 17410.

(64)   Jing, M. X.; Han, C.; Li, M.; Shen, X. Q. *Nanoscale Res. Lett.* **2014**, *9.*

(65)   Madaria, A. R.; Kumar, A.; Ishikawa, F. N.; Zhou, C. W. *Nano Res.* **2010**, *3*, 564.

(66)   Hu, L.; Kim, H.; Lee, J.-Y.; Peumans, P.; Cui, Y. *ACS Nano* **2010**, *5*, 2955.

(67)   Song, M.; You, D. S.; Lim, K.; Park, S.; Jung, S.; Kim, C. S.; Kim, D. H.; Kim, D. G.; Kim, J. K.; Park, J.; Kang, Y. C.; Heo, J.; Jin, S. H.; Park, J. H.; Kang, J. W. *Adv. Funct. Mater.* **2013**, *23*, 4177.

(68)   Celle, C.; Mayousse, C.; Moreau, E.; Basti, H.; Carella, A.; Simonato, J.-P. *Nano Res.* **2012**, *5*, 427.

(69)   Lee, J. Y.; Connor, S. T.; Cui, Y.; Peumans, P. *Nano Lett.* **2010**, *10*, 1276.

(70)   Leem, D. S.; Edwards, A.; Faist, M.; Nelson, J.; Bradley, D. D. C.; de Mello, J. C. *Adv. Mater.* **2011**, *23*, 4371.

(71)   Chen, Y.; Lan, W.; Wang, J.; Zhu, R.; Yang, Z.; Ding, D.; Tang, G.; Wang, K.; Su, Q.; Xie, E. *Physica. E.* **2016**, *76*, 88.

(72)   Scardaci, V.; Coull, R.; Lyons, P. E.; Rickard, D.; Coleman, J. N. *Small* **2011**, *7*, 2621.

(73)   Akter, T.; Kim, W. S. *ACS Appl. Mater. Interfaces* **2012**, *4*, 1855.

(74)   Miller, M. S.; O'Kane, J. C.; Niec, A.; Carmichael, R. S.; Carmichael, T. B. *ACS Appl. Mater. Interfaces* **2013**, *5*, 10165.

(75)   Junaidi; Triyana, K.; Harsojo; Suharyadi, E. *4th International Conference on Advanced Materials Science and Technology* **2017**, *202*.

(76)   Bae, S.; Kim, H.; Lee, Y.; Xu, X. F.; Park, J. S.; Zheng, Y.; Balakrishnan, J.; Lei, T.; Kim, H. R.; Song, Y. I.; Kim, Y. J.; Kim, K. S.; Ozyilmaz, B.; Ahn, J. H.; Hong, B. H.; Iijima, S. *Nat. Nanotechnol* **2010**, *5*, 574.

(77)   Zeng, X.-Y.; Zhang, Q.-K.; Yu, R.-M.; Lu, C.-Z. *Adv. Mater.* **2010**, *22*, 4484.

(78)   Tokuno, T.; Nogi, M.; Karakawa, M.; Jiu, J.; Nge, T. T.; Aso, Y.; Suganuma, K. *Nano Res.* **2011**, *4*, 1215.

(79)   Moreno, I.; Navascues, N.; Arruebo, M.; Irusta, S.; Santamaria, J. *Nanotechnology* **2013**, *24*, 275603.

(80)   Liang, J.; Li, L.; Niu, X.; Yu, Z.; Pei, Q. *Nat. Photonics* **2013**, *7*, 817.

(81)   Kim, D.-H.; Yu, K.-C.; Kim, Y.; Kim, J.-W. *ACS Appl. Mater, Interfaces* **2015**, *7*, 15214.

(82)   Hu, W.; Niu, X.; Li, L.; Yun, S.; Yu, Z.; Pei, Q. *Nanotechnology* **2012**, *23*, 344002.

(83)   Kim, D. H.; Yu, K. C.; Kim, Y.; Kim, J. W. *ACS Appl. Mater. Interfaces* **2015**, *7*, 15214.

(84)   Yu, Z. B.; Zhang, Q. W.; Li, L.; Chen, Q.; Niu, X. F.; Liu, J.; Pei, Q. B. *Adv. Mater.* **2011**, *23*, 664.

(85)   Madaria, A. R.; Kumar, A.; Ishikawa, F. N.; Zhou, C. *Nano Res.* **2010**, *3*, 564.

(86)   Ko, Y.; Kim, J.; Kim, D.; Yamauchi, Y.; Kim, J. H.; You, J. *Sci. Rep.* **2017**, *7*, 2282.

(87)   Liang, J.; Li, L.; Chen, D.; Hajagos, T.; Ren, Z.; Chou, S.-Y.; Hu, W.; Pei, Q. *Nat. Commun.* **2015**, *6*, 7647.

(88)   Tybrandt, K.; Stauffer, F.; Vörös, J. *Sci. Rep.* **2016**, *6*, 25641.

(89)   Song, C.-H.; Han, C. J.; Ju, B.-K.; Kim, J.-W. *ACS Appl. Mater. Interfaces* **2016**, *8*, 480.

(90)   Elechiguerra, J. L.; Larios-Lopez, L.; Liu, C.; Garcia-Gutierrez, D.; Camacho-Bragado, A.; Yacaman, M. J. *Chem. Mater.* **2005**, *17*, 6042.

(91)   Hillman, C.; Arnold, J.; Binfield, S.; Seppi, J. In: *SMTA International Conference*, MD, USA, 2007.

(92)   Jiu, J. T.; Wang, J.; Sugahara, T.; Nagao, S.; Nogi, M.; Koga, H.; Suganuma, K.; Hara, M.; Nakazawa, E.; Uchida, H. *RSC Adv.* **2015**, *5*, 27657.

(93)   Mayousse, C.; Celle, C.; Fraczkiewicz, A.; Simonato, J.-P. *Nanoscale* **2015**, *7*, 2107.

(94)   Vohra, A.; Carmichael, R. S.; Carmichael, T. B. *Langmuir* **2016**, *32*, 10206.

(95)   Lee, H.; Hong, S.; Lee, J.; Suh, Y. D.; Kwon, J.; Moon, H.; Kim, H.; Yeo, J.; Ko, S. H. *ACS Appl. Mater. Interfaces* **2016**, *8*, 15449.

(96)   Eom, H.; Lee, J.; Pichitpajongkit, A.; Amjadi, M.; Jeong, J.-H.; Lee, E.; Lee, J.-Y.; Park, I. *Small* **2014**, *10*, 4171.

(97)   Jiu, J.; Nogi, M.; Sugahara, T.; Suganuma, K.; Tsujimoto, M.; Isoda, S. *J. Nanopart. Res.* **2012**, *14*, 1241.

(98)   Wang, J.; Jiu, J.; Sugahara, T.; Nagao, S.; Nogi, M.; Koga, H.; He, P.; Suganuma, K.; Uchida, H. *ACS Appl. Mater. Interfaces* **2015**, *7*, 23297.

(99)   Das, S. R.; Nian, Q.; Saei, M.; Jin, S.; Back, D.; Kumar, P.; Janes, D. B.; Alam, M. A.; Cheng, G. J. *ACS Nano* **2015**, *9*, 11121.

(100)   Zhang, Q.; Di, Y.; Huard, C. M.; Guo, L. J.; Wei, J.; Guo, J. *J. Mater. Chem. C* **2015**, *3*, 1528.

(101)   Dong, H.; Wu, Z.; Jiang, Y.; Liu, W.; Li, X.; Jiao, B.; Abbas, W.; Hou, X. *ACS Appl. Mater. Interfaces* **2016**, *8*, 31212.

(102)   Vohra, A.; Filiatrault, H. L.; Amyotte, S. D.; Carmichael, R. S.; Suhan, N. D.; Siegers, C.; Ferrari, L.; Davidson, G. J. E.; Carmichael, T. B. *Adv. Funct. Mater.* **2016**, *26*, 5222.

(103)   White, M. S.; Kaltenbrunner, M.; Głowacki, E. D.; Gutnichenko, K.; Kettlgruber, G.; Graz, I.; Aazou, S.; Ulbricht, C.; Egbe, D. A. M.; Miron, M. C.; Major, Z.; Scharber, M. C.; Sekitani, T.; Someya, T.; Bauer, S.; Sariciftci, N. S. *Nat. Photonics* **2013**, *7*, 811.

(104) Filiatrault, H. L.; Porteous, G. C.; Carmichael, R. S.; Davidson, G. J. E.; Carmichael, T. B. *Adv. Mater.* **2012**, *24*, 2673.

(105) Wang, J.; Yan, C.; Chee, K. J.; Lee, P. S. *Adv. Mater.* **2015**, *27*, 2876.

(106) Wang, J.; Yan, C.; Cai, G.; Cui, M.; Eh, A. L.-S.; Lee, P. S. *Adv. Mater.* **2015**.

(107) Cutnell, J. D.; Johnson, K. W. *Physics, 9th ed*; John Wiley & Sons: New York, 2012.

(108) Xu, L.; Gutbrod, S. R.; Bonifas, A. P.; Su, Y.; Sulkin, M. S.; Lu, N.; Chung, H.-J.; Jang, K.-I.; Liu, Z.; Ying, M.; Lu, C.; Webb, R. C.; Kim, J.-S.; Laughner, J. I.; Cheng, H.; Liu, Y.; Ameen, A.; Jeong, J.-W.; Kim, G.-T.; Huang, Y.; Efimov, I. R.; Rogers, J. A. *Nat. Commun.* **2014**, *5*, 3329.

(109) Yang, S. X.; Chen, Y. C.; Nicolini, L.; Pasupathy, P.; Sacks, J.; Su, B.; Yang, R.; Sanchez, D.; Chang, Y. F.; Wang, P. L.; Schnyer, D.; Neikirk, D.; Lu, N. S. *Adv. Mater.* **2015**, *27*, 6423.

(110) Wu, Y.; Mechael, S. M.; Chen, Y. *Adv. Mater. Technol.* **2018**, *3*, 1700292.

(111) Xiang, Y.; Li, T.; Suo, Z. G.; Vlassak, J. J. *Appl. Phys. Lett.* **2005**, *87*, 161910.

(112) Li, T.; Huang, Z. Y.; Suo, Z.; Lacour, S. P.; Wagner, S. *Appl. Phys. Lett.* **2004**, *85*, 3435.

(113) Li, T.; Suo, Z. *Int. J. Solids Struct.* **2006**, *43*, 2351.

(114) Lacour, S. P.; Wagner, S.; Huang, Z. Y.; Suo, Z. *Appl. Phys. Lett.* **2003**, *82*, 2404.

(115) Lacour, S. P.; Chan, D.; Wagner, S.; Li, T.; Suo, Z. *Appl. Phys. Lett.* **2006**, *88*, 204103.

(116) Wang, X. L.; Hu, H.; Shen, Y. D.; Zhou, X. C.; Zheng, Z. J. *Adv. Mater.* **2011**, *23*, 3090.

(117) Jones, J.; Lacour, S. P.; Wagner, S.; Suo, Z. G. *J. Vac. Sci. Technol. A* **2004**, *22*, 1723.

(118) Kim, D.-H.; Song, J.; Choi, W. M.; Kim, H. S.; Kim, R. H.; Liu, Z.; Huang, Y.; Hwang, K. C.; Zhang, Y.; Rogers, J. A. *Proc. Natl. Acad. Sci. USA* **2008**, *105*, 18675.

(119) Gray, D. S.; Tien, J.; Chen, C. S. *Adv. Mater.* **2004**, *16*, 393.

(120) Brosteaux, D.; Axisa, F.; Gonzalez, M.; Vanfleteren, J. *IEEE Electr. Device L* **2007**, *28*, 552.

(121) Mandlik, P.; Lacour, S. P.; Li, J. W.; Chou, S. Y.; Wagner, S. *IEEE Electr. Device L* **2006**, *27*, 650.

(122) Robinson, A. P.; Minev, I.; Graz, I. M.; Lacour, S. P. *Langmuir* **2011**, *27*, 4279.

(123) Filiatrault, H. L.; Carmichael, R. S.; Boutette, R. A.; Carmichael, T. B. *ACS Appl. Mater. Interfaces* **2015**, *7*, 20745.

(124) Lambricht, N.; Pardoen, T.; Yunus, S. *Acta Materialia* **2013**, *61*, 540.

(125) *Electroless Plating: Fundamentals and Applications*; Mallory, G. O.; Hajdum, J. B., Eds.; American Electroplaters and Surface Finishers Society: Orlando, FL, 1990.

(126) Cohen, R.; West, K. W. *J. Electrochem. Soc.* **1973**, *120*, 502.

(127) Osaka, T.; Takematsu, H. *J. Electrochem. Soc.* **1980**, *127*, 1021.

(128) Feldstein, N.; Schlesinger, M.; Hedgecock, N. E.; Chow, S. L. *J. Electrochem. Soc.* **1974**, *121*, 738.

(129) Cohen, R. L.; Meek, R. L. *J. Colloid Interface Sci.* **1976**, *55*, 156.

(130) Osaka, T.; Nagasaka, H.; Goto, F. *J. Electrochem. Soc.* **1980**, *127*, 2343.

(131) Horkans, J.; Kim, J.-Y.; McGrath, C.; Romankiw, L. T. *J. Electrochem. Soc.* **1984**, *134*, 301.

(132) Miller, M. S.; Davidson, G. J. E.; Sahli, B. J.; Mailloux, C. M.; Carmichael, T. B. *Adv. Mater.* **2008**, *20*, 59.

(133) Miller, M. S.; Filiatrault, H. L.; Davidson, G. J. E.; Luo, M.; Carmichael, T. B. *J. Am. Chem. Soc.* **2010**, *132*, 765.

(134) Xia, Y.; Whitesides, G. M. *Annu. Rev. Mater. Sci.* **1998**, *28*, 153.

(135) Guo, R. S.; Yu, Y.; Xie, Z.; Liu, X. Q.; Zhou, X. C.; Gao, Y. F.; Liu, Z. L.; Zhou, F.; Yang, Y.; Zheng, Z. J. *Adv. Mater.* **2013**, *25*, 3343.

(136) Guo, R.; Yu, Y.; Xie, Z.; Liu, X.; Zhou, X.; Gao, Y.; Liu, Z.; Zhou, F.; Yang, Y.; Zheng, Z. *Adv. Mater.* **2013**, *25*, 3343.

2. Chapter 2

Patterned and Compliant Transparent Conductive Electrode Based

on Silver Nanowires

2.1. Introduction

Transparent conductive electrodes (TCEs) are fundamental components of optoelectronic devices, possessing the dual functionality of acting as electrodes and as windows for light to enter or leave devices. TCEs are used extensively in solar cells,[1,2] light emitting devices,[3,4] touch screens,[5] photodetectors,[6] and transparent heaters.[7] Requirements for useful TCEs include high conductivity and high optical transparency, low surface roughness to enable integration into thin-film optoelectronic devices, and low-cost, high-throughput methods to generate patterned TCEs for use in devices. The standard TCE material, indium tin oxide (ITO), sets the benchmark for these requirements, with a high transparency (> 80%), low sheet resistance ($R_s < 20$ Ω/sq), and low surface roughness (~3 nm).[8,9] The dominance of ITO in optoelectronics is waning, however, as optoelectronics evolve toward applications requiring mechanical flexibility and stretchability. These new mechanical requirements are incompatible with ITO, which is a brittle ceramic that cracks at strains less than 1%.[10-12] Although depositing ITO on plastic substrates like polyethylene terephthalate (PET) increases its flexibility to 2-3% strain,[13] the low processing temperature that PET substrates can tolerate significantly limits the electrical performance of the produced ITO. Here, we report the fabrication of patterned silver nanowire (AgNW) networks embedded in an optically clear polymer matrix on polydimethylsiloxane (PDMS) substrates. Our patterning method uses plasma oxidation to define a surface wettability pattern on PDMS, which directs the deposition of AgNWs within that pattern to produce a variety of feature geometries with features as small as 50 μm. Embedding the patterned AgNW films in a polymer matrix provides composite coatings are highly transparent and conductive, with

high flexibility and stretchability. We demonstrate their use as transparent electrodes in bendable alternating-current electroluminescent (ACEL) devices.

The need for flexible and stretchable TCEs has prompted extensive research using carbon nanotubes,[14] conductive polymers,[15] graphene,[16] metal grids,[17] or random meshes of metal nanowires[18,19] to prepare flexible and stretchable TCEs with transparency and conductivity comparable to that of ITO on glass. Among these candidates, silver nanowires (AgNWs) are especially promising for several reasons: AgNWs form an interconnected network comprising AgNW-AgNW junctions, creating a network of redundant conductive pathways throughout the film with openings between AgNWs that allow light to pass through to make the film process an optical transmittance as high as 90% and a sheet resistance as low as 3 Ω/sq[20] exceeding the benchmark set by ITO. Compatibility with cost-effective solution processing and the mechanical flexibility of AgNW films make these materials suitable for the fabrication of large-area, flexible TCEs; furthermore, the processing temperature of AgNWs of < 200 °C is compatible with most plastic and elastomeric substrates.[21,22] In addition, the high aspect ratio of AgNWs make them intrinsically flexible and the interconnected silver nanowires slide and rearrange to accommodate the applied stretching strain, making the network intrinsically stretchable,[23] suitable for the fabrication of mechanically deformable TCEs. Despite these advantages, two specific challenges hinder the adoption of AgNWs as electrodes in flexible and stretchable optoelectronic devices. The first is the high roughness and poor adhesion of AgNWs deposited from solution onto a substrate, which results in the formation of poorly-adhered, irregular piles with protrusions > 100 nm from the surface. These protrusions lead to lower device efficiencies compared to ITO-based

devices and create pathways for electrical shorting.[18,21] A useful strategy to solve this problem has been to embed AgNWs into a polymer matrix. The polymer fills in the voids among AgNWs and thus creates a composite with a smooth surface. Strong adhesion between the polymer and AgNW network improves the robustness of the resulting composite. Both flexible polymers, such as polyvinyl alcohol,[24] polyurethane,[25] or poly(3,4-ethylenedioxythiophene) poly(styrenesulfonate),[26] and stretchable polymers, such as PDMS,[27] polydopamine,[28] and polyacrylate[29] have been used as the polymer matrix to embed AgNWs. Among them, polyvinyl alcohol, PDMS, and polyacrylate have been directly used as the substrate, whereas polyurethane, poly(3,4-ethylenedioxythiophene) poly(styrenesulfonate), and polydopamine were applied as coatings on a PDMS substrate. The second challenge is the difficulty in producing patterned AgNW films over large substrate areas, which is necessary for practical device applications. Although various patterning techniques have been reported to produce patterned AgNW films, each process has limitations. Photolithography and wet etching have the advantage of mass production in industry,[30,31] but the costly multi-step manufacturing procedure and the use of toxic etchants needs to be addressed. Focused pulsed laser scribing over the AgNW network can selectively remove AgNWs to form patterned AgNW films without using conventional chemical etching or lithography.[32,33] However, the slow processing rate of spot etching results in low throughput, reducing the feasibility of using this method to commercialize products. Although solution printing onto a substrate using methods such as screen printing[34] and gravure printing[35,36] enables the mass production of large-area patterned AgNW films, these techniques require expensive instrumentation and the resolution of the patterns is limited by the nozzle

geometry, the mask resolution, and solution viscosity. Spin-coating is another commonly used solution-based deposition technique, which generates uniform AgNW films.[37] Yet, the loss of material makes it less economical. Vacuum filtration of a AgNW dispersion through a patterned photoresist layer positioned atop a polymer filter produces patterned AgNW films with features as small as 10 μm.[38] Dry transfer printing of AgNWs from an aluminum oxide filter to PET substrate using a PDMS stamp generates patterned AgNW lines or pixels.[39] Nevertheless, the overall area of the AgNW patterns generated using these two methods is limited by the size of the filtering apparatus.

Recent research to solve this patterning problem has developed wetting/dewetting processes for AgNW dispersion deposition to produce patterned AgNW films.[40-42] The general approach produces patterned hydrophobic and hydrophilic regions on a substrate surface; the differences in wettability guide the AgNW dispersion within predefined hydrophilic areas. This wetting/dewetting approach offers significant advantages of scalability as well as low-cost solution deposition over potentially large areas. For example, Kim et al. selectively deposited a hydrophobic fluoropolymer on a polyethylene naphthalate (PEN) substrate using microcontact printing. Subsequently spray coating AgNW dispersion causes the AgNWs to dewet from the hydrophobic fluoropolymer, which can subsequently be removed, to produce flexible and patterned AgNW films with a minimum feature size of ~25 μm.[40] However, this process can produce connected residues between the patterned areas, creating undesired conductive pathways. Multiple deposition/transfer/etching steps also make this approach less practical. Liu et al. treated a PDMS substrate with UV/ozone through a shadow mask to selectively create etched hydrophilic regions with a depression of ~600 nm, which enables the spread of an AgNW

dispersion in the exposed area.[41] Before transferring the AgNW patterns onto flexible or stretchable receiving substrates such as PET, PVA, paper, and PDMS, the authors used the chemical vapor deposition of hexamethyldisilazane to lower the surface free energy of the oxidized PDMS to enable the release of the AgNW film from the surface. The generated AgNW patterns have a minimum dimension of ~100 μm and withstand a bending radius of 0.5 mm while remaining conductive. However, the effect of the chemical treatment on the properties of AgNWs remains unclear. Additionally, these two studies did not indicate if the flexibility of the patterned AgNW TCEs can be extended to stretchability. Akter et al. fabricated patterned AgNW networks with stretchability by modifying the surface of PDMS through the deposition of polydopamine through a stencil mask to selectively create hydrophilic regions.[28] Spray-coating an AgNW dispersion on the modified surface resulted in AgNW deposition only on the dopamine-modified regions to produce patterned and stretchable conductive films. However, this report explored the optical, electrical, and mechanical properties of unpatterned AgNW/dopamine/PDMS composites rather than investigating these properties of patterned films. Despite the demonstrated advantages of wetting/dewetting patterning, the surface roughness of the resulting patterned AgNW films, an important factor that affects the device performance,[43] is not reported by any of these studies.

Here we describe a new wetting/dewetting process to fabricate flexible and stretchable patterned AgNW coatings without the limitations discussed in previous reports. Instead of etching the PDMS surface with a long UV/ozone treatment, we selectively create a thin, hydrophilic silicate layer by exposing the PDMS surface briefly to air plasma through a stencil mask. The resulting surface wettability pattern acts as a

template to direct the deposition of AgNWs from solution. To lower the surface free energy and also eliminate the use of chemical vapor deposition, we simply leave the PDMS in ambient conditions to allow hydrophobic recovery of the PDMS template, which enables facile release of the AgNWs from the surface and allows the patterned AgNW film to be embedded into an optically transparent polymer matrix (AgNW/polymer) and adhered to a PDMS substrate. The resulting patterned composite possesses a low surface roughness and strong adhesion to the substrate with either flexibility or stretchability by simply altering the elasticity of the polymer matrix. The resulting AgNW/polymer films are highly transparent and conductive with a low surface roughness (< 30 nm) that makes these films suitable as mechanically deformable TCEs.

2.2. Results and Discussion

2.2.1. Fabrication of Patterned AgNW/Polymer Coatings

The process to fabricate patterned AgNW/polymer coatings combines commercially available AgNWs with optically clear polymers, according to Scheme 2.1. We investigated two optically clear polymers, optical adhesive (OA) and Clear Flex 50 (CF). OA is a liquid polyurethane adhesive that cures when exposed to long wavelength ultraviolet light. The cured OA has a Young's Modulus of 1.1 GPa and is flexible. To fabricate stretchable coatings, we employed CF, a urethane rubber that cures at room temperature to produce a stretchable coating with a Young's Modulus of 2.47 MPa. OA coatings on oxidized PDMS substrates remain adhered to ~20% elongation, at which point the composite fractures, whereas CF coatings on oxidized PDMS substrates remain adhered to 106% linear strain, at which point where the composite fractures (Figure S2.1 in the supporting information).
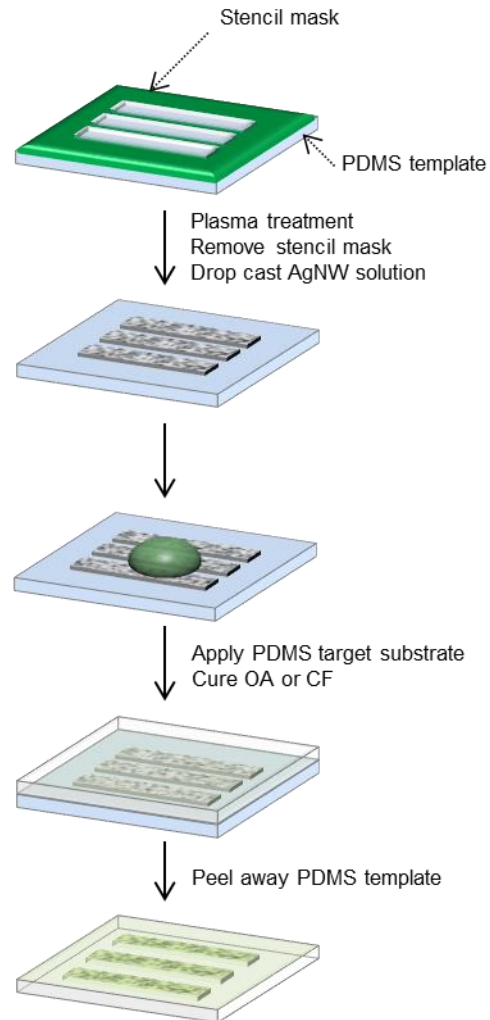
Scheme 2.1. *Process used to fabricate patterned AgNW/OA and AgNW/CF coatings on PDMS substrates.*

To produce patterned AgNW/polymer coatings, we first fabricate a PDMS template with a hydrophobic/hydrophilic pattern on the surface. Native PDMS has an intrinsically hydrophobic surface (water contact angle, $\theta = 123.8 \pm 0.8°$) that is not wet by AgNW dispersions in ethanol. After placing a stencil mask with the desired pattern on the native PDMS surface, brief (40 s) exposure to air plasma creates a thin, hydrophilic silicate layer ($\theta < 20°$) bearing surface hydroxyl groups.[42] The areas covered by the

stencil mask remain hydrophobic ($\theta = 123.2 \pm 1.4°$). The resulting patterned

hydrophobic/hydrophilic PDMS surface defines the AgNW deposition area. Drop-

casting a AgNW dispersion (1 mg/mL, 2 mg/mL, or 4 mg/mL) in ethanol (48 µL/cm^2)

onto the patterned PDMS template followed by air-drying on an agitator forms patterned

AgNW films. During the drying process, the AgNW dispersion spontaneously flows into

the hydrophilic regions on the PDMS template and dewets from the hydrophobic regions.

Annealing the patterned AgNW film at 200 °C for 20 min fuses the AgNWs at their

junctions and removes the residual solvent. To enable peel-off of the AgNW films from

the PDMS template, we lower the surface free energy of the PDMS template by simply

allowing the PDMS surface to undergo hydrophobic recovery in ambient conditions for

24 hours. During hydrophobic recovery, low molecular weight chains (i.e., uncrosslinked

linear PDMS chains or residual crosslinking agent) diffuse to the surface through

microcracks in the brittle plasma-induced silicate layer,[44] lowering the surface free

energy and restoring the hydrophobicity of the PDMS surface ($\theta = 123.1 \pm 0.7°$) to

enable the release of the patterned AgNW network to that target substrate, which is a

plasma-oxidized PDMS substrate. Applying a drop of either OA or CF onto the surface

of the AgNW film on the PDMS template, placing the target PDMS substrate on top, and

then curing the polymer adheres the AgNW/polymer film to the target PDMS substrate;

the template can then be easily peeled away. This process completely transfers the

patterned AgNW network from the PDMS template to the target PDMS substrate (Figure

S2.2). We subjected the AgNW/polymer coating surfaces to repeated peel tests with

Scotch tape and did not observe AgNW residue on the tape after 10 peel tests (Figure

S2.3).

2.2.2. Pattern Dimensions and Resolution

Patterning by wetting/dewetting produces patterned AgNW/polymer films with various curved and square edges and line widths that correspond to the features of the stencil mask used to produce the hydrophilic pattern. The feature sizes of the patterned AgNW films range from millimeters to micrometers (Figure 2.1a-d, S2.4). Figure 2.1a shows AgNW/OA films patterned into mm-scale letters with curvatures as small as 20°. Figure 2.1b displays a pattern comprising square wave designs with line widths ranging from 50 μm to 150 μm and square shapes with side lengths of 600 μm to 1500 μm. We used a single 5 cm x 5 cm stencil mask to fabricate the patterns in Figure 2.1 a and b. For Figure 2.1c, we placed four 2.5 cm x 2.5 cm stencil masks onto a PDMS substrate at the same time to fabricate four sets of interdigitated electrodes at once. Each set of electrodes consisted of six individual electrodes with line widths of 1 mm. We also generated more complex patterns, such as AgNW grids, that are impossible to achieve with a single stencil mask. Exposing the PDMS surface to air plasma through a shadow mask with 2-mm-wide lines spaced by 2.5 mm, rotating the mask 90° and exposing the surface to air plasma a second time creates the hydrophilic grid pattern. A photograph of the patterned AgNW/OA grid with overall dimensions of 2.5 cm x 2.5 cm is shown in Figure 2.1d.
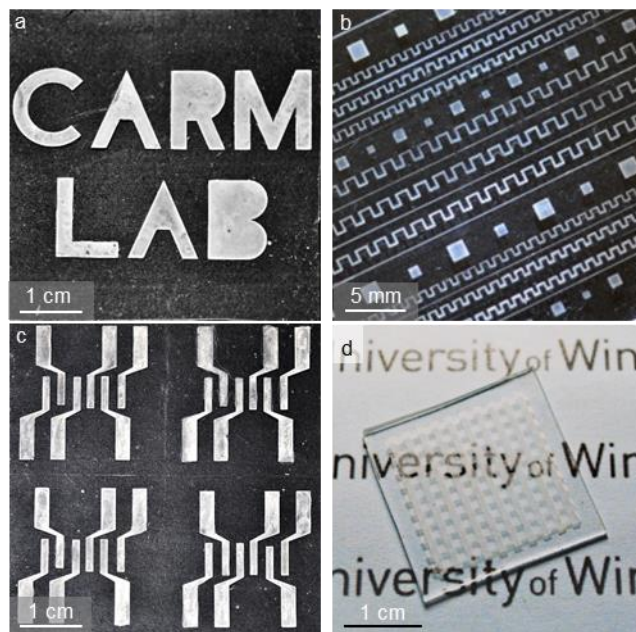
Figure 2.1. *(a) Optical micrograph of letters with various curvatures. (b) Optical micrograph of square and square wave patterns. (c) Optical micrograph of four sets of electrodes. Each set consisted of six polygonal chains. (d) Photograph of a patterned grid. Overall sample dimensions are (a-c) 5 cm x 5 cm and (d) 2.5 cm x 2.5 cm.*

2.2.3. Morphology of Patterned AgNW/Polymer Coatings

We used scanning electron microscopy (SEM) to examine the uniformity and edge definition of the patterned AgNW/polymer coatings. Top-view SEM images of patterned AgNW/OA lines (Figure 2.2a, b) show that the AgNW line edges with widths of 50 μm and 300 μm are sharp, without AgNW residue outside the pattern, thus indicating the hydrophilic patterns of the PDMS template control the deposition of the AgNW dispersion well. The embedded AgNWs are homogeneously distributed and interconnected, forming a network (Figure 2.2c). The cross-sectional SEM image of an AgNW/OA coating on a silicon wafer (Figure S2.5a) shows that the thickness of the OA layer is ~31 μm, similar to that of the CF layer (~30 μm) (Figure S2.5b). The AgNWs

reside at the top of the coating (Figure S2.5c). SEM images also reveal that a higher density of AgNWs accumulates at the edges of the patterned features, a common phenomenon in drop casting referred to as the 'coffee ring effect' (Figure 2.2d). During the drying of the AgNW dispersion, liquid evaporating from the edge is replenished by liquid from the interior due to capillary flow and leading to mass transfer and aggregation of AgNWs at the edge of the patterned area. The width of the zone depends on the linewidth of the patterned feature: Coffee-ring zones have a width of ~80 μm for features with linewidths of 2000 μm and 1500 μm, ~60 μm for features with linewidths of 1000 μm and 800 μm, and ~40 μm for a linewidth of 500 μm and 300 μm. Features of linewidths of 100 μm and 50 μm do not show a distinct coffee-ring zone.
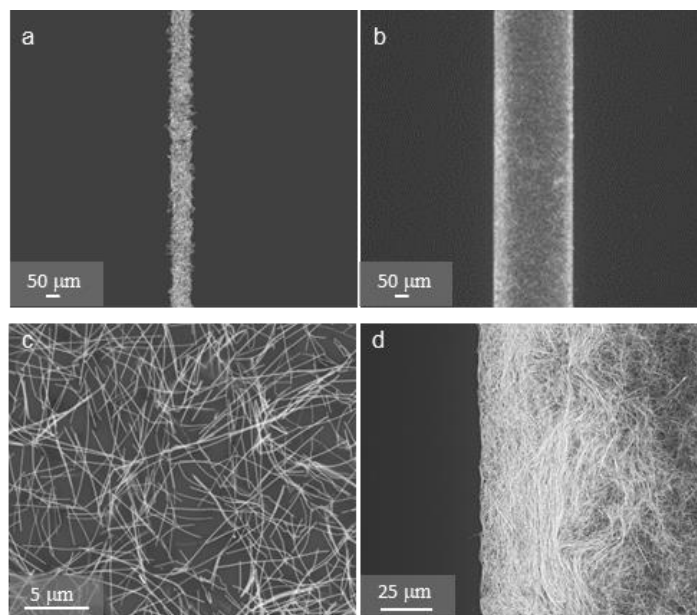
Figure 2.2. SEM images of patterned AgNW/OA lines with widths of (a) 50 *μm* and (b) 300 *μm* on PDMS substrate. Higher magnification of AgNW networks at the (c) centre and (d) edge of 2000-*μm*-wide AgNW/OA lines.

2.2.4. Topography of Patterned AgNW/Polymer Coatings

The inherent roughness of AgNW networks not embedded in polymer is problematic for thin-film devices, where a smooth surface is required.[18,21,43] Embedding the patterned AgNW networks in OA and CF polymers significantly decreases the surface roughness compared to AgNW networks without polymer. Over an area of 10 μm x 10 μm (Figure 2.3a, b), the root-mean-square roughness (R_{RMS}) of patterned AgNW/OA coatings fabricated from a 2 mg/mL dispersion is 21.6 ± 0.7 nm, similar to that of patterned AgNW/CF coatings made using the same dispersion concentration (22.7 ± 2.6 nm). These values are ~4x lower than the R_{RMS} of AgNW films fabricated using the same dispersion concentration without the polymer matrix (84.6 ± 7.4 nm) (Figure 2.3c). Moreover, AFM profile measurements (Figure 2.3d, e, f) reveal lower peak-to-

valley-distances for AgNW/OA and AgNW/CF coatings (~65 nm) compared to AgNW films without the polymer matrix (~350 nm).

We also scanned the edges of the 2 mm x 20 mm patterned AgNW/OA line on PDMS over an area of 100 μm x 100 μm to characterize the consequence of the coffee-ring effect on the roughness (Figure S2.6a). The width of the coffee-ring zone is ~80 μm. The higher density of AgNW at pattern edges increases the number of overlapped AgNW-AgNW junctions. As a result, the RMS roughness of the edge of the patterns (R_{RMS} = 36.2 ± 3.8 nm) is 50% higher than the RMS roughness at the center. The profile measurement (Figure S2.6b) also shows an increased maximum peak-to-valley distance over the scan area for the AgNW patterns of ~150 nm.
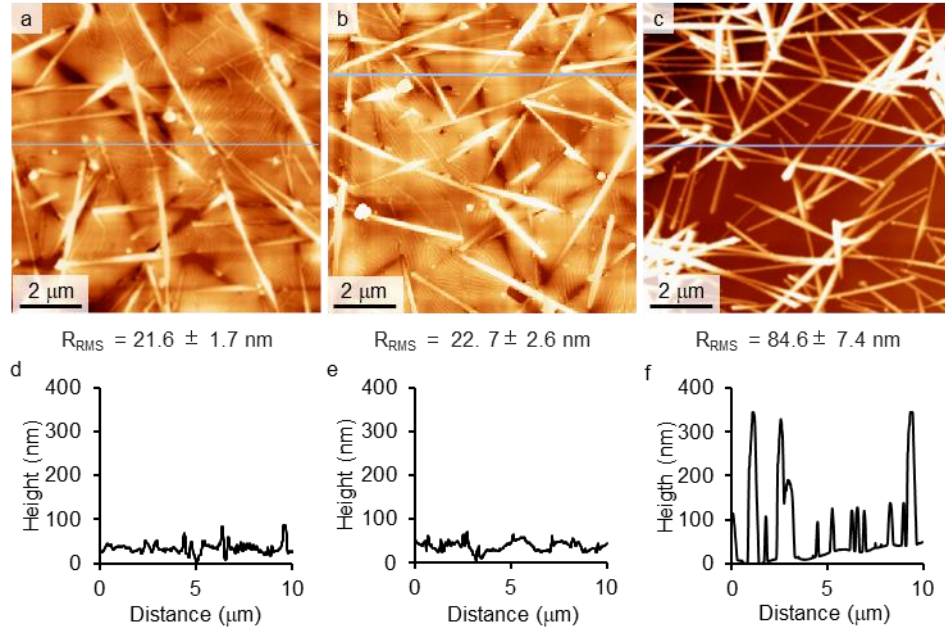
Figure 2.3. *AFM height images (Z scale = 150 nm) with R_{RMS} measurements and corresponding profile measurements of patterned (a, d) AgNW/OA and (b, e) AgNW/CF lines (20 mm x 2 mm) on PDMS fabricated using a 2 mg/mL AgNW dispersion. AFM height image (Z scale = 350 nm) with R_{RMS} measurements and corresponding profile measurement of (c, f) an unpatterned AgNW network fabricated by drop-casting a 2 mg/mL AgNW dispersion onto a silicon wafer substrate.*

2.2.5. Electrical and Transmittance Properties of AgNW/Polymer Coatings

Both AgNW/OA and AgNW/CF coatings on PDMS substrates are highly transparent and conductive. We collected transmittance spectra and measured the corresponding R_s of AgNW/OA and AgNW/CF coatings patterned into five 20 mm x 2 mm lines using AgNW dispersion concentrations of 1 mg/mL, 2 mg/mL, and 4 mg/mL (Figure 2.4, Table S2.1). We measured the R_s of each line separately and report the average of measurements from at least three samples. The R_s and optical transparency of AgNW/polymer coatings depend on the concentration of the AgNW dispersion, with the expected trade-off between R_s and optical transmittance: Increasing the concentration of

AgNW dispersion increases the density of AgNWs in the network that decreases R_s as well as the optical transmittance. The choice of polymer (OA or CF) does not affect the optical transparency, since both polymers are transparent throughout the visible light range. The comparable R_s of OA- and CF-based coatings made with same AgNW dispersion concentration indicates that the electrical network formed by the AgNWs are independent of the choice of polymer. The R_s is also not significantly influenced by the linewidth: We patterned AgNW/OA and AgNW/CF into lines of the same length (2 cm) and widths ranging from 50 to 2000 μm (Figure 2.5a). Despite the slight variation in the width of the coffee-ring zone of accumulated AgNWs at the pattern edge, decreasing the line width from 2000 μm to 50 μm did not show a measurable increase in the R_s (Figure 2.5b, c). We chose AgNW/OA and AgNW/CF coatings made from a 2 mg/mL AgNW dispersion (R_s = 6 Ω/sq) for the remainder of this study.
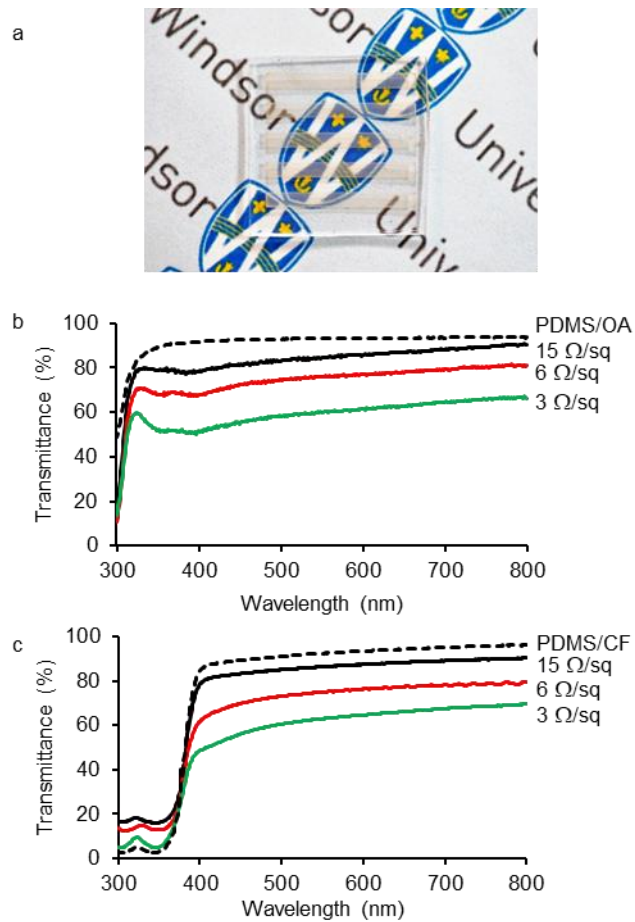
Figure 2.4. *(a) Photograph of patterned AgNW/OA lines on PDMS substrate used for R_s and transmittance measurements. Transmittance spectra of patterned (b) AgNW/OA and (c) AgNW/CF lines on PDMS substrates with corresponding R_s. Dotted line shows the transmittance spectrum of the (b) PDMS/OA and (c) PDMS/CF composite without AgNWs.*
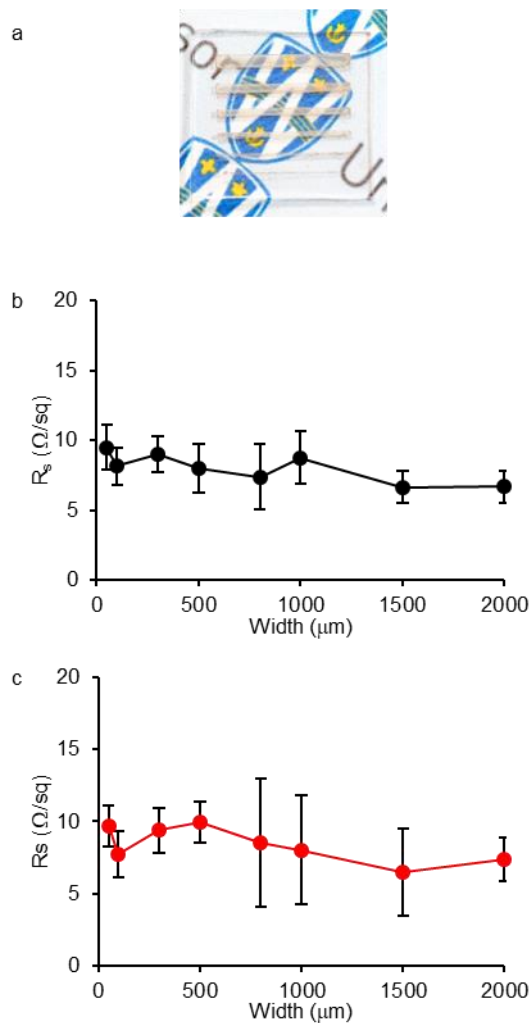
Figure 2.5. (a) Photograph of patterned AgNW/OA lines on PDMS substrate with various line widths and lengths of 2 cm. R_s as a function of linewidth for patterned (b) AgNW/OA and (c) AgNW/CF lines made from a 2 mg/mL AgNW dispersion.

2.2.6. Flexibility and Stretchability of Patterned AgNW/Polymer Coatings

Patterned AgNW/OA coatings are highly flexible. We measured the change in resistance of patterned AgNW/OA lines with a dimension of 20 mm x 2 mm on 1-mm-thick PDMS substrates at various bending radii. The bending strain is calculated

according to equation 2.1, where ε is the bending strain, d is the thickness of the substrate, and r is the radius of the curvature.

$$\varepsilon = d/2r \qquad (2.1)$$

The change in resistance (R/R_0) versus the bending strain is plotted in Figure 2.6a. The resistance of AgNW/OA lines negligibly changed ($R/R_0 = 1.00 \pm 0.12$) when bending the films to radii as small as 0.7 mm (71% strain). Flexible TCEs are required to remain conductive in the process of reuse; therefore, we also tested the durability of the AgNW/OA lines to repetitive bending. After 200 cycles of 15% bending strain, the resistance of the AgNW lines increased by less than twofold its initial value (Figure 2.6b).

Using CF as the polymer matrix produces AgNW/CF coatings on PDMS that remain conductive with stretching. We stretched 20 mm x 2 mm AgNW/CF lines on 1-mm-thick PDMS substrates and measured the resistance at 5% strain intervals until the films were no longer conductive. The R/R_0 versus the stretching strain is plotted in Figure 2.6c. The resistance of the AgNW/CF lines increases with elongation, which can be attributed to the increase in the length of the conductive pathway, as well as damage to AgNW-AgNW contacts within the network.[27] The patterned AgNW/CF lines remain conductive up to 70% stretching strain, and become non-conductive beyond this elongation likely due to separation of AgNW-AgNW contacts within the network. Releasing the strain, however, enables the reformation, albeit incomplete, of AgNW-AgNW contacts to recover the network conductivity with an R/R_0 value of 9.5 ± 0.8. Stretchable TCEs have potential applications in wearable optoelectronics which require functionality during the repeated bending of joints such as the wrist (~30% strain). We

subjected patterned AgNW/CF coatings to repetitive cycles of 30% strain and measured the resistance in the relaxed state (0%) after every 20 cycles. The plot of the change in resistance as a function of the number of strain cycles (Figure 2.6d) shows a slightly gradual increase in R/R_0 with the number of strain cycles. After 200 cycles, the R/R_0 increases to 3.6 ± 0.2, likely due to irrecoverable loss of AgNW-AgNW junctions during repetitive stretching.
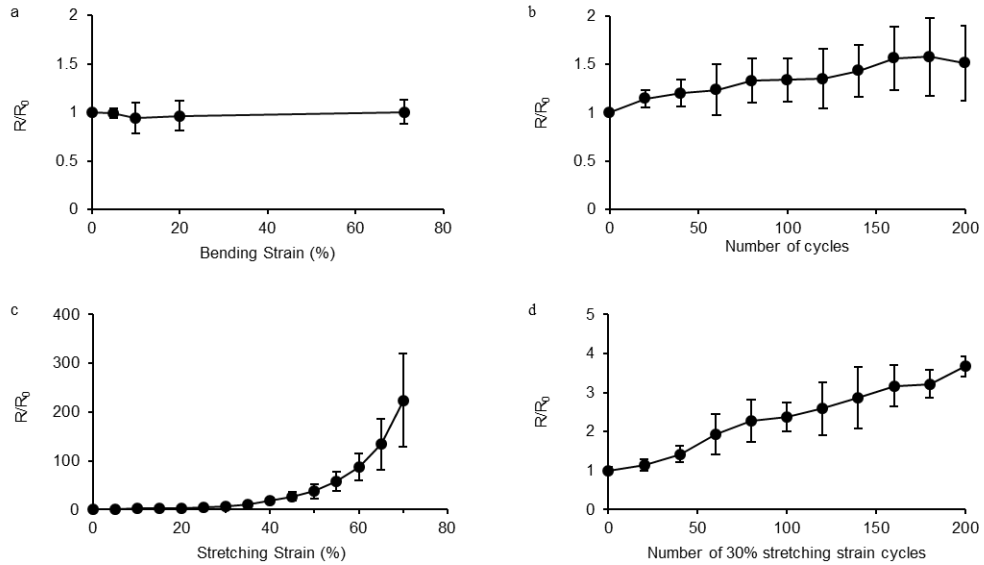
Figure 2.6. (a) Change in resistance of 20 mm x 2 mm AgNW/OA lines on PDMS substrate as a function of bending strain. (b) Change in resistance of 20 mm x 2 mm AgNW/OA lines on PDMS versus the number of 15% bending strain cycles. (c) Change in resistance of 20 mm x 2 mm AgNW/CF lines on PDMS as a function of stretching strain. (d) Change in resistance of 20 mm x 2 mm AgNW/CF lines on PDMS versus the number of 30% stretching strain cycles. The concentration of the AgNW dispersion used in all cases was 2 mg/mL.

2.2.7. Flexible ACEL Devices with Patterned AgNW/OA TCEs

We demonstrated the use of a patterned AgNW/OA film on a PDMS substrate as the TCE in flexible alternating-current electroluminescent (ACEL) devices and characterized the devices before and after cycles of bending. ACEL devices use a simple architecture that consists of a phosphor deposited between two electrodes; this simple architecture has previously been exploited in the fabrication of flexible[45] and stretchable devices[46] that use flexible or stretchable electrodes with an emissive composite comprising ZnS:Cu phosphor microparticles dispersed in PDMS. We used the patterned AgNW/OA coating on PDMS to fabricate flexible ACEL devices according to the structure shown in Figure 2.7a. The device consists of an AgNW/OA coating patterned into five 20 mm x 2 mm lines on 1-mm-thick PDMS substrates as the TCE. We deposited the emissive composite of ZnS:Cu phosphor microparticles in PDMS onto the TCE surface by spin-coating, cured the PDMS at 60 °C, and then completed the device by simply adhering copper tape to the surface as the top electrode. Unstrained ACEL devices immediately emit bright, uniform light over the patterned AgNW electrode area when a voltage of 150 V AC is applied. The flexible ACEL devices maintain light emission when bent to 5%, 10%, and 20% strain (radii of 10.0 mm, 5.0 mm, 2.5 mm, respectively), as shown in Figure 2.7b. Bending beyond 20% strain causes delamination of the copper tape electrode. Although it would be ideal to replace the copper tape electrode with a second flexible AgNW/OA coating on PDMS, this integration is challenging due to the weak adhesion between the laminated top AgNW/OA electrode and the emissive layer resulting in delamination at low bending strains.
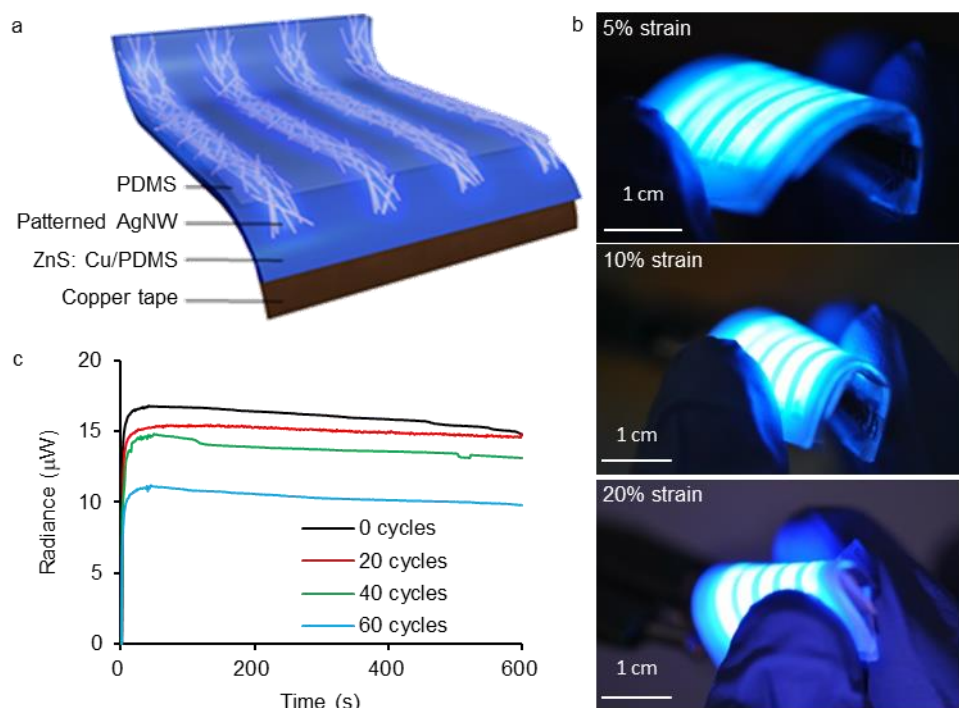
Figure 2.7. (a) Diagram of the flexible ACEL device structure. (b) Photographs of flexible ACEL devices fabricated with a patterned AgNW/OA (2 mg/mL) coating on PDMS as the TCE, bent to various strains. (c) Temporal evolution of radiance of a typical device operated under 150 V AC in ambient conditions before and after being subjected to repetitive 20% bending strain cycles.

We tested the durability of these ACEL devices by subjecting them to repetitive 20% bending strain cycles (bending radius of 2.5 mm). We measured the radiance of an unstrained device and then measured the radiance of the same device after subjecting it to 20, 40, and 60 bending cycles (Figure 2.7c). Three samples were measured, and the resulting maximum radiance values were averaged. The maximum radiance values decreased to $91.9 \pm 0.3\%$, 85.8 ± 0.5 %, and $66.5 \pm 0.1\%$ of the maximum radiance of unstrained devices, after subjecting the devices to 20, 40, and 60 cycles of 20% bending strain respectively. The decrease in maximum radiance with strain cycles may be due to a combination of several factors: First, the increase in resistance of the AgNW/OA

coating due to repetitive bending may lower the applied voltage on the emissive layer.[47] Second, tens of bending cycles degrade the contact between the top flexible Cu electrode and the ZnS:Cu emissive layer (Figure S2.7). Third, the degradation of the light-emissive material itself is typical of ACEL devices and can be attributed to the structural relaxation at the ZnS:Cu interface resulting in Cu diffusion into the vacancies within the electroluminescent materials.[48,49] Previous studies have reported that the electroluminescent intensity of unstrained ACEL devices decreases ~10% each time the device is operated.[49]

Replacing the AgNW/OA coating on PDMS with an AgNW/CF coating on PDMS as both top TCE and bottom electrode is a path to fabricating intrinsically stretchable ACEL devices; however, the integration of these layers remains challenging. Pressing the AgNW/CF surface onto the emissive layer results in weak lamination between the coating and the emissive material, and voids between the AgNW/CF surface and emissive layer causes an uneven electrical field distribution that consequently affects the performance of the resulting devices. Stretching these devices easily destroys this three-layer structure by catastrophic delamination. Future work on these systems will focus on methods to solve these integration problems.

2.3. Conclusions

We have successfully developed a simple, solution-based and scalable method to fabricate patterned AgNW networks embedded in both flexible and stretchable polymers and adhered to a PDMS substrate. The resulting AgNW/polymer composites are highly transparent, conductive, and remain conductive under mechanical bending, stretching, and repetitive mechanical deformations, possessing all the essential features that are

needed for compliant TCEs. We believe that these optical, electrical, and mechanical properties of AgNW/OA and AgNW/CF coatings, along with the simplicity and scalability of preparation, can be helpful in the development of new flexible and stretchable optoelectronic devices. We have demonstrated that ACEL devices fabricated using flexible AgNW/OA coatings on PDMS as the TCE remain functional with bending. However, it is still challenging to fabricate ACEL devices that use two AgNW/OA electrodes or stretchable light-emitting devices that use two stretchable AgNW/CF electrodes due to challenges with integrating the top electrode in the device via lamination. Future work will focus on solving this integration problem to create robust flexible and stretchable optoelectronic devices.

2.4. Experimental

Materials. AgNW dispersed in ethanol (20 mg/mL) with an average diameter of 60 nm and an average length of 90 μm was purchased from ACS Material Inc. (Pasadena, CA, USA). PDMS (Sylgard 184) elastomer base and curing agent kits were purchased from Dow Corning (Midland, MI, USA). Polyurethane optical adhesive NOA 73 (OA) was obtained from Norland Products Inc. (Cranbury, NJ, USA). Urethane rubber Clear Flex 50 (CF) was purchased from Smooth-On Inc. (Macungie, PA, USA). ZnS: Cu microparticles were purchased from Shanghai KPT (Shanghai, China). All the materials were used as received without further purifications.

Preparation of AgNW suspensions. The stock AgNWs suspension in ethanol was diluted to 1 mg/mL, 2 mg/mL, and 4 mg/mL with anhydrous ethanol. The diluted solutions were sonicated for 2 min before using.

Preparation of patterned AgNW films. The PDMS base and curing agent (Sylgard 184) were mixed in a weight ratio of 10:1 and degassed. The liquid mixture was coated on flat polystyrene Petri dishes and cured overnight in an oven at 60 °C. Cured PDMS films were cut into squares with a size of 2.5 cm x 2.5 cm or 5.0 cm x 5.0 cm. A stainless-steel stencil mask with the desired pattern was placed onto PDMS surface and then the covered PDMS was subjected to air plasma for 40 s in a Harrick plasma cleaner at air pressure of 15 psig and flow rate of 10.6 mL/min at medium discharge setting. The stencil mask was then removed from the PDMS surface, and the patterned PDMS template was placed onto an agitator (KS 130 Basic, IKA) with an agitation rate of 160 rpm. The diluted AgNW solution was drop cast onto the PDMS template at 48 μL/cm^2 while agitating. The AgNW dispersion spontaneously spread in the hydrophilic regions and dewetted from the hydrophobic areas followed by air-dried on the agitator with agitation. After annealing at 200 °C for 20 min on a hot plate and cooling to room temperature, the patterned AgNW films on PDMS template were set aside for 24 h to undergo hydrophobic recovery. A drop (5 μL/cm^2 of AgNW film) of OA or CF, was then placed onto the surface of the patterned AgNW film, and oxidized PDMS substrate was placed on top after air Plasma for 40 s. OA or CF was allowed to spread for 1 min and then OA was cured under a UV light (Spectroline Model SB-100p) for 15 min while CF was cured at room temperature for 16 h. The target PDMS substrate was then peeled off from the PDMS template, with either AgNW/OA or AgNW/CF coating adhered to its surface.

Fabrication of bendable ACEL devices. Patterned AgNW/OA coatings were oxidized in air plasma for 30 s. ZnS:Cu microparticles were mixed with PDMS

prepolymer (weight ratio of base to curing agent = 10: 1) in the weight ratio of 2:1 to produce a phosphor paste. The prepared ZnS:Cu/PDMS composite was then spin-coated onto the patterned AgNW/OA coating on PDMS substrate at 500 rpm for 1 min. The film was then cured in an oven at 60 °C overnight. A copper tape cathode was adhered onto the surface of the resulting ZnS:Cu/PDMS emissive material.

Characterization. Optical microscopy images were taken using an Olympus BX51 microscope equipped with an Olympus Q-Color 3 camera. SEM images were collected with a Quanta 200 FEG Environmental SEM (FEI, USA). AFM images (10 μm x 10 μm and 100 μm x 100 μm) were collected using the tapping mode of a Digital Instruments Multimode AFM. Transmittance spectra were recorded using a Varian Cary 50 UV-Visible spectrophotometer. Resistance values were measured using Keithley 2601 source meter with a minimum of five measurements for each sample. The R_s was measured using the four-point probe method with all four probes placed on a single AgNW line. Bending experiments were performed by wrapping patterned AgNW/OA stripes around cylindrical objects with radii varying from 10 mm to 0.7 mm and measuring the resistance of the patterned AgNW lines at each bending radius. Stretching tests were conducted by clamping samples in a microvice stretching (S. T. Japan, USA, Inc.) and the resistance was measured at 5% increments of strain. Data sets consisted of a minimum of five samples, and the average was reported. The ACEL device was driven by a DC power supply (Keithley 2601) together with a TDK CXA-L10A Inverter. The ACEL light emission radiance was measured with a calibrated UDT S470 optometer using an integrating sphere.

2.5. References

(1)   Bi, H.; Huang, F. Q.; Liang, J.; Xie, X. M.; Jiang, M. H. *Adv. Mater.* **2011**, *23*, 3202.

(2)   Leem, D.-S.; Edwards, A.; Faist, M.; Nelson, J.; Bradley, D. D. C.; Mello, J. C. *Adv. Mater.* **2011**, *23*, 4371.

(3)   Li, L.; Liang, J.; Chou, S.-Y.; Zhu, X.; Niu, X.; ZhibinYu; Pei, Q. *Sci. Rep.* **2014**, *4*, 4307.

(4)   Yu, Z.; Zhang, Q.; Li, L.; Chen, Q.; Niu, X.; Liu, J.; Pei, Q. *Adv. Mater.* **2010**, *23*, 664.

(5)   Lee, J.; Lee, P.; Lee, H.; Lee, D.; Lee, S. S.; Ko, S. H. *Nanoscale* **2012**, *4*, 6408.

(6)   Zheng, Z.; Gan, L.; Li, H.; Ma, Y.; Bando, Y.; Golberg, D.; Zhai, T. *Adv. Funct. Mater.* **2015**, *25*, 5885.

(7)   Kim, T.; Kim, Y. W.; Lee, H. S.; Kim, H.; Yang, W. S.; Suh, K. S. *Adv. Funct. Mater.* **2013**, *23*, 1250.

(8)   Yang, Y.; Huang, Q.; Metz, A. W.; Ni, J.; Jin, S.; Marks, T. J.; Madsen, M. E.; DiVenere, A.; Ho, S. T. *Adv. Mater.* **2004**, *16*, 321.

(9)   Gaynor, W.; Burkhard, G. F.; McGehee, M. D.; Peumans, P. *Adv. Mater.* **2011**, *23*, 2905.

(10)   Tahar, R. B. H.; Ban, T.; Ohya, Y.; Takahashi, Y. *J. Appl. Phys.* **1998**, *83*, 2631.

(11)   Fortunato, E.; Ginley, D.; Hosono, H.; Paine, D. C. *MRS Bull.* **2007**, *32*, 242.

(12)   Kumar, A.; Zhou, C. W. *ACS Nano* **2010**, *4*, 11.

(13)   Cairns, D. R.; Crawford, G. P. *Proc. IEEE* **2005**, *93*, 1451.

(14)   Sekitani, T.; Nakajima, H.; Maeda, H.; Fukushima, T.; Aida, T.; Hata, K.; Someya, T. *Nat. Mater.* **2009**, *8*, 494.

(15)   Liu, Z. Y.; Parvez, K.; Li, R. J.; Dong, R. H.; Feng, X. L.; Mullen, K. *Adv. Mater.* **2015**, *27*, 669.

(16)   Kim, K. S.; Zhao, Y.; Jang, H.; Lee, S. Y.; Kim, J. M.; Kim, K. S.; Ahn, J. H.; Kim, P.; Choi, J. Y.; Hong, B. H. *Nature* **2009**, *457*, 706.

(17)   Hong, S.; Yeo, J.; Kim, G.; Kim, D.; Lee, H.; Kwon, J.; Lee, H.; Lee, P.; Ko, S. H. *ACS Nano* **2013**, *7*, 5024.

(18)   Hu, L. B.; Kim, H. S.; Lee, J. Y.; Peumans, P.; Cui, Y. *ACS Nano* **2010**, *4*, 2955.

(19)   Chu, H. C.; Chang, Y. C.; Lin, Y.; Chang, S. H.; Chang, W. C.; Li, G. A.; Tuan, H. Y. *ACS Appl. Mater. Interfaces* **2016**, *8*, 13009.

(20)   Lee, P.; Lee, J.; Lee, H.; Yeo, J.; Hong, S.; Nam, K. H.; Lee, D.; Lee, S. S.; Ko, S. H. *Adv. Mater.* **2012**, *24*, 3326.

(21)   Lee, J. Y.; Connor, S. T.; Cui, Y.; Peumans, P. *Nano Lett.* **2008**, *8*, 689.

(22) Gong, C. K.; Liang, J. J.; Hu, W.; Niu, X. F.; Ma, S. W.; Hahn, H. T.; Pei, Q. B. *Adv. Mater.* **2013**, *25*, 4186.

(23) Yan, C.; Kang, W.; Wang, J.; Cui, M.; Wang, X.; Foo, C. Y.; Chee, K. J.; Lee, C. P. *ACS Nano* **2014**, *8*, 316.

(24) Zeng, X.-Y.; Zhang, Q.-K.; Yu, R.-M.; Lu, C.-Z. *Adv. Mater.* **2010**, *22,* 4484.

(25) Miller, M. S.; O'Kane, J. C.; Niec, A.; Carmichael, R. S.; Carmichael, T. B. *ACS Appl. Mater. Interfaces* **2013**, *5*, 10165.

(26) Yang, L.; Zhang, T.; Zhou, H.; Price, S. C.; Wiley, B. J.; You, W. *ACS Appl. Mater. Interfaces* **2011**, *3*, 4075.

(27) Xu, F.; Zhu, Y. *Adv. Mater.* **2012**, *24*, 5117.

(28) Akter, T.; Kim, W. S. *ACS Appl. Mater. Interfaces* **2012**, *4*, 1855.

(29) Hu, W.; Niu, X.; Li, L.; Yun, S.; Yu, Z.; Pei, Q. *Nanotechnology* **2012**, *23*, 344002.

(30) Ok, K.-H.; Kim, J.; Park, S.-R.; U., K.; Lee, C.-J.; Hong, S.-J.; Kwak, M.-G.; Kim, N.; Han, C. J.; Kim, J.-W. *Sci. Rep.* **2015**, *5*, 9464.

(31) Ko, Y.; Kim, J.; Kim, D.; Yamauchi, Y.; Kim, J. H.; You, *J. Sci. Rep.* **2017**, *7*, 2282.

(32) Henley, S. J.; Cann, M.; Jurewicz, I.; Dalton, A.; Milne, D. *Nanoscale* **2014**, *6*, 946.

(33) Spechler, J. A.; Arnold, C. B. *Appl. Phys. A* **2012**, *108*, 25.

(34) Chou, N.; Kim, Y.; Kim, S. *ACS Appl. Mater. Interfaces* **2016**, *8*, 6269.

(35) Gupta, R.; Walia, S.; Hosel, M.; Jensen, J.; Angmo, D.; Krebs, F. C.; Kulkarni, G. U. *J. Mater. Chem. A* **2014**, *2*, 10930.

(36) Scheideler, W. J.; Smith, J.; Deckman, I.; Chung, S.; Arias, A. C.; Subramanian, V. *J. Mater. Chem. C* **2016**, *4*, 3248.

(37) Liu, S. Y.; Ho, S. H.; So, F. *ACS Appl. Mater. Interfaces* **2016**, *8*, 9268.

(38) Tybrandt, K.; Stauffer, F.; Vörös, J. *Sci. Rep.* **2016**, *6*, 25641.

(39) Madaria, A. R.; Kumar, A.; Ishikawa, F. N.; Zhou, C. *Nano Res*. **2010**, *3*, 564.

(40) Kim, M. S.; Lee, D. H.; Kim, K. B.; Jung, S. H.; Lee, J. K.; O, B. H.; Lee, S. G.; Park, S. G. *Thin Solid Films* **2015**, *587*, 100.

(41) Liu, G.-S.; Liu, C.; Chen, H.-J.; Cao, W.; Qiu, J.-S.; Shieh, H.-P., D.; Yang, B.-Y. *Nanoscale* **2016**, *8*, 5507.

(42) Hillborg, H.; Ankner, J. F.; Gedde, U. W.; Smith, G. D.; Yasuda, H. K.; Wikström, K. *Polymer* **2000**, *41*, 6851.

(43) Gaynor, W.; Burkhard, G. F.; McGehee, M. D.; Peumans, P. *Adv. Mater.* **2011**, *23*, 2905.

(44) Eddington, D. T.; Puccinelli, J. P.; Beebe, D. J. Sens. *Actuators B* **2006**, *114*, 170.

(45)   Schrage, C.; Kaskel, S. *ACS Appl. Mater. Interfaces* **2009**, *1*, 1640.

(46)   Wang, J. X.; Yan, C. Y.; Chee, K. J.; Lee, P. S. *Adv. Mater.* **2015**, *27*, 2876.

(47)   Zhang, J. H.; Wang, L.; Zhang, Y.; Li, L.; Tang, S. I.; Xing, C. G.; Kim, S. H.; Jiang, C.; Lu, J. X. *Molecular Carcinogenesis* **2015**, *54*, 1567.

(48)   Brese, N. E.; Rohrer, C. L.; Rohrer, G. S. *Solid State Ionics* **1999**, *123*, 19.

(49)   Popovych, K. O. *Semicond. Phys. Quantum Electron. Optoelectron.* **2007**, *10*, 77.

2.6. Supporting Information
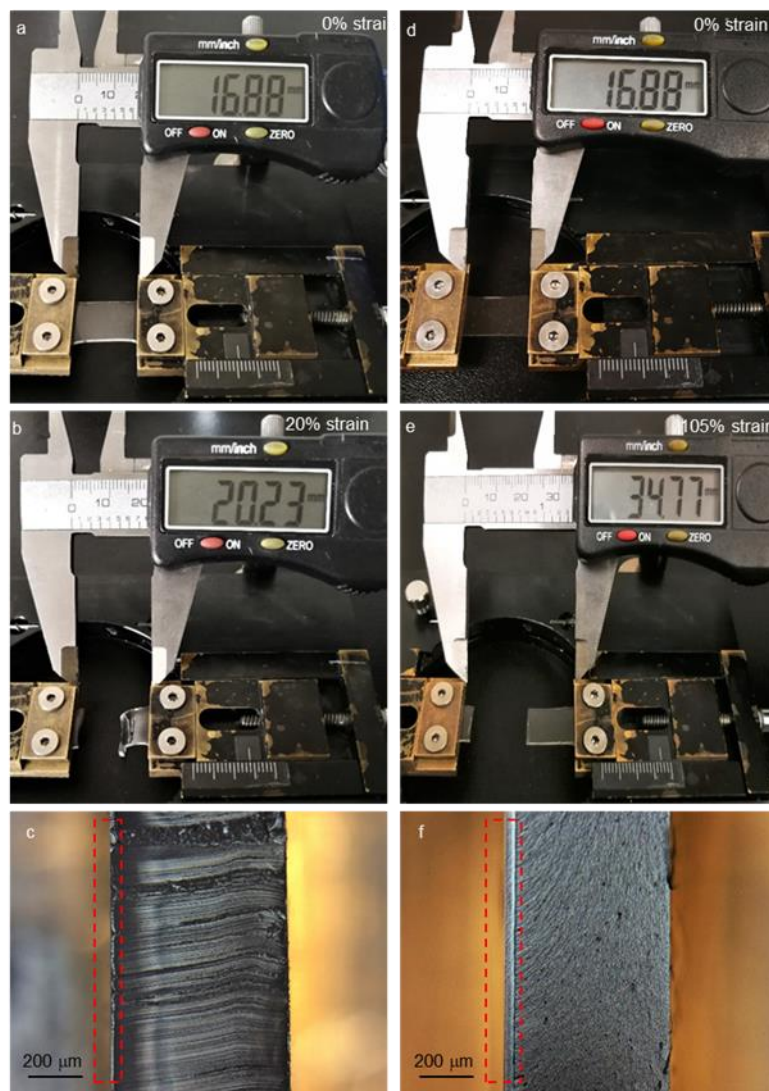
Figure S2.1. *Photographs of OA coating on PDMS substrate (a) at 0% strain and (b) fractured at 20% strain. (c) Cross-sectional optical micrograph of OA coating on PDMS substrate after fracture at 20% strain. The OA coating (in the red frame) remains adhered to the PDMS substrate after fracture. Photographs of CF coating on PDMS substrate (d) at 0% strain and (e) fractured at 106% strain. (f) Cross-sectional optical micrograph of CF coating on PDMS substrate after fracture at 106% strain. The CF coating (in the red frame) remains adhered to the PDMS substrate after fracture.*
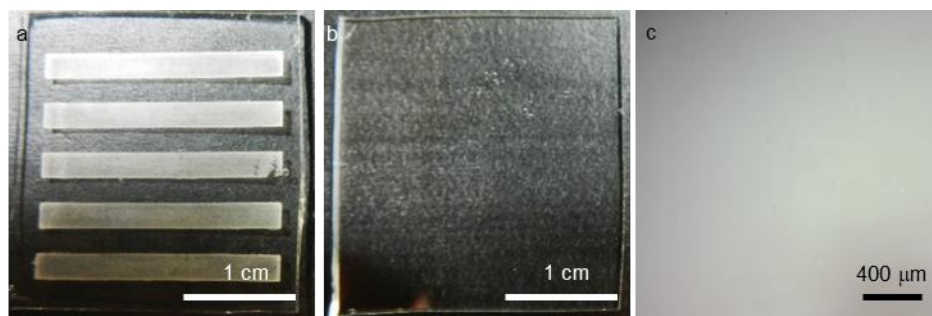
Figure S2.2. *Photographs of (a) AgNW/OA coating on PDMS substrate and (b) PDMS template after the transferring process. (c) Optical micrograph of PDMS template after the transferring process, showing that no AgNW residue was observed.*
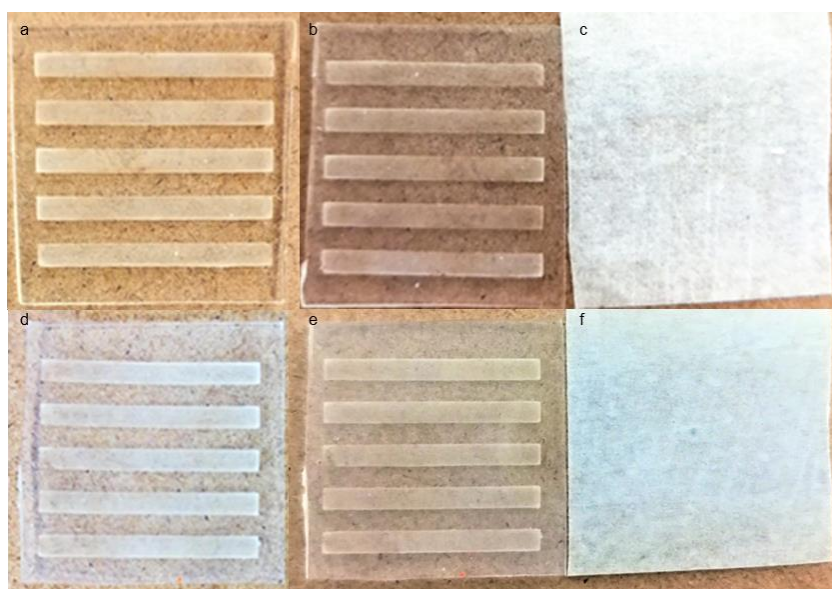
Figure S2.3. *Photographs of AgNW/OA coatings on PDMS substrate (a) before and (b) after 10 peel-off tests. (c) Optical micrograph of the tape after 10 peel-off tests of AgNW/OA coating on PDMS substrate. Photographs of AgNW/CF coatings on PDMS substrate (d) before and (e) after 10 peel-off tests. (f) Optical micrograph of the tape after 10 peel-off tests of AgNW/CF coating on PDMS substrate.*
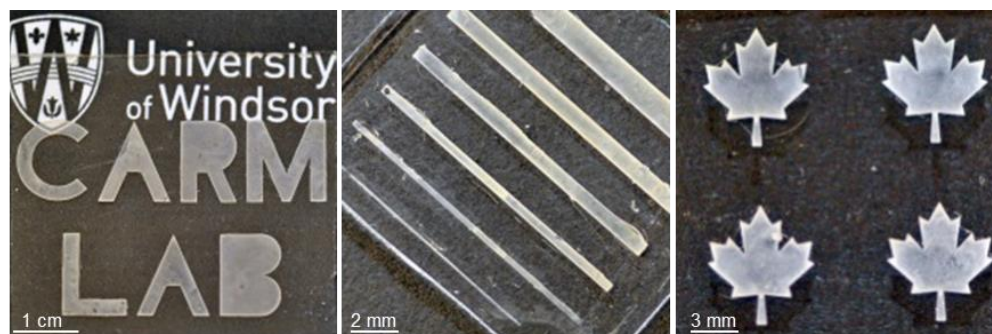
Figure S2.4. Photographs of patterned AgNW/CF coatings on PDMS substrates.
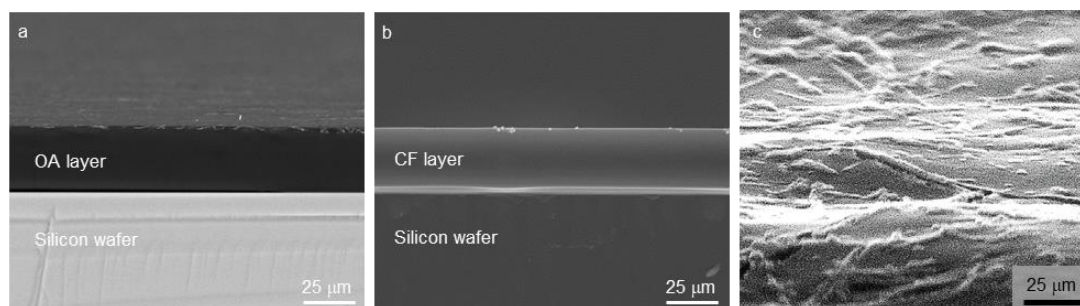
Figure S2.5. Cross-sectional SEM image of a freeze-fractured (a) AgNW/OA and (b) AgNW/CF coating on silicon wafer fabricated using a 2 mg/mL AgNW dispersion. (c) SEM image of the AgNW/CF coating surface on silicon wafer.
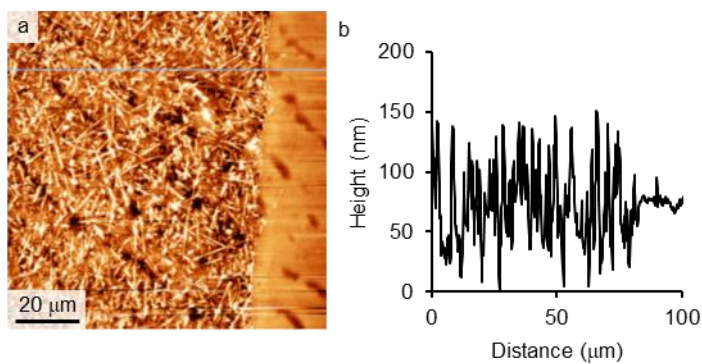
Figure S2.6. *(a) AFM height image with R_{RMS} measurement and (b) corresponding profile measurement of the edge of a 2 mm x 20 mm patterned AgNW/OA line on PDMS substrate over a scanning area of 100 μm x 100 μm (z scale = 150 nm). The concentration of the AgNW dispersion used was 2 mg/mL.*

Table S2.1. *Electrical and optical properties of patterned AgNW/OA and AgNW/CF lines on PDMS substrate.*

Concentration of AgNW dispersion (mg/mL)	%T (at 550 nm)		R_s (Ω/sq)	
	AgNW/OA	AgNW/CF	AgNW/OA	AgNW/CF
1	86	85	15.4 ± 3.6	15.3 ± 2.3
2	75	76	6.2 ± 1.6	6.4 ± 1.4
4	62	60	2.9 ± 0.7	3.0 ± 0.6

73
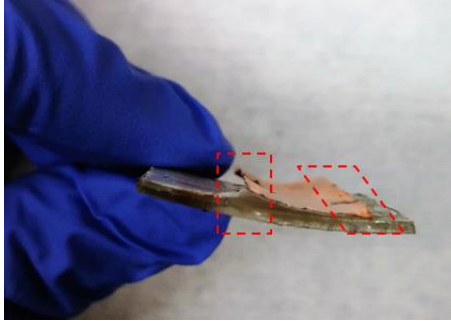
Figure S2.7. Delaminated copper tape (in the red frame) from the emissive layer of a flexible ACEL device after 60 cycles of 20% bending strain.

3. Chapter 3

Stretchable and Durable AgNW Composites on Transparent Butyl

Rubber

3.1. Introduction:

Stretchable optoelectronics that remain functional with mechanical deformation create opportunities to seamlessly integrate electronics with human beings in fields spanning solar cells, touch screens, displays, photodetectors, and biomedical light therapies.[1] Transparent conductive electrodes (TCEs) possessing high optical transparency, high electrical conductivity, and mechanical stretchability are essential components of these optoelectronics. The research community has spent extensive effort to develop new stretchable TCEs using thin metal films,[2-3] metallic grids,[4-5] carbon nanotubes,[6-8] graphene,[9-10] conductive polymers,[11-12] and metallic nanowires.[13-14] Among these materials, silver nanowires (AgNWs) are promising because of their easily adjustable transparency, intrinsically high conductivity, and solution-based deposition methods.[1,15] Interconnected AgNWs form a conductive percolation network through AgNW-AgNW junctions with openings between AgNWs that allow light to pass through and create an optically transparent film. AgNWs slide with stretching, leading to the macroscale elongation of the AgNW network.[16-17] The main strategy to impart stretchability to AgNW-based TCEs relies on the elastomer poly(dimethylsiloxane) (PDMS) as a stretchable platform for the AgNW network. Embedding AgNWs within a elastomeric matrix such as polyacrylate,[20] polyurethane,[21] or poly(urethane acrylate)[18, 22-27] fills in the voids in the AgNW network, smoothing the surface and adhering to the AgNW network to generate AgNW/polymer coating that is then transferred to the PDMS platform. The strong adhesion between AgNW network and the polymer matrix constrains the slide of AgNW between each other and the disconnection between

AgNWs.[16,19,23] Stretching AgNW/polymer coatings causes the AgNWs to reorient along the stretching direction, narrowing the space between them.[22]

Although the high elasticity and transparency of PDMS make it a standard substrate for the fabrication of stretchable AgNW films, its high gas permeability[28,29] limits the practical applications of AgNW/PDMS composites. Air readily permeates through the PDMS substrate to oxidize and sulfurize AgNWs, forming silver oxide and silver sulfide nanocrystals on the surface. Water vapor accelerates the degradation rate.[30-33] These degradation products damage the conductive pathways and eventually increase the sheet resistance (R_s) of the AgNW network, leading to electrical failure of the AgNW network and eventually the failure of AgNW-based electronics.[34] Therefore, it is important to protect AgNW films from these deleterious environmental factors to improve the stability and extend the life span of electronic devices made from AgNWs. One solution has been to coat individual AgNWs with a film of photoresist,[34] metals such as nickel[35,36] or gold,[31] or metal oxide[37] and use the resulting core-shell structures to form the transparent and conductive network. However, this method can increase the contact resistance between nanowires and introduce less conductive impurities, leading to a higher R_s.[34] The additional processing to coat individual AgNWs before transferring to the target substrate also increases the complexity of the fabrication. A second method encapsulates the entire AgNW network with a barrier material such as graphene,[38-40] a polymer blend such as poly(dopamine)-alginic acid[41] and polyethoxysiloxane,[42] or a hybrid of graphene and a polymer such as polycarbonate and polyvinyl alcohol.[43] Although these coatings successfully protect AgNWs from air and humidity, the

stretchability of these films has not been studied. Additionally, for both methods, the additional coating layer can reduce the optical transmittance of the film.[35,41,43]

Our approach to protect AgNW transparent and conductive networks replaces the PDMS substrate with a new elastomer, transparent butyl rubber, which exhibits a low gas permeability. Butyl rubber (poly (isobutylene-co-isoprene), IIR) is a well-known elastomer used in applications requiring low gas permeability, although IIR typically used in industrial applications is not optically transparent. We previously developed transparent butyl rubber (T-IIR) with an optical transmittance of 75% and oxygen permeation rate of 216 ± 3 cc-mm/m^2-day, and showed that this material is an effective gas barrier layer to protect sensitive optoelectronic materials and devices such as mixed-halide perovskite films and light-emitting electrochemical cells.[29] As part of this study, we showed that laminating a membrane of T-IIR as an encapsulant over an AgNW network deposited on a glass substrate protects the AgNWs from corrosion due to exposure to nitric acid vapor for 24 h. In contrast, using PDMS as the encapsulant resulted in corrosion of the AgNWs and destruction of the conductive network. The low gas permeability combined with the elasticity of T-IIR makes it not only an effective encapsulant to protect AgNW network on rigid substrate, but also an ideal platform for durable and stretchable AgNW network fabrication. Here, we describe the fabrication of a stretchable TCE coating by adhering a transparent and stretchable AgNW and polyurethane composite to a T-IIR elastomeric substrate. The resulting transparent composites remain conductive up to 110% strain. We further used several extreme conditions to accelerate the degradation of AgNW films – exposure to humidified air, storage underwater, and exposure to corrosive acid vapor – and compared the integrity of

the stretchable AgNW network encapsulated in T-IIR with that of a control system fabricated using a PDMS platform. T-IIR encapsulated AgNW composites retain their electrical and mechanical functionality, making them ideal to act as long-term stable TCEs.

3.2. Results and Discussion

3.2.1. Fabrication of stretchable AgNW/CF coatings

Our group has previously developed a simple method to fabricate flexible and transparent AgNW coatings composed of an annealed AgNW network embedded in a flexible polyurethane adhesive, and applied these coatings to various substrates such as glass, polyethylene terephthalate, and PDMS.[44] To fabricate stretchable AgNW coatings, we used a similar method, replacing the flexible polyurethane adhesive with the optically clear polyurethane rubber Clear Flex 50 (CF), which has a low Young's modulus of 2.47 MPa. The low Young's modulus of CF, T-IIR (0.41 MPa) and PDMS (2.05 MPa) makes each material suitable for the fabrication of stretchable TCEs. We produced stretchable AgNW/CF coatings on T-IIR and PDMS substrates according to Scheme 3.1. We first fabricated a PDMS carrier substrate for the formation of the AgNW network by exposing a native PDMS surface to air plasma for 40 s, which creates a silicate layer[45] that enables the AgNW dispersion in ethanol (0.5 mg/mL, 0.7 mg/mL, 1.0 mg/mL, and 2.0 mg/mL) to spread on the surface. After drop casting the AgNW dispersion (48 μL/cm^2) and drying in air, we annealed the AgNW films at 200 °C for 20 min to fuse the AgNWs at their intersection points.[44] We then reduced the surface free energy of the PDMS carrier substrate to enable release of the AgNW network by allowing the PDMS to undergo

hydrophobic recovery in ambient conditions overnight. Hydrophobic recovery of PDMS is a spontaneous process in which low molecular weight residues in the bulk PDMS diffuse to the surface to lower the surface free energy and restore the hydrophobicity of the PDMS surface.[46,47] We then deposited a drop (5 µL/cm^2) of CF onto the surface of the AgNW film on the PDMS carrier, and placed the target substrate on top. Target substrates were T-IIR or PDMS substrates exposed to oxygen or air plasma to allow the CF adhesive to wet and bind to the surface.[48] After curing the CF, the PDMS carrier easily peels away to leave AgNW/CF coating strongly adhered to the target substrate (Figure S3.1 in the supporting information). The abbreviations designated to the AgNW/CF coatings on these two substrates are T-IIR/[AgNW]$_n$ and PDMS/[AgNW]$_n$, respectively, where n represents the concentration of the AgNW dispersion (0.5, 0.7, 1.0, and 2.0 mg/mL) used to fabricate these coatings.

PDMS carrier

1. Plasma treatment
2. Drop cast AgNW solution

1. Anneal AgNW films and leave for 24 h
2. Apply polyurethane CF

1. Apply target substrate, PDMS or T-IIR
2. Cure CF

1. Remove PDMS carrier
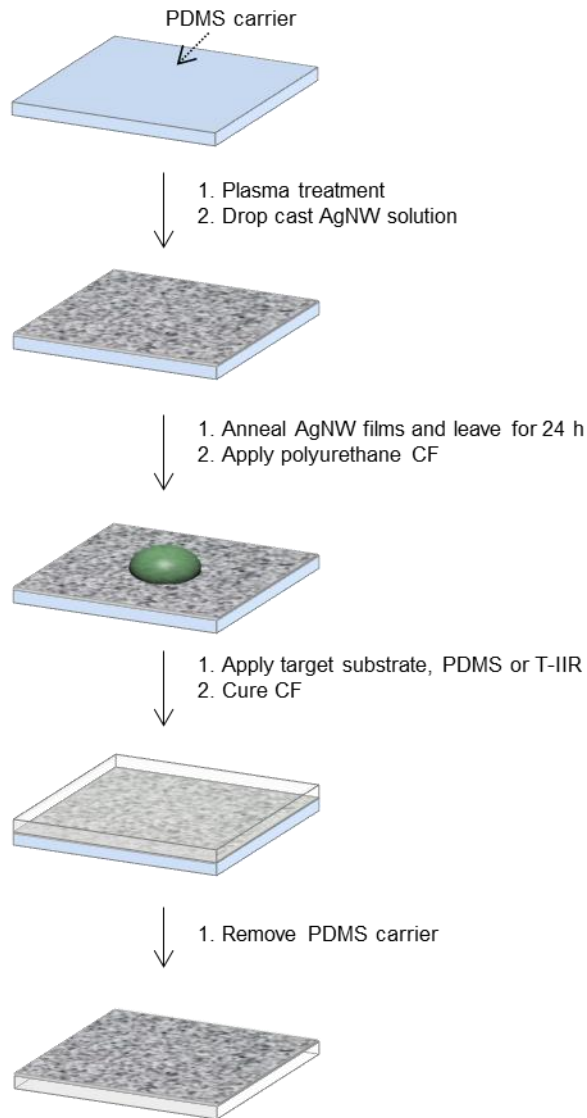
Scheme 3.1. *Process used to fabricate AgNW/CF coatings on T-IIR or PDMS substrate.*

3.2.2. Surface Morphology of T-IIR/[AgNW]$_n$ and PDMS/[AgNW]$_n$ Composites

Scanning electron microscopy (SEM) images of T-IIR/[AgNW]$_n$ and PDMS/[AgNW]$_n$ composites reveal that AgNWs are uniformly distributed on the surface, forming a network structure (Figure 3.1a-d and S3.2a-d). As the concentration of the

AgNW dispersion increases, the density of AgNWs in the CF film also increases. Circular particles with sizes ranging from 100 to 300 nm, and triangular particles with sizes ranging from 0.75 to 2.24 µm, were present in all AgNW films. These particles likely arise from storing AgNWs in ambient conditions, which causes the migration of Ag atoms from AgNWs to form silver particles.[30,33,36] Cross-sectional SEM images of a AgNW/CF coating (1 mg/mL) on a silicon wafer (Figure S3.3a, b) shows that the AgNW network resides at the surface of a ~30-µm-thick film of CF adhered to the underlying substrate.
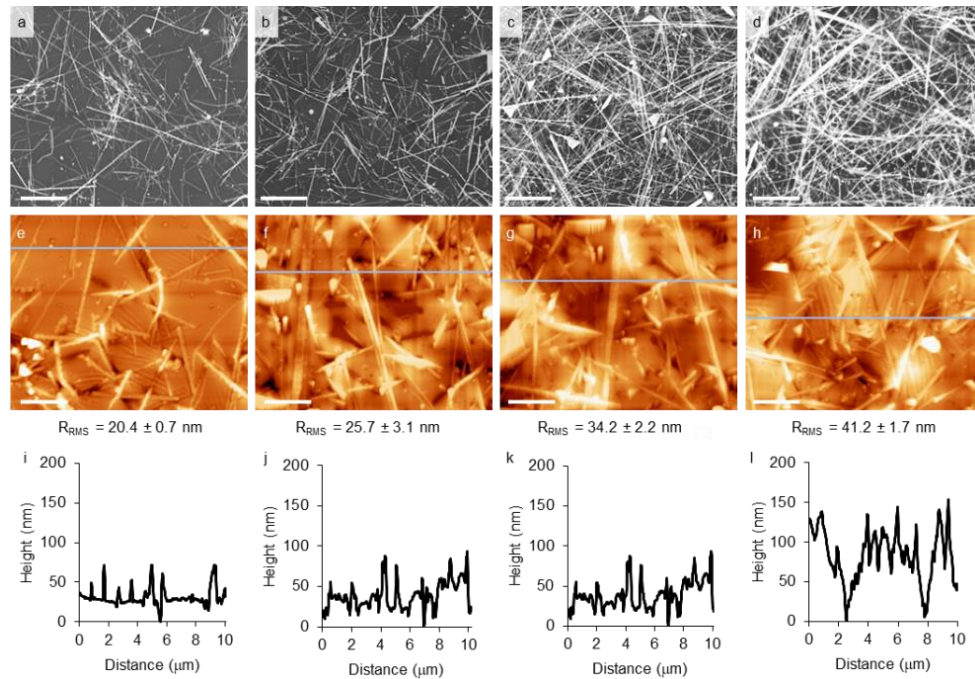
Figure 3.1. *Top view SEM images (scale = 5 µm) of (a) T-IIR/[AgNW]$_{0.5}$, (b) T-IIR/[AgNW]$_{0.7}$, (c) T-IIR/[AgNW]$_{1.0}$, and (d) T-IIR/[AgNW]$_{2.0}$ composites. AFM height images (scale = 2 µm, z-scale = 250 nm) with R$_{RMS}$ measurements and corresponding profile measurements of (e, i) T-IIR/[AgNW]$_{0.5}$, (f, j) T-IIR/[AgNW]$_{0.7}$, (g, k) T-IIR/[AgNW]$_{1.0}$, and (h, l) T-IIR/[AgNW]$_{2.0}$ composites.*

Atomic force microscopy (AFM) reveals that T-IIR/[AgNW]$_n$ and PDMS/[AgNW]$_n$ composites prepared with the same AgNW dispersion concentration exhibit similar root-mean-square roughness (R$_{RMS}$) values, indicating that surface roughness is a property of the coating and is independent of the substrate (Table S3.1). For both substrates, increasing the concentration of the AgNW dispersion to form the network increases the density of AgNWs in the film, and consequently R$_{RMS}$ values (Figure 3.1e-h and S3.2e-h). For example, the R$_{RMS}$ values of T-IIR/[AgNW]$_{2.0}$ and PDMS/[AgNW]$_{2.0}$ composites (42.2 ± 1.7 and 38.4 ± 1.1 nm, respectively) are ~2 times higher than that of T-IIR/[AgNW]$_{0.5}$ and PDMS/[AgNW]$_{0.5}$ composites (20.4 ± 0.7 and 17.2 ± 1.6 nm, respectively). AFM profile measurements indicate that peak-to-valley distances also increase as the concentration of AgNW dispersion increases (Figure 3.1i-l and S3.2i-l). The peak-to-valley distance values for T-IIR/[AgNW]$_{0.5}$ and PDMS/[AgNW]$_{0.5}$ composites are 79.2 ± 4.6 and 76.7 ± 1.7 nm, one order of magnitude lower than for T-IIR/[AgNW]$_{2.0}$ and PDMS/[AgNW]$_{2.0}$ composites (156.3 ± 4.5 and 143.7 ± 11.7 nm). Overall, however, embedding the AgNW networks in CF polymer decreases the surface roughness compared to AgNW networks without polymer matrix. The R$_{RMS}$ of both T-IIR/[AgNW]$_{2.0}$ and PDMS/[AgNW]$_{2.0}$ composites are ~2.4 x lower than the R$_{RMS}$ of AgNW films fabricated without the polymer matrix by drop casting the same dispersion concentration (2.0 mg/mL) on a silicon wafer substrate (R$_{RMS}$ = 94.1 ± 6.7 nm) (Figure S3.4a, b).

3.2.3. Electrical and Transmittance Properties of T-IIR/[AgNW]$_n$ and PDMS/[AgNW]$_n$ Composites

Varying the concentration of the AgNW dispersion used to prepare T-IIR/[AgNW]$_n$ and PDMS/[AgNW]$_n$ composites provides AgNW networks with different R_s values and transparencies (Figure 3.2 and Table 3.1). We collected transmittance spectra and measured the corresponding R_s of T-IIR/[AgNW]$_n$ and PDMS/[AgNW]$_n$ composites with a size of 2 cm x 2 cm. AgNWs exhibit a signature absorbance peak at 365 nm due to the surface plasma resonance;[29,49] however, this peak is obscured in both T-IIR/[AgNW]$_n$ and PDMS/[AgNW]$_n$ composites due to the absorbance of the CF coating in the range of 300-400 nm (Figure S3.5). Increasing the concentration of the AgNW dispersion produces films with a high density of AgNW conductive paths, resulting in lower R_s; at the same time, the high AgNW density results in a lower transparency (Figure 3.2). T-IIR/[AgNW]$_n$ and PDMS/[AgNW]$_n$ composites prepared from the same AgNW dispersion concentration exhibit similar R_s values, indicating that the electrical pathways formed by the AgNW/CF coating are independent of the choice of substrate. However, T-IIR/[AgNW]$_n$ composites are less transparent than PDMS/[AgNW]$_n$ composites due to the intrinsically lower transparency of the T-IIR substrate: At 550 nm, the % transmittance (%T) is 91% for PDMS and 69% for T-IIR.
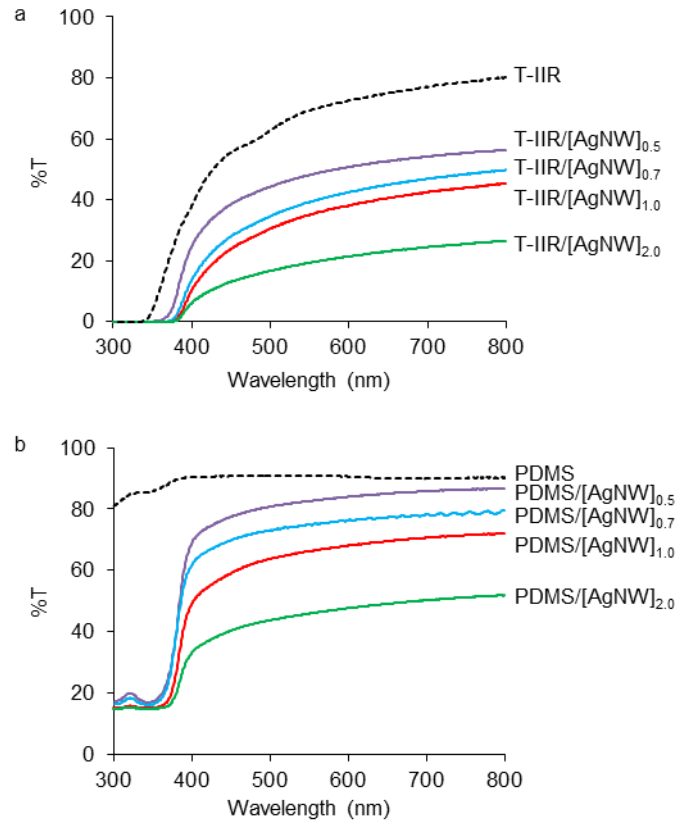
Figure 3.2. Transmittance spectra of (a) T-IIR/[AgNW]$_n$ and (b) PDMS/[AgNW]$_n$ composites. Dotted line represents the transmittance spectrum of (a) T-IIR substrate and (b) PDMS substrate.

Table 3.1. Summary of electrical and optical properties of T-IIR/[AgNW]$_n$ and PDMS/[AgNW]$_n$ composites.

Concentration (n) (mg/mL)	% T (at 550 nm)		R$_s$ (Ω/sq)	
	T-IIR/[AgNW]$_n$	PDMS/[AgNW]$_n$	T-IIR/[AgNW]$_n$	PDMS/[AgNW]$_n$
0.5	48.2	82.4	20 ± 2.2	16.2 ± 3.6
0.7	39.3	74.7	6.2 ± 0.9	7.8 ± 1.7
1.0	36.3	66.0	4.2 ± 1.0	4.4 ± 0.6
2.0	19.3	45.6	2.0 ± 0.4	1.6 ± 0.3

3.2.4. Stretchability of T-IIR/[AgNW]$_n$ and PDMS/[AgNW]$_n$ Composites

Both T-IIR/[AgNW]$_n$ and PDMS/[AgNW]$_n$ composites remain conductive with stretching. We stretched 2.5 cm x 1.0 cm T-IIR/[AgNW]$_n$ and PDMS/[AgNW]$_n$ composites using a micro-vice system and measured the resistance at 5% strain intervals until the films were no longer conductive. The resistance as a function of elongation is plotted in Figure 3.3. In general, the resistances of T-IIR/[AgNW]$_n$ and PDMS/[AgNW]$_n$ composites increase with stretching, which can be attributed to the increase in conductive path length as well as the breakage of AgNW-AgNW junctions that interrupt conductive pathways through the network.[21,23,50] Increasing the AgNW dispersion concentration used to form the network from 0.5 mg/mL to 2.0 mg/mL enables the AgNW networks of both T-IIR/[AgNW]$_n$ and PDMS/[AgNW]$_n$ composites to remain conductive to higher elongations. Increasing the dispersion concentration increases the density of AgNWs in the coating, thus providing an increased number of conductive pathways through the network via AgNW-AgNW junctions.[51] Damage to the network and/or AgNW-AgNW junctions with elongation increases the resistance, but enough AgNW-AgNW junctions remain connected to maintain conductivity to higher elongations. For example, T-IIR/[AgNW]$_{0.5}$ and PDMS/[AgNW]$_{0.5}$ composites remain conductive to 40% elongation, while T-IIR/[AgNW]$_{2.0}$ and PDMS/[AgNW]$_{2.0}$ composites remain conductive up to 95% and 110% elongation, respectively.
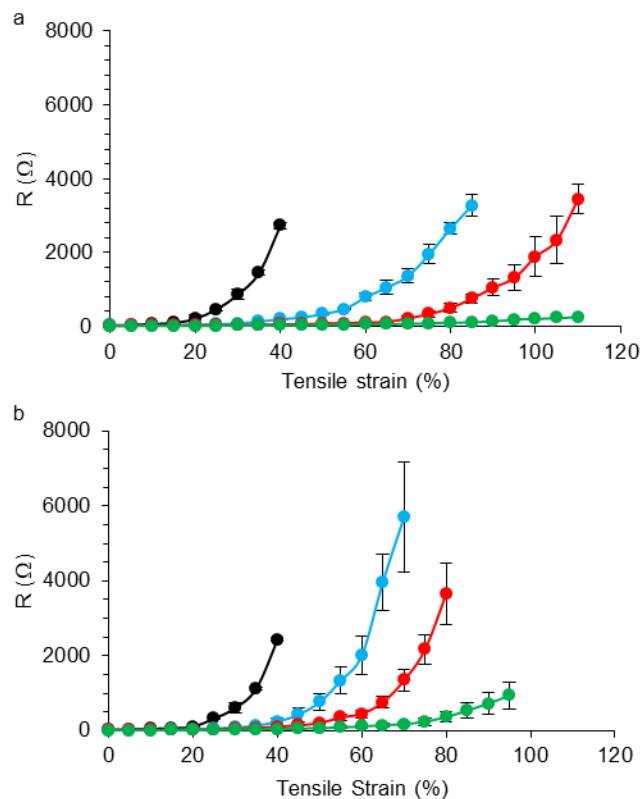
Figure 3.3. *Resistance as a function of tensile strain of (a) T-IIR/[AgNW]$_n$ and (b) PDMS/[AgNW]$_n$ composites, where n = 0.5 mg/mL (black lines), 0.7 mg/mL (blue lines), 1.0 mg/mL (red lines), and 2.0 mg/mL (green lines).*

For AgNW networks formed using AgNW dispersions of 0.7, 1.0, and 2.0 mg/mL, T-IIR/[AgNW]$_n$ composites exhibit a smaller change in resistance with stretching compared to PDMS/[AgNW]$_n$ composites. The resistance of T-IIR/[AgNW]$_{0.7}$, T-IIR/[AgNW]$_{1.0}$, and T-IIR/[AgNW]$_{2.0}$ composites remains < 50 Ω to 25%, 35%, and 55% strain, respectively. In contrast, the resistance of PDMS/[AgNW]$_{0.7}$, PDMS/[AgNW]$_{1.0}$, and PDMS/[AgNW]$_{2.0}$ composites remains < 50 Ω to lower elongations (20%, 25%, and 40% strain, respectively). Further elongation leads to a lower resistance increase of T-IIR/[AgNW]$_n$ composites than PDMS/[AgNW]$_n$

composites. At 70% elongation, the resistance of T-IIR/[AgNW]$_{0.7}$, T-IIR/[AgNW]$_{1.0}$, and T-IIR/[AgNW]$_{2.0}$ composites (R = 1356.7 ± 186.1 Ω, 215.4 ± 50.6 Ω, 62.4 ± 2.5 Ω, respectively) is 4x, 6x and 3x lower than that of the PDMS/[AgNW]$_{0.7}$, PDMS/[AgNW]$_{1.0}$, and PDMS/[AgNW]$_{2.0}$ composites (5699.8 ± 751.3 Ω, 1345.0 ± 285.7 Ω, and 176.1 ± 58.7 Ω, respectively). T-IIR/[AgNW]$_{0.7}$, T-IIR/[AgNW]$_{1.0}$, and T-IIR/[AgNW]$_{2.0}$ composites also remain conductive to higher strains (85%, 110% and 110%, respectively) than PDMS/[AgNW]$_{0.7}$, PDMS/[AgNW]$_{1.0}$, and PDMS/[AgNW]$_{2.0}$ composites (70%, 80%, and 95% strain, respectively).

The difference in resistance with stretching between T-IIR/[AgNW]$_n$ and PDMS/[AgNW]$_n$ composites may be attributed to differences in adhesion between the CF coating and the elastomeric substrate. It has been previously reported that exposure of the T-IIR substrate to oxygen plasma for 15 min results in the formation of -COOH, -OH, and ketone groups on the surface in low density.[48] In contrast, plasma oxidation of PDMS is known to produce a uniform layer of Si-OH groups on the surface. These oxidized elastomer surfaces exhibit different bonding and adhesion to the CF elastomer. We fabricated T-IIR/CF and PDMS/CF composites without the AgNW network to permit imaging of the elastomer-CF interfaces under strain. Optical micrographs of the T-IIR/CF interface at 0% strain are featureless, but upon elongation to 10% strain web-like features appear and persist to high elongations (70%) (Figure S3.6a-c). We attribute these features to small, localized delaminations of the CF from the T-IIR substrate, consistent with the low density of oxidized functional groups on this surface. Further elongation to 115% strain results in delamination of the CF layer from the T-IIR substrate. Images of the PDMS/CF interface did not show these features (Figure S3.6d-

f); instead, these two layers deform together without delamination, ultimately fracturing into two pieces at 106% strain. We propose that the differences in adhesion between the CF layer and substrate change the effect of applied stress on the embedded AgNW networks. In T-IIR/$[AgNW]_n$ composites, the small delaminations over the interface absorb the strain energy and permit localized out-of-plane deformations of the CF/AgNW layer, which enables the preservation of the percolation network.[53-55] These out-of-plane deformations are similar to the stretching mechanism reported for tortuous metal wires and meshes deposited on elastomeric substrates. Out-of-plane deformations have been shown to protect these metal-on-elastomer structures from damage due to stretching, unless separation of the metal from the elastomer occurs, which forms free-standing metal films that fracture easily. In our T-IIR/$[AgNW]_n$ composites, the AgNWs are embedded in and adhered to the CF matrix, preventing the formation of free-standing AgNWs; thus, the small delaminations between the CF layer and T-IIR substrate are beneficial. In contrast, the strong adhesion between oxidized PDMS and CF constrains out-of-plane deformation, compelling the AgNW/CF layer to elongate along with the PDMS substrate. Absorption of the strain energy by the AgNW network, along with the inability of the network to deform out of plane, results in damage and loss of conductivity.

3.2.5. T-IIR as a Gas-Diffusion Barrier for AgNW/CF Coatings

We chose T-IIR/$[AgNW]_{1.0}$ and PDMS/$[AgNW]_{1.0}$ composites to compare the efficacies of T-IIR and PDMS as protective gas-diffusion barriers. We prepared T-IIR/$[AgNW]_{1.0}$ and PDMS/$[AgNW]_{1.0}$ composites, laminated a 1-mm-thick T-IIR membrane over the surface of T-IIR/$[AgNW]_{1.0}$ composites followed by sealing the

edges using a waterproof butyl sealant to produce T-IIR/[AgNW]$_{1.0}$/T-IIR structures, as well as adhered a 1-mm-thick PDMS membrane over the surface of PDMS/[AgNW]$_{1.0}$ composites followed by sealing the edges using a waterproof silicone sealant to produce PDMS/[AgNW]$_{1.0}$/PDMS structures. We then exposed the resulting composite structures to three different environments: (1) 45 °C/ 95% relative humidity (RH) for 30 days, (2) underwater for 7 days, and (3) nitric acid vapor for 24 h. After these experiments, we peeled away the top laminated layer (T-IIR or PDMS) for examination and testing.

T-IIR protected the AgNW network of T-IIR/[AgNW]$_{1.0}$ composites in all three environments. There is a negligible change in morphology and structure for the well-protected AgNW networks of T-IIR/[AgNW]$_{1.0}$ composites, with no indication of the growth of new nanoparticles on the AgNW surface or drastic changes to the AgNW network (Figure 3.4a-c). In contrast, the morphology of PDMS/[AgNW]$_{1.0}$ composites changed significantly after exposure to all three environments. In addition to the large particles that were present before exposure, the SEM images in Figure 3.4d and e reveal that both humidity and immersion in water result in the formation of nanoparticles on the surface of the AgNWs, which is likely silver sulfide (Ag$_2$S) and silver oxide (Ag$_2$O) nanoparticles formed by corrosion of AgNWs by ambient sulfur-containing gases such as sulfur dioxide and carbonyl sulfide as well as water.[56] SEM images of PDMS/[AgNW]$_{1.0}$ composites exposed to the humid environment furthermore show shortening of the AgNWs, consistent with the AgNWs being broken into short rods after storing in the humidified environment for one month (Figure 3.4d).[33] Figure 3.4f shows that the permeation of nitric acid vapor through the PDMS encapsulant etches the AgNWs, destroying the structure of the network.
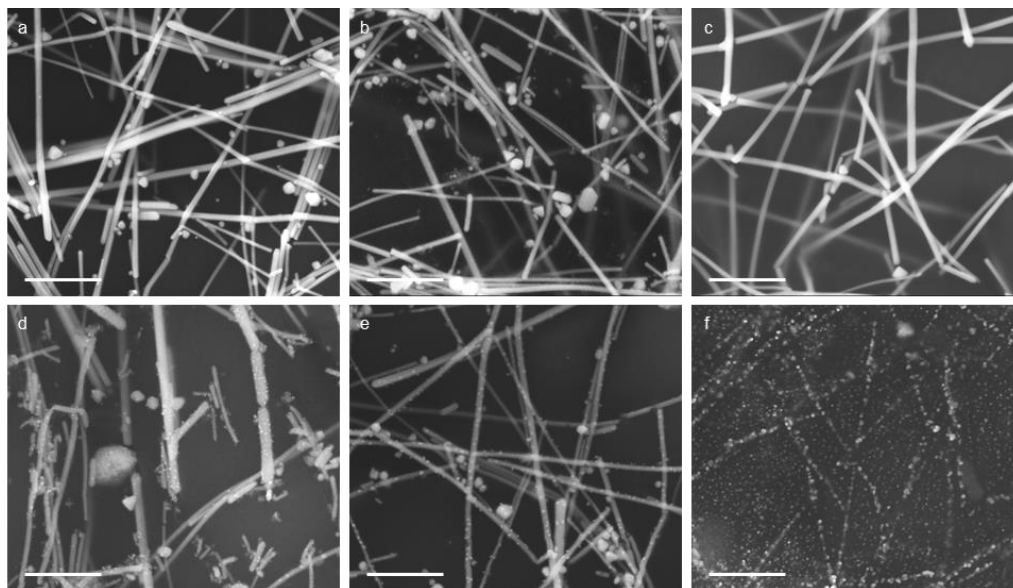
Figure 3.4. *SEM images (scale = 1 μm) of T-IIR/[AgNW]$_{1.0}$ composites after (a) exposure to 45 °C/ 95% RH for 30 days, (b) immersed in water for 7 days, and (c) exposure to nitric acid vapor for 24 hours. SEM images of PDMS/[AgNW]$_{1.0}$ composites after (d) exposure to 45 °C/ 95% RH for 30 days, (e) immersed in water for 7 days, and (f) exposure to nitric acid vapor for 24 hours.*

The optical transmittance and electrical conductivity of T-IIR/[AgNW]$_{1.0}$ composites negligibly changed after exposure to all three environments, consistent with the superior gas barrier properties of T-IIR that protect and preserve the AgNW network (Table 3.2, Figure S3.7). However, the changes to the morphology of the AgNW network of PDMS/[AgNW]$_{1.0}$ composites caused by the environmental stress strongly affect the %T and R_s values. The %T of PDMS/[AgNW]$_{1.0}$ composites decreased after exposure to humidity or immersion in water due to the scattering of light by the particles formed on the surfaces of the AgNWs or by the formation of discontinuous AgNW structures.[53] The changes to the AgNW network caused by humidity and underwater exposure increased the R_s of PDMS/[AgNW]$_{1.0}$ composites to 3.2x and 21.4x the initial value. Changes due to nitric acid vapor permeation through PDMS were more dramatic: The destruction of

91

the AgNW network resulted in an increase in %T at 550 nm from 66% to 92%, accompanied by a loss of conductivity.

Table 3.2. *Summary of electrical and optical properties of T-IIR/[AgNW]$_{1.0}$ and PDMS/[AgNW]$_{1.0}$ composites before and after exposure to deleterious environments.*

	% T (at 550 nm)		R$_s$ (Ω/sq)	
	T-IIR/[AgNW]$_{1.0}$	PDMS/[AgNW]$_{1.0}$	T-IIR/[AgNW]$_{1.0}$	PDMS/[AgNW]$_{1.0}$
Before	35.6	66.2	4.1 ± 1.3	4.5 ± 0.6
Environment 1: 45 °C/ 95% RH for 30 days	35.9	35.9	5.0± 0.3	107.1± 9.0
Environment 2: underwater for 7 days	33.8	39.4	5.1± 1.0	15.5 ± 3.1
Environment 3: nitric acid vapor for 24 h	34.9	92.2	5.6 ± 1.2	Not conductive

We further assessed how the environmental stresses of humidity exposure and underwater storage affected the ability of T-IIR/[AgNW]$_{1.0}$ and PDMS/[AgNW]$_{1.0}$ composites to retain conductivity with stretching. After exposure, we measured the resistance at 5% strain intervals until the composites were no longer conductive and plotted the resistance as a function of strain in Figure 3.5. We compared these results to T-IIR/[AgNW]$_{1.0}$ and PDMS/[AgNW]$_{1.0}$ control composites that had not been exposed., also plotted in Figure 3.5. Compared to T-IIR/[AgNW]$_{1.0}$ composites, the environmental stress affects the resistance with stretching of PDMS[AgNW]$_{1.0}$ composites more appreciably. Resistance changes with stretching of T-IIR/[AgNW]$_{1.0}$ composites exposed to humidity and stored underwater remained similar to control T-IIR/[AgNW]$_{1.0}$ composites to 95% strain, after which the resistance of humidity-exposed composites slightly increased (Figure 3.5a). In contrast, humidity exposure caused the resistance of PDMS/[AgNW]$_{1.0}$ composites to increase abruptly from 372 ± 116 Ω to 16902 ± 6153 Ω

when stretched from 0% to 40% strain, 161x higher than the control. The elongation at electrical failure of the humidity-exposed composites occurred at 40% lower strain than that of the control PDMS/[AgNW]$_{1.0}$ composite. Underwater storage also caused the resistance of PDMS/[AgNW]$_{1.0}$ composite to increase rapidly from 29 ± 9 Ω to 9235 ± 2691 Ω at 75% strain, 4.3x higher than control PDMS/[AgNW]$_{1.0}$ composites at this elongation.
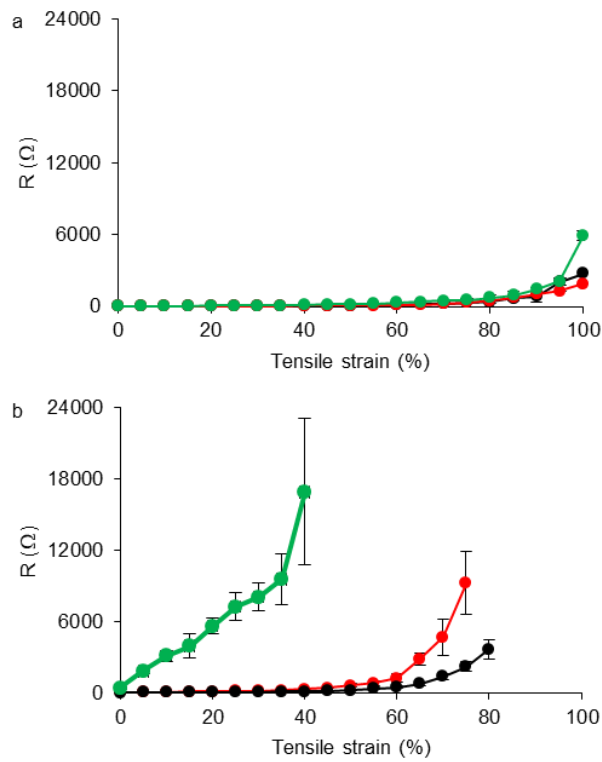
Figure 3.5. *Resistance of (a) T-IIR/[AgNW]$_{1.0}$ and (b) PDMS/[AgNW]$_{1.0}$ composites as a function of tensile strain before (black lines) and after exposure to 45 °C/ 95% RH for 30 days (green lines) and immersion in water for 7 days (red lines).*

3.2.6. Durability of T-IIR/[AgNW]$_{1.0}$ and PDMS/[AgNW]$_{1.0}$ Composites

For wearable light-emitting devices, touch panels, and touch screens, the stretchable TCEs not only need to function under environmental stress, they must also remain operational with repetitive deformations. To test the durability of T-IIR/[AgNW]$_{1.0}$ and PDMS/[AgNW]$_{1.0}$ composites to repetitive strain and environmental stress, we exposed the composites to humidity and stored them underwater, removing them from these environments at 24 and 48 h intervals, respectively, to apply 50 cycles of 15% tensile strain and then measure the electrical resistance. The resistance versus time in days and the number of cycles is plotted in Figure 3.6. After 30 days of exposure to humidity and a total of 750 cycles, and 7 days stored underwater and a total of 350 strain cycles, the resistance of T-IIR/[AgNW]$_{1.0}$/T-IIR structures was negligibly affected. In contrast, the resistance of PDMS/[AgNW]$_{1.0}$/PDMS structures increased by 96x the initial value (from $13.7 \pm 1.6\ \Omega$ to $1308.5 \pm 440.5\ \Omega$) and 3.5x the initial value (from $13.7 \pm 1.4\ \Omega$ to $42 \pm 16.1\ \Omega$).
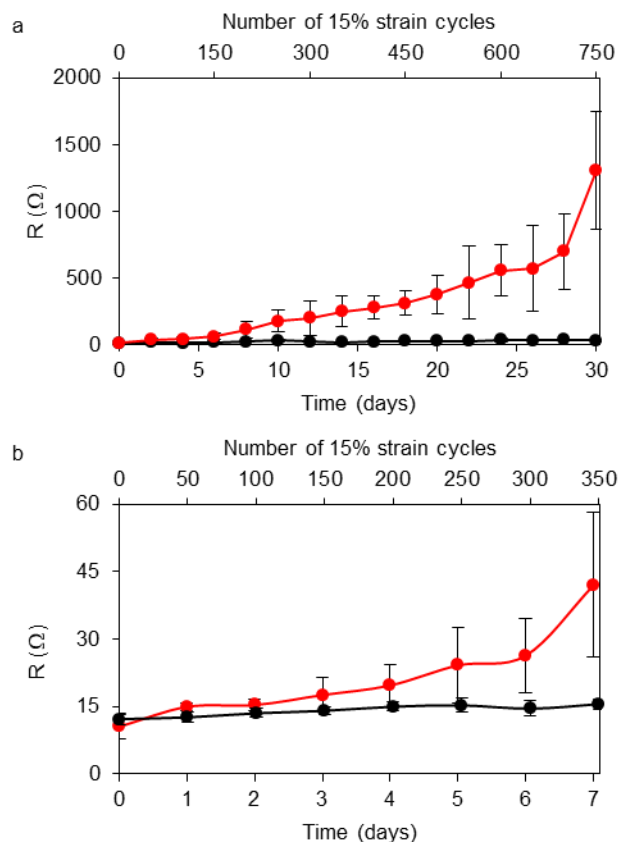
Figure 3.6. *(a) Resistance of T-IIR/[AgNW]$_{1.0}$/T-IIR (black line) and PDMS/[AgNW]$_{1.0}$/PDMS (red line) structures as a function of the time and 15% strain/relaxation cycles after exposure to 45 °C/ 95% RH for 30 days. (b) Resistance of T-IIR/[AgNW]$_{1.0}$/T-IIR/ (black line) and PDMS/[AgNW]$_{1.0}$ /PDMS (red line) structures as a function of the time and 15% strain/relaxation cycles after immersion in water at room temperature for 7 days.*

3.3. Conclusions

We have successfully fabricated AgNW/CF coatings on T-IIR substrates that not only possess optical transparency, electrical conductivity, and mechanical stretchability in ambient conditions but also remain so under environmental stress due to the excellent gas barrier properties of the T-IIR substrate. In contrast, the facile permeation of humidified air, water, and corrosive nitric acid vapor through the PDMS substrate of

PDMS/$[AgNW]_n$ composites causes significant changes to the resistance, transmittance, and stretchability of these composites. Future use of these new T-IIR/$[AgNW]_n$ composites as stretchable, TCEs will open up new applications in robust and reliable stretchable optoelectronics. Furthermore, the fascinating differences in the resistance changes with stretching of AgNW/CF layers on T-IIR and PDMS attributed to differences in interfacial adhesion motivate future studies to further study this effect experimentally and through modelling. Adjusting interfacial adhesion in layered composites may provide a way to fine-tune electrical changes with stretching, leading to new methods for the design and fabrication of stretchable electronics.

3.4. Experimental

Materials. PDMS (Sylgard 184) elastomer base and curing agent kits were purchased from Dow Corning (Midland, MI, USA). T-IIR substrates were prepared according to literature.[29] AgNW dispersed in ethanol (20 mg/mL) with an average diameter of 50 nm and an average length of 120 μm was purchased from ACS Material Inc. (Pasadena, CA, USA). CF was purchased from Smooth-On Inc. (Macungie, PA, USA). All the materials were used as received without further purification.

Preparation of oxidized T-IIR substrates. T-IIR sheets (~1 mm thick) were cut into the desired size and sonicated in acetone and isopropanol for 10 min each followed by drying in a stream of nitrogen. They were then exposed to oxygen plasma for 15 min in a Harrick plasma cleaner at O_2 pressure of 10 psig and flow rate of 10.6 mL/min at medium discharge setting to generate an oxidized surface.

Preparation of oxidized PDMS substrates. PDMS pre-polymer base was mixed with the curing agent in a weight ratio of 10:1. The liquid mixture was cast against smooth polystyrene Petri dishes and cured in an oven at 60°C overnight. Cured PDMS films were cut to the desired size of films and exposed to air plasma for 40 s in a Harrick plasma cleaner at air pressure of 10 psig and flow rate of 32 mL/min at medium discharge setting to generate an oxidized surface.

Fabrication of T-IIR/[AgNW]$_n$ and PDMS/[AgNW]$_n$. AgNW dispersion was diluted in anhydrous ethanol to 0.5 mg/mL, 0.7 mg/mL, 1 mg/mL, and 2 mg/mL and ultrasonicated for 1 min before use to reduce aggregation. 48 μL/cm^2 diluted AgNW dispersion was then drop-cast onto the oxidized PDMS carrier. The samples were allowed to dry on a KS 130 basic (IKA) shaker at 160 rpm at room temperature. After drying, AgNW films on PDMS carriers were annealed at 200 $^{\circ}$C for 20 min on a hot plate to fuse the AgNWs and then set aside for 24 h to undergo hydrophobic recovery. A drop (5 μL/cm^2 of AgNW film) of CF Part A mixed with Part B in a weight ratio of 1:2 was then placed onto the surface of the AgNW film. The oxidized target substrate (T-IIR or PDMS) was then placed facing down onto the AgNW film. The CF was allowed to spread for 1 min and then was cured in an oven at 60 $^{\circ}$C for 16 h. The PDMS carrier was then removed to obtain the T-IIR/[AgNW]$_n$ and PDMS/[AgNW]$_n$ composites.

Stability tests. Copper tape was adhered at the edge of AgNW/CF coatings to act as the contact for the measurement of resistance. A T-IIR barrier was adhered on top of T-IIR/[AgNW]$_n$ composites and sealed using a waterproof Butyl sealant (Tremco, USA) to create a T-IIR/T-IIR/[AgNW]$_n$ structure. A PDMS barrier was adhered on top of

PDMS/[AgNW]$_n$ composites and sealed using a waterproof Silicone I White Silicone (GE, USA) to create a PDMS/PDMS/[AgNW]$_n$ structure.

Environment 1, underwater test: The T-IIR/T-IIR/[AgNW]$_n$ and PDMS/PDMS/[AgNW]$_n$ structures were immersed in water in a glass jar at room temperature for 7 days. Then the protective layer, either T-IIR or PDMS, was carefully removed from the composites. For the durability test, samples were subjected to 50 cycles of 15 % repetitive strain after removing from water at 24 h intervals.

Environment 2, 45 °C/95% RH test: The T-IIR/T-IIR/[AgNW]$_n$ and PDMS/PDMS/[AgNW]$_n$ structures were exposed to 45 °C/ 95% RH in a humidity control chamber (MicroClimate® Benchtop Test Chamber, CSZ, USA). Then the protecting layer, either T-IIR or PDMS, was carefully removed from the composites. For the durability test, samples were subjected to 50 cycles of 15 % repetitive strain after removing from the humidity control chamber at 48 h intervals.

Environment 3, nitric acid test: The T-IIR/T-IIR/[AgNW]$_n$ and PDMS/PDMS/[AgNW]$_n$ structures were placed in a vapor chamber. 10 drops of concentrated nitric acid were added to the chamber, and the samples were exposed to nitric acid vapor for 24 h, removed from the chamber, and the barrier layers were then carefully removed from the samples.

Characterization: Optical microscopy images were taken using an Olympus BX51 microscope equipped with an Olympus Q-Color 3 camera. SEM images were collected with a Quanta 200 FEG Environmental SEM (FEI, USA). AFM images (10 μm × 10 μm) were collected using the tapping mode of a Digital Instruments Multimode

AFM. R_{RMS} values from three different areas of three samples were averaged. Transmission spectra were recorded using a Varian Cary 50 UV-Visible Spectrophotometer. Electrical characterization was conducted using a Keithley 2601A Sourcemeter. EGaIn (~5 μL) was first deposited by syringe to the corners (for R_s measurements) or ends (for resistance measurements) of the AgNW/CF surface to facilitate electrical contact. R_s measurements were carried out using a four-point wire setup. Stretching properties were tested using a microvice stretcher (S.T. Japan, USA, Inc.) in which each end of the T-IIR/[AgNW]$_n$ and PDMS/[AgNW]$_n$ composites was secured, and the resistance was measured at 5% increments of strain. A minimum of three samples was averaged.

3.5. References

(1) McCoul, D.; Hu, W.; Gao, M.; Mehta, V.; Pei, Q. *Adv. Electron. Mater.* **2016**, *2*, 1500407.

(2) Filiatrault, H. L.; Porteous, G. C.; Carmichael, R. S.; Davidson, G. J. E.; Carmichael, T. B. *Adv. Mater.* **2012**, *24*, 2673.

(3) Guo, C. F.; Sun, T. Y.; Liu, Q. H.; Suo, Z. G.; Ren, Z. F. *Nat. Commun.* **2014**, *5*, 3121.

(4) Jang, H. Y.; Lee, S. K.; Cho, S. H.; Ahn, J. H.; Park, S. *Chem. Mater.* **2013**, *25*, 3535.

(5) Park, S. M.; Jang, N. S.; Ha, S. H.; Kim, K. H.; Jeong, D. W.; Kim, J.; Lee, J.; Kim, S. H.; Kim, J. M. *J. Mater. Chem. C* **2015**, *3*, 8241.

(6) Vohra, A.; Imin, P.; Imit, M.; Carmichael, R. S.; Meena, J. S.; Adronov, A.; Carmichael, T. B. *RSC Adv.* **2016**, *6*, 29254.

(7) Lipomi, D. J.; Vosgueritchian, M.; Tee, B. C. K.; Hellstrom, S. L.; Lee, J. A.; Fox, C. H.; Bao, Z. N. *Nat. Nanotechnol.* **2011**, *6*, 788.

(8) Yu, Z. B.; Niu, X. F.; Liu, Z. T.; Pei, Q. B. *Adv. Mater.* **2011**, *23*, 3989.

(9) Kim, K. S.; Zhao, Y.; Jang, H.; Lee, S. Y.; Kim, J. M.; Kim, K. S.; Ahn, J. H.; Kim, P.; Choi, J. Y.; Hong, B. H. *Nature* **2009**, *457*, 706.

(10)   Xu, P.; Kang, J.; Choi, J. B.; Suhr, J.; Yu, J. Y.; Li, F. X.; Byun, J. H.; Kim, B. S.; Chou, T. W. *ACS Nano* **2014**, *8*, 9437.

(11)   Lipomi, D. J.; Lee, J. A.; Vosgueritchian, M.; Tee, B. C. K.; Bolander, J. A.; Bao, Z. A. *Chem. Mater.* **2012**, *24*, 373.

(12)   Kim, Y. H.; Lee, J.; Hofmann, S.; Gather, M. C.; Muller-Meskamp, L.; Leo, K. *Adv. Funct. Mater.* **2013**, *23*, 3763.

(13)   Liang, J. J.; Li, L.; Niu, X. F.; Yu, Z. B.; Pei, Q. B. *Nat. Photonics* **2013**, *7*, 817.

(14)   Liang, J. J.; Li, L.; Chen, D.; Hajagos, T.; Ren, Z.; Chou, S. Y.; Hu, W.; Pei, Q. B. *Nat. Commun.* **2015**, *6*, 7647.

(15)   Liu, H. S.; Pan, B. C.; Liou, G. S. *Nanoscale* **2017**, *9*, 2633.

(16)   Liang, J. J.; Li, L.; Tong, K.; Ren, Z.; Hu, W.; Niu, X. F.; Chen, Y. S.; Pei, Q. B. *ACS Nano* **2014**, *8*, 1590.

(17)   Wu, J.; Zang, J.; Rathmell, A. R.; Zhao, X.; Wiley, B. J. *Nano Lett.* **2013**, *13*, 2381.

(18)   Hu, W. L.; Niu, X. F.; Li, L.; Yun, S. R.; Yu, Z. B.; Pei, Q. B. *Nanotechnology* **2012**, *23*, 344002.

(19)   Hu, W. L.; Niu, X. F.; Zhao, R.; Pei, Q. *Appl. Phys. Lett.* **2013**, *102*, 083303.

(20)   Liang, J.; Li, L.; Niu, X.; Yu, Z.; Pei, Q. *Nat. Photonics* **2013**, *7*, 817.

(21)   Xu, F.; Zhu, Y. *Adv. Mater.* **2012**, *24*, 5117.

(22)   Lee, J.-Y.; Shin, D.; Park, J. *Thin Solid Films* **2016**, *608*, 34.

(23)   Amjadi, M.; Pichitpajongkit, A.; Lee, S.; Ryu, S.; Park, I. *ACS Nano* **2014**, *8*, 5154.

(24)   Song, L.; Myers, A. C.; Adams, J. J.; Zhu, Y. *ACS Appl. Mater. Interfaces* **2014**, *6*, 4248.

(25)   Yao, S.; Zhu, Y. *Nanoscale* **2014**, *6*, 2345.

(26)   Cheng, T.; Zhang, Y. Z.; Lai, W. Y.; Chen, Y.; Zeng, W. J.; Huang, W. *J. Mater. Chem. C* **2014**, *2*, 10369.

(27)   Kim, D. H.; Yu, K. C.; Kim, Y.; Kim, J. W. *ACS Appl. Mater. Interfaces* **2015**, *7*, 15214.

(28)   Aoki, T. *Prog. Polym. Sci.* **1999**, *24*, 951.

(29)   Vohra, A.; Filiatrault, H. L.; Amyotte, S. D.; Carmichael, R. S.; Suhan, N. D.; Siegers, C.; Ferrari, L.; Davidson, G. J. E.; Carmichael, T. B. *Adv. Funct. Mater.* **2016**, *26*, 5222.

(30)   Elechiguerra, J. L.; Larios-Lopez, L.; Liu, C.; Garcia-Gutierrez, D.; Camacho-Bragado, A.; Yacaman, M. *J. Chem. Mater.* **2005**, *17*, 6042.

(31)   Hillman, J. A. C.; Binfield, S. *SMTA International* **2007**, Edina, MN, 13.

(32)   Mayousse, C.; Celle, C.; Fraczkiewicz, A.; Simonato, J.-P. *Nanoscale* **2015**, *7*, 2107.

(33)   Jiu, J. T.; Wang, J.; Sugahara, T.; Nagao, S.; Nogi, M.; Koga, H.; Suganuma, K.; Hara, M.; Nakazawa, E.; Uchida, H. *RSC Adv.* **2015**, *5*, 27657.

(34)   Wang, J.; Jiu, J.; Sugahara, T.; Nagao, S.; Nogi, M.; Koga, H.; He, P.; Suganuma, K.; Uchida, H. *ACS Appl. Mater. Interfaces* **2015**, *7*, 23297.

(35)   Eom, H.; Lee, J.; Pichitpajongkit, A.; Amjadi, M.; Jeong, J.-H.; Lee, E.; Lee, J.-Y.; Park, I. *Small* **2014**, *10*, 4171.

(36)   Lee, H.; Hong, S.; Lee, J.; Suh, Y. D.; Kwon, J.; Moon, H.; Kim, H.; Yeo, J.; Ko, S. H. *ACS Appl. Mater. Interfaces* **2016**, *8*, 15449.

(37)   Jiu, J. T.; Nogi, M.; Sugahara, T.; Suganuma, K.; Tsujimoto, M.; Isoda, S. *J. Nanopart. Res.* **2012**, *14*, 1241.

(38)   Das, S. R.; Nian, Q.; Saei, M.; Jin, S.; Back, D.; Kumar, P.; Janes, D. B.; Alam, M. A.; Cheng, G. J. *ACS Nano* **2015**, *9*, 11121.

(39)   Chu, J. H.; Lee, D. H.; Jo, J.; Kim, S. Y.; Yoo, J. W.; Kwon, S. Y. *Adv. Funct. Mater.* **2016**, *26*, 7234.

(40)   Manikandan, A.; Lee, L.; Wang, Y. C.; Chen, C. W.; Chen, Y. Z.; Medina, H.; Tseng, J. Y.; Wang, Z. M. M.; Chueh, Y. L. *J. Mater. Chem. A* **2017**, *5*, 13320.

(41)   Jin, Y.; Deng, D.; Cheng, Y.; Kong, L.; Xiao, F. *Nanoscale* **2014**, *6*, 4812.

(42)   Liu, B.-T.; Huang, S.-X. *RSC Adv.* **2014**, *4*, 59226.

(43)   Zhang, Q.; Di, Y.; Huard, C. M.; Guo, L. J.; Wei, J.; Guo, J. *J. Mater. Chem. C* **2015**, *3*, 1528.

(44)   Miller, M. S.; O'Kane, J. C.; Niec, A.; Carmichael, R. S.; Carmichael, T. B. *ACS Appl. Mater. Interfaces* **2013**, *5*, 10165.

(45)   Chaudhury, M. K.; Whitesides, G. M. *Langmuir* **1991**, *7*, 1013.

(46)   Eddington, D. T.; Puccinelli, J. P.; Beebe, D. *J. Sensors and Actuators B* **2006**, *114*, 170.

(47)   Bhattacharya, S.; Datta, A.; Berg, J. M.; Gangopadhyay, S. *J. Microelectromechanical Sys.* **2005**, *14*, 590.

(48)   Vohra, A.; Carmichael, R. S.; Carmichael, T. B. *Langmuir* **2016**, *32*, 10206.

(49)   Weiss, N.; Muller-Meskamp, L.; Selzer, F.; Bormann, L.; Eychmuller, A.; Leo, K.; Gaponik, N. *Rsc Adv.* **2015**, *5*, 19659.

(50)   Akter, T.; Kim, W. S. *ACS Appl. Mater. Interfaces* **2012**, *4*, 1855.

(51)   De, S.; Coleman, J. N. *MRS Bull.* 2011, 36, 774.

(52)   Hu, L. B.; Kim, H. S.; Lee, J. Y.; Peumans, P.; Cui, Y. *ACS Nano* **2010**, *4*, 2955.

(53)   Guo, C. F.; Liu, Q.; Wang, G.; Wang, Y.; Shi, Z.; Suo, Z.; Chu, C.-W.; Ren, Z. *Proc. Natl. Acad. Sci. USA.* **2015**, *112*, 12332.

(54)   Li, T.; Suo, Z. *Int. J. Solids and Structures* **2007**, *44*, 1696.

(55)   Li, T.; Huang, Z. Y.; Suo, Z.; Lacour, S. P.; Wagner, S. *Appl. Phys. Lett.* **2004**, *85*, 3435.

(56)   Graedel, T. E. *J. Electrochem. Soc.* **1992**, *139*, 1963.

3.6. Supporting Information
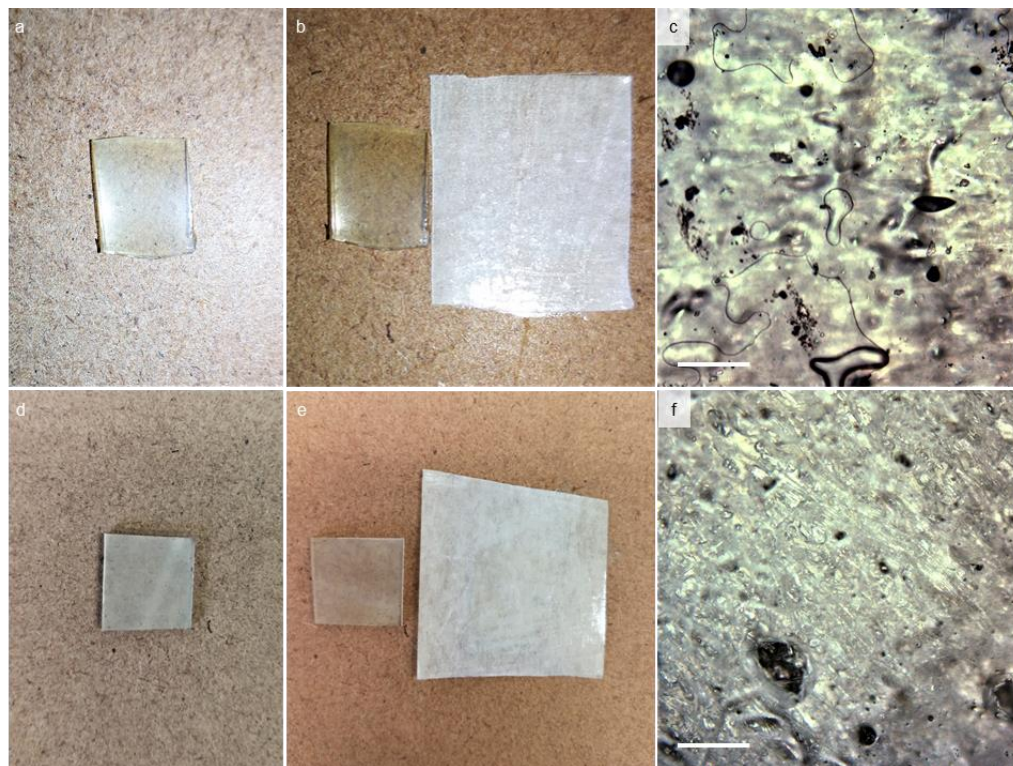
Figure S3.1. *Photograph of T-IIR/[AgNW]$_{1.0}$ composites (a) before and (b) after adhesion test with a Scotch tape. (c) Optical micrograph (scale = 200 μm) of the Scotch tape after adhesion test for T-IIR/[AgNW]$_{1.0}$ composites. Photograph of PDMS/[AgNW]$_{1.0}$ composites (d) before (e) and after adhesion test with a Scotch tape. (f) Optical micrograph (scale = 200 μm) of the Scotch tape after adhesion test for PDMS/[AgNW]$_{1.0}$ composites.*
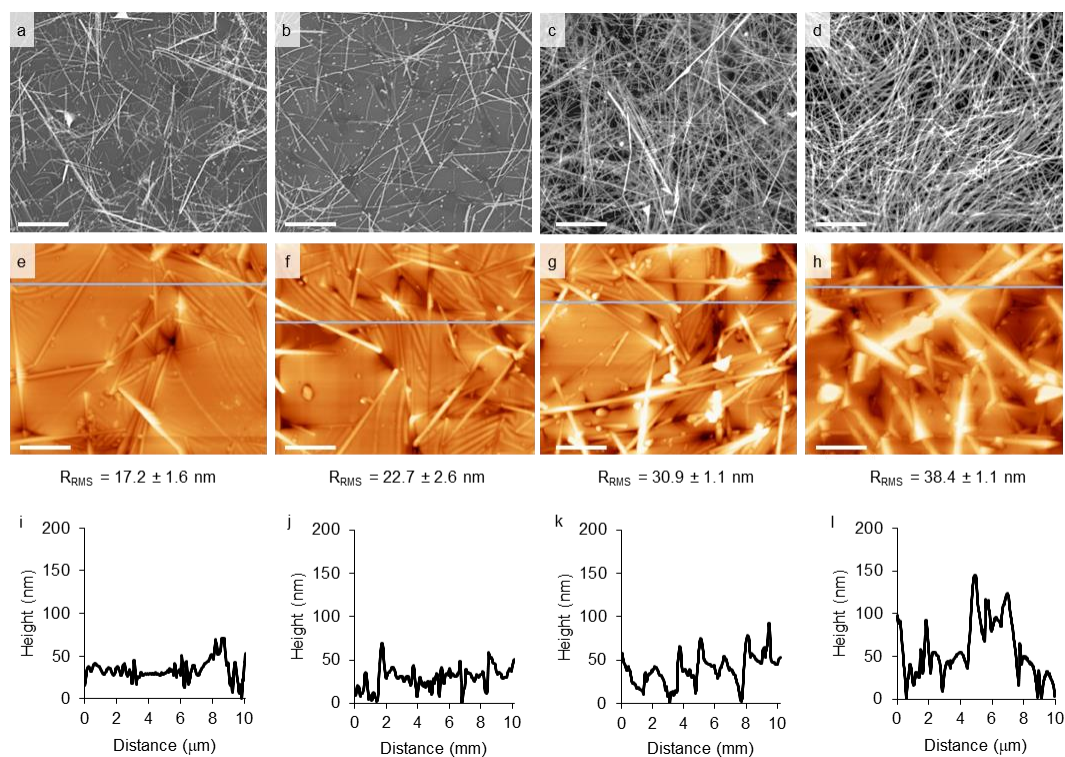
Figure S3.2. Top view SEM images (scale = 5 μm) of (a) PDMS/[AgNW]$_{0.5}$, (b) PDMS/[AgNW]$_{0.7}$, (c) PDMS/[AgNW]$_{1.0}$, and (d) PDMS/[AgNW]$_{2.0}$ composites. AFM height images (scale = 2 μm, z-scale = 250 nm) with R_{RMS} measurements and corresponding profile measurements of (e, i) PDMS/[AgNW]$_{0.5}$, (f, j) PDMS/[AgNW]$_{0.7}$, (g, k) PDMS/[AgNW]$_{1.0}$, and (h, i) PDMS/[AgNW]$_{2.0}$ composites.
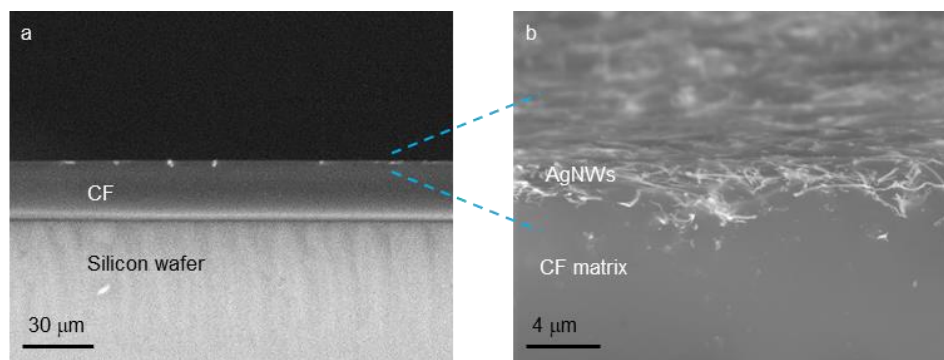
Figure S3.3. (a, b) Cross-sectional SEM images of a freeze-fractured AgNW/CF coating (1 mg/mL) on a silicon wafer. The AgNW network resides at the surface of a ~30-μm-thick CF layer.

Table S3.1. *Summary of root-mean-square roughness (R_{RMS}) values and peak-to-valley distances of T-IIR/[AgNW]$_n$ and PDMS/[AgNW]$_n$ composites.*

Concentration (n) (mg/mL)	R_{RMS}		Peak-to-valley distances	
	T-IIR/[AgNW]$_n$	PDMS/[AgNW]$_n$	T-IIR/[AgNW]$_n$	PDMS/[AgNW]$_n$
0.5	20.4 ± 0.7	17.2 ± 1.6	79.2 ± 4.6	76.7 ± 1.5
0.7	25.7 ± 3.1	22.7 ± 2.6	92.9 ± 10.8	93.0 ± 6.4
1.0	34.2 ± 2.2	30.9 ± 1.1	126.8 ± 10.4	127.6 ± 15.3
2.0	41.2 ± 1.7	38.4 ± 1.1	156.3 ± 4.5	143.7 ± 11.7

R_{RMS} = 94.1 ± 6.7 nm
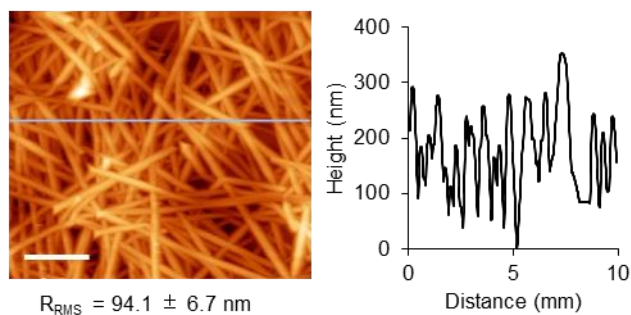
Figure S3.4. *AFM height image (scale = 2 μm, z-scale = 250 nm) with R_{RMS} measurements and corresponding profile measurement of AgNW network (2 mg/mL) on silicon wafer without CF matrix.*
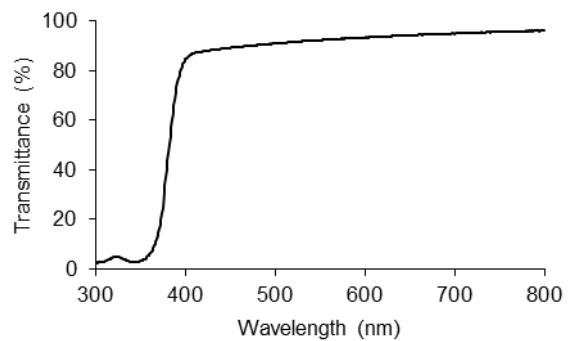
Figure S3.5. *Transmission spectrum of CF/PDMS composite.*
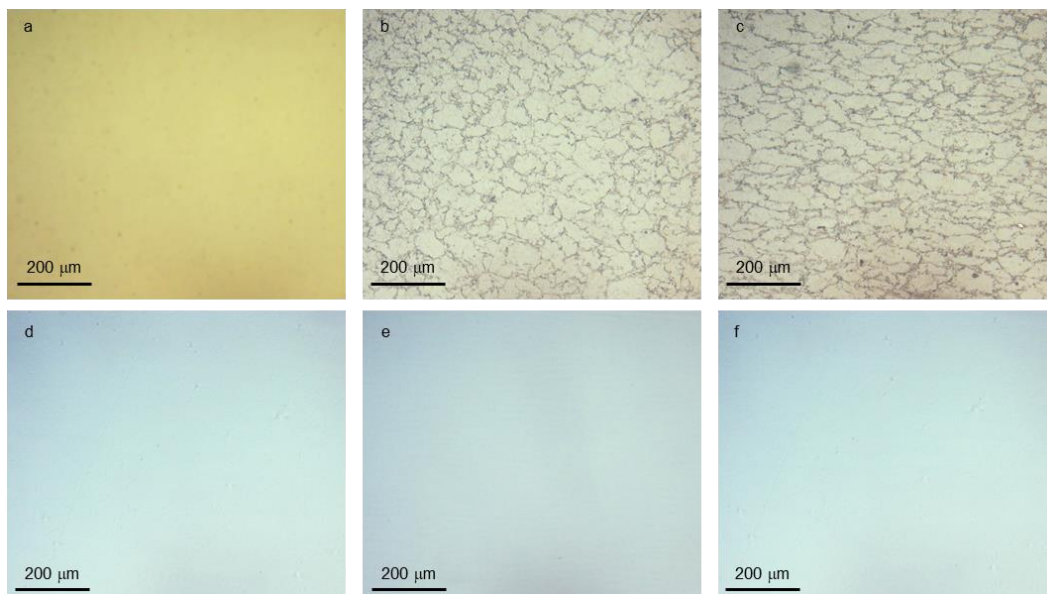
Figure S3.6. *Optical micrographs of the interface between CF and T-IIR substrate at (a) 0%, (b) 10%, and (c) 70% strain. Optical micrographs of the interface between CF and PDMS substrate at (d) 0%, (e) 10%, and (f) 70% strain. The samples were stretched in the horizontal direction.*
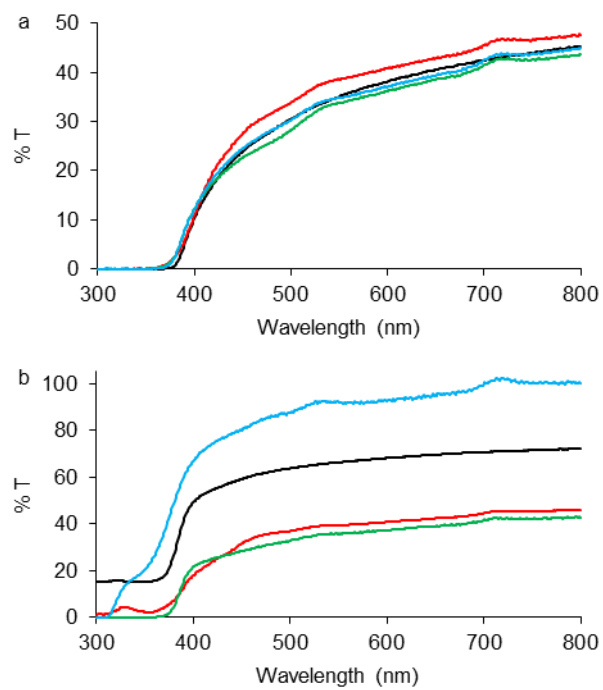
Figure S3.7. *Transmittance spectra of (a) T-IIR/[AgNW]$_{1.0}$ and (b) PDMS/[AgNW]$_{1.0}$ composites before (black lines) and after exposure to 45 °C/ 95% RH for 30 days (green lines), immersed in water for 7 days (red lines), and exposure to nitric acid vapor for 24 hours (blue lines).*

4. Chapter 4

Stretchable Light-Emitting Electrochemical Cells Incorporating Butyl

Rubber-Poly(Ethylene Oxide) Graft Copolymers

4.1. Introduction

Stretchable light-emitting devices function during mechanical deformation and can conform to curved or irregularly shaped surfaces while continuing to emit light. These devices are opening up opportunities in areas previously limited by the rigidity of conventional electronics, with exciting demonstrations of soft interactive displays for electronic skins,[1] stretchable displays,[2] biomedical imaging apparatus for internal tissues,[3] electronic textiles,[4] volumetric 3D displays,[5] and illuminated panels that can conform to the human body to provide useful therapies to accelerate wound healing,[6] activate chemotherapy drugs,[7] and aid in pain management.[8]

There are two strategies to impart stretchability to light-emitting electronic devices. The first connects rigid light-emitting devices using interconnects with either stretchable structures[9,10] or made from intrinsically stretchable conductive materials,[11] which absorb the strain during elongation. The second strategy develops ways to make intrinsically stretchable light-emitting devices, in which all device layers – electrodes, luminescent materials, injection and transport materials – are engineered to be inherently stretchable so the device itself accommodates mechanical deformation. This approach enables the fabrication of large-area, conformable, and illuminated panels.[12,13] The leading methodology for fabricating intrinsically stretchable light-emitting devices uses simple device architectures that minimize the number of thin-film layers to thereby reduce the number of interfaces that can delaminate under strain and cause device failure. Alternating current electroluminescence (ACEL) devices and light-emitting electrochemical cells (LEECs) are two device types with suitably simple architectures, consisting of an electroluminescent material between two electrodes. Intrinsically

stretchable ACEL devices use a stretchable electroluminescent material – a phosphor dispersed in an elastomer – sandwiched between two stretchable electrodes. ACEL devices fabricated using ZnS:Cu microparticles dispersed in poly(dimethylsiloxane) (PDMS) between stretchable silver nanowire electrodes emit blue light to 100% strain.[14] The stretchability of the ACEL device was further improved to 700% elongation by using ZnS:Cu/EcoFlex composite as the emissive material and ionic conductors on 3M VHB tapes as both electrodes.[12] LEECs have a similar device architecture, in which the emissive layer supports charge injection, charge transport, and emissive recombination.[15,16] The luminescent material is either a conjugated semiconducting polymer blended with a solid electrolyte that provides mobile ions, referred to as polymer-LEECs, or an ionic transition metal complex (iTMC) that serves as both an electronic and ionic conductor, referred to as iTMC-LEECs. The key feature of both LEEC types is the enhancement of charge injection that occurs at the electrode interfaces: Under an applied voltage, ions in the emissive material migrate to the respective electrode interfaces, where they accumulate to form electric double layers to reduce the barrier for electron/hole injection.[15,17] High ionic mobility facilitates this redistribution of ions, reducing the time it takes to form the electric double layer and reducing the response time of the LEEC. Imparting stretchability to LEECs has used the incorporation of stretchable polymers with the emissive material to create a stretchable emissive composite, similar to the phosphor-elastomer composites described above stretchable ACEL devices. For example, Liang et al. reported intrinsically stretchable polymer-LEECs by blending a stretchable crosslinked polymer with the emissive polymer, and sandwiching the resulting composite between two AgNW-based electrodes. These

devices emit light to 120% strain.[18] Our approach to the fabrication of intrinsically stretchable light-emitting devices has focused on iTMC-LEECs. We demonstrated the first example of intrinsically stretchable ruthenium-based LEECs by dispersing the ionic transition metal complex $Ru(dtb-bpy)_3(PF_6)_2$ in an elastomeric PDMS matrix to create an emissive composite.[13] Employing a semitransparent gold film on PDMS as the anode and a drop of indium gallium eutectic (EGaIn) as the cathode produced stretchable LEECs that emitted light to 27% strain, the point of electrical failure of the semitransparent gold electrode. These LEECs also sustained 50 cycles of repetitive 15% strains without diminishing the peak radiance.

An advantage of iTMC-LEECs is that emission throughout the visible spectrum as well as white light emission can be accessed by changing the metal center (Ru, Ir, Os, Cu^I) or modifying its ligand sphere.[11,19-22] Iridium complexes are a particularly interesting class of materials, as these species can provide emission throughout the visible spectrum.[23] However, low ion conductivity in films of iridium complexes causes a long delay in the turn-on time (t_{on}), defined as the time it takes for the device to emit light above a particular threshold, because the counterions are slow to redistribute under the applied voltage. Values of t_{on} for Ir-based LEECs range from a few minutes to several hours. A typical method to reduce t_{on} for iTMC-LEECs, as well as polymer-LEECs, is to blend the iTMC or polymer with a polar additive to increase the dielectric constant of the film. Such polar materials have included the solid electrolyte $PEO/LiCF_3SO_3$,[24,25] polymerizable ion-pair monomers and ion transporters,[26] oligoether monomers,[27] and ionic liquids.[28,29] This approach not only increases the ion conductivity, but it also effectively solubilizes polar iTMCs without leading to problematic phase separation.

Phase separation decelerates and abates the process of electrochemical doping at the electrodes, leading to a slow charge recombination and light emission,[30] and can also cause the inhomogeneous development of electric field distributions that leads to a degradation of the device stability.[31] For example, adding the solid electrolyte poly(ethylene oxide)/lithium trifluoromethanesulfonate ($PEO/LiCF_3SO_3$) to either polymer-LEECs or iTMC-LEECs produces uniform films and improves the device response by reducing t_{on} as well as improving t_{max}, the time it takes for the device to reach maximum radiance.[24,25,32] The $PEO/LiCF_3SO_3$ solid electrolyte facilitates the movement of the Li^+ cations of $LiCF_3SO_3$ by dynamic bond making/breaking with the ether oxygen atoms of PEO. Despite these impressive device improvements, the intrinsic brittleness of the $PEO/LiCF_3SO_3$ solid electrolyte eliminates the possibility of intrinsic stretchability. Ionic liquids have also been shown to solubilize iTMCs, increase the ion conductivity, and reduce t_{on}. LEECs fabricated from the iTMC $Ir(ppy)_2(dtb-bpy)(PF_6)$ and the ionic liquid 1-ethyl-3-methylimidazolium hexafluorophosphate decreases the t_{on} from 5 h to 40 min.[28] However, the advantages of LEECs fabricated using brittle solid electrolytes or ionic liquids to reduce t_{on} and t_{max} are accompanied by a critical drawback: These additives cause an unfavorable trade-off with the device stability. The low t_{max} (30 s) of Ru-based iTMC LEECs incorporating the $PEO/LiCF_3SO_3$ solid electrolyte is accompanied by a corresponding decrease in the lifetime of these LEECs.[24] The light output decays to half its maximum value (termed the $t_{1/2}$ value) after 1-2 hours of device operation. For Ir-based LEECs incorporating ionic liquids, reduction of t_{on} decreases the device lifetime (the time at which the radiance decayed to one-fifth of the maximum radiance) by a factor of 3.[28] The trade-off between t_{on} and device lifetime is thought to be

caused by electrochemical degradation reactions due to space-charge accumulation near the electrodes, suggesting that fine control over the dielectric properties of the emissive film may be an effective way to reach a reasonable compromise between t_{on} and device lifetime.

The trade-off described above, along with the intrinsic brittleness typical of many highly polar additives, indicates it is a challenging problem to prepare iTMC-LEECs that not only balance reasonable t_{on} values with acceptable device lifetimes, but also support intrinsic device stretchability. Here, we introduce a new approach to solve these problems that blends an amphiphilic graft copolymer with the emissive iridium complex $[Ir(ppy)_2(dtb\text{-}bpy)]^+[PF_6^-]$, in which the graft copolymer combines the necessary disparate properties into a single material and provide a way to control the dielectric properties of the resulting film. The amphiphilic graft copolymer consists of a backbone of butyl rubber (poly(isobutylene-co-isoprene), IIR) bearing PEO side chains (IIR-g-PEO, RgP) according to Scheme 4.1. The RgP copolymer is a soft material, designed to impart stretchability.[33] The polar PEO side chains are designed to solubilize the iTMC (the emissive iridium complex $[Ir(ppy)_2(dtb\text{-}bpy)]^+[PF_6^-]$) and additionally form a solid electrolyte with $LiCF_3SO_3$ to improve the ionic mobility. By varying the molecular weight of the PEO sidechains, we demonstrate the effect of different PEO content (16, 34, and 69 wt%) on phase separation in the film, responsiveness and lifetime of the LEECs, and the ability of the LEECs to sustain mechanical deformation.
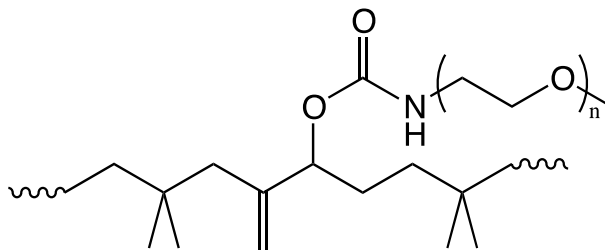
Scheme 4.1. *Structure of butyl rubber-PEO graqqqft copolymer (RgP).*

4.2. Results and Discussion

We synthesized RgP graft copolymers with three different PEO weight percentages by varying the MW of the PEO sidechains attached to the IIR backbone, according to the published procedure of Bonduelle et al.[34] RgP copolymers with PEO contents of 16, 34, and 69 wt% are designated RgP**16**, RgP**34**, and RgP**69**, respectively. Previous studies have shown that nonpolar butyl rubber and polar PEO are incompatible, and noncovalent blends undergo nanoscale phase separation during film formation.[35] Bonduelle et al. previously demonstrated that combining these components covalently in the RgP copolymer also produces films with phase separation that depends on the PEO content of the copolymer. Copolymers with very low PEO content (< 12 wt%) formed microscale patterns consistent with a kinetic trapping mechanism; as the PEO content was increased from 18 to 65 wt%, the films evolved from micrometer-scale patterns to nanoscale patterns governed primarily by thermodynamic phase separation. We prepared films of RgP**16**, RgP**34**, and RgP**69** using 50 mg/mL solutions in dichloromethane onto ITO/glass substrates and observed a similar trend through analysis of the resulting films using atomic force microscopy (AFM). AFM phase images show that each copolymer undergoes phase separation, with domain sizes that depend on the PEO content of the

114

copolymer. In Figure 4.1, we assign the phase with small phase shift angle (blue color) to

IIR domains due to the lower attraction of the AFM tip to the soft regions and the phase

with large phase shift angle (red color) to PEO domains. The AFM phase image of the

RgP**16** film reveals the largest IIR domains, which range from the nano- to microscale

(~0.15 to 3.0 μm^2), consistent with the low PEO content of the graft copolymer (Figure

4.1a). Both RgP**34** and RgP**69** films exhibit nanoscale IIR domains, consistent with the

higher PEO content of these copolymers and the results reported by Bonduelle et al.

(Figure 4.1b, c). AFM topographical images show that films of RgP**16** exhibit large (~16

μm) depressions, whereas RgP**34** and RgP**69** films both exhibit a fine surface texture

(Figure 4.1d-f). The roughness of all of these films increases as the PEO content

increases, with RMS roughness values for RgP**16**, RgP**34**, and RgP**69** films of 2.8 ± 0.1

nm, 3.5 ± 0.3 nm, and 4.2 ± 0.8 nm, respectively. This trend is likely due to the

crystallinity of the PEO, which increases the surface roughness.[34]
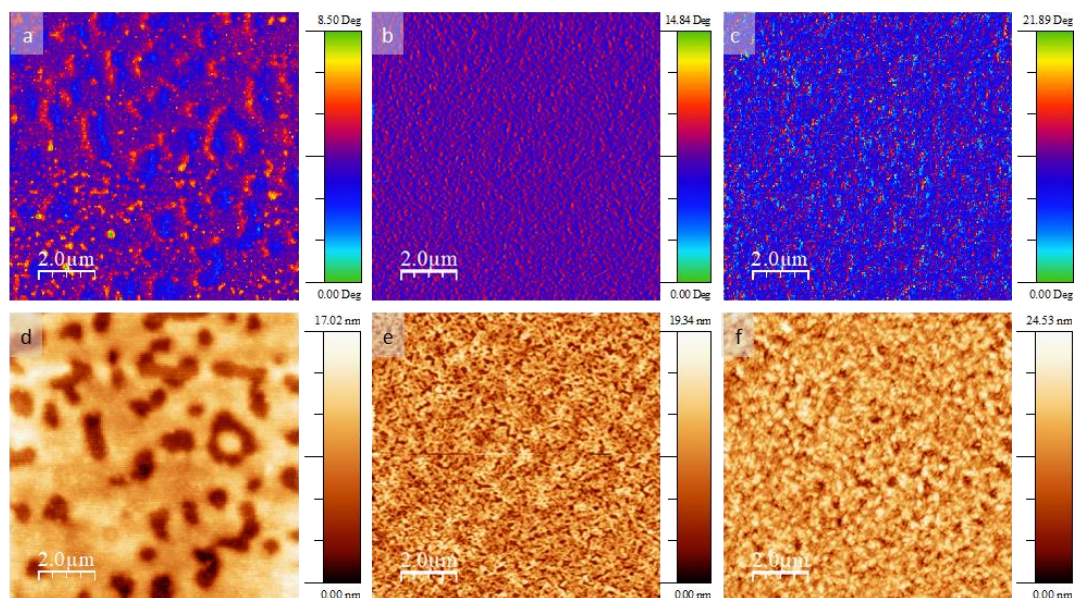
Figure 4.1. AFM phase images of (a) RgP**16**, (b) RgP**34**, and (c) RgP**69** films on ITO/glass. AFM height images of (d) RgP**16**, (e) RgP**34**, and (f) RgP**69** films on ITO/glass.

4.2.1. RgP/LiCF$_3$SO$_3$/Ir Emissive Films

We studied the ability of the three RgP copolymers, as well as that of the two parent polymers (PEO and IIR), to effectively disperse the ionic components used in LEECs. We prepared composite films that incorporated LiCF$_3$SO$_3$ (to form the solid electrolyte with PEO), and the emissive ionic iridium complex [Ir(ppy)$_2$(dtb-bpy)]$^+$[PF$_6^-$]. Individually, the PEO and IIR parent polymers of RgP copolymers display very different compatibilities with these ionic components. Films of PEO, LiCF$_3$SO$_3$, and [Ir(ppy)$_2$(dtb-bpy)]$^+$[PF$_6^-$] (PEO/LiCF$_3$SO$_3$/Ir) prepared by spin coating a 10:0.2:1 molar ratio in dichloromethane onto an ITO/glass substrate appear featureless under the optical microscope (Figure 4.2a), and the AFM phase image presents a homogeneous surface without phase separation (Figure 4.2b), consistent with the well-known ability of PEO to dissolve ionic salts. The AFM topographical image reveals dendritic structures that can

116

be attributed to the crystallinity of the PEO and an RMS roughness of 14.0 ± 1.7 nm (Figure 4.2c). In contrast, films of IIR and $[Ir(ppy)_2(dtb-bpy)]^+[PF_6^-]$ prepared by spin-coating a 10:1 molar ratio in dichloromethane display significant surface texture and phase separation in optical micrographs and AFM topographical and phase images (Figure 4.2d-e). AFM phase images reveal irregularly shaped microscale domains of $[Ir(ppy)_2(dtb-bpy)]^+[PF_6^-]$ (the red features in Figure 4.2e), consistent with the incompatibility of the polar Ir salt with the nonpolar IIR polymer. AFM topographical images reveal that the poor mixing results in films with a high RMS roughness value of 61.1 ± 7.2 nm, ~4 times higher than that of $PEO/LiCF_3SO_3/Ir$ films, and microscale thickness variations with a maximum peak-to-valley distance of 369.2 ± 57.1 nm.
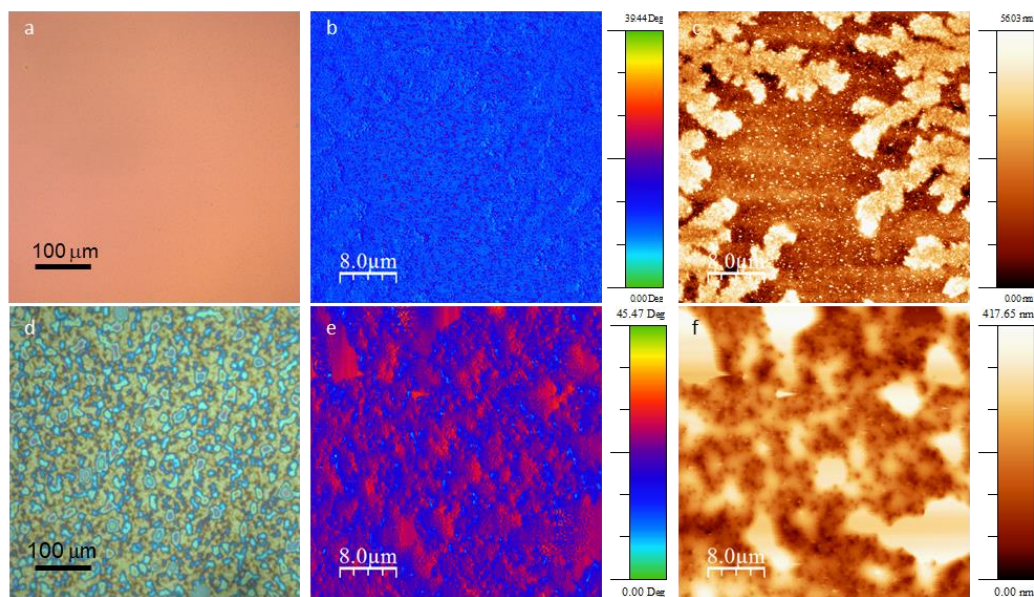
Figure 4.2. (a) Optical micrograph, (b) AFM phase image, and (c) AFM height image of $PEO/LiCO_3SO_3/Ir$ films on ITO/glass. (d) Optical micrograph, (e) AFM phase image, and (f) AFM height image of IIR/Ir films on ITO/glass.

Using PEO sidechains on an IIR backbone in RgP graft copolymers enables the incorporation of the soft IIR in a composite film that also solubilizes the ionic salts. This solubilization depends on the PEO content in the RgP copolymer. We spin coated a solution of the RgP copolymer, $LiCF_3SO_3$, $[Ir(ppy)_2(dtb-bpy)]^+[PF_6^-]$ (24 mg/mL), in a molar ratio of 10:0.2:1 in dichloromethane onto ITO/glass. Optical micrographs of the resulting films reveal microscale features for RgP**16**/$LiCF_3SO_3$/Ir composite films, whereas RgP**34**/$LiCF_3SO_3$/Ir composite films appear featureless and RgP**69**/ $LiCF_3SO_3$/Ir composite films exhibit fine surface features (Figure 4.3a-c). We further analyzed the composite films using AFM to characterize the effect of the added iTMC and lithium salt on the phase separation and topography of the copolymer films at the nanoscale. AFM phase images (Figure 4.3d-f) reveal that all three films exhibit phase separation that differs significantly from films of the RgP copolymers alone. RgP**16**/$LiCF_3SO_3$/Ir films exhibit an inhomogeneous surface with microscale aggregation of IIR, the majority component of RgP**16**. The aggregation is accompanied by broad features in the AFM topographical image (Figure 4.3g). This inhomogeneity is consistent with the low PEO content of RgP**16**, which appears insufficient to effectively solubilize the ionic salts. RgP**34**/$LiCF_3SO_3$/Ir and RgP**69**/$LiCF_3SO_3$/Ir composite films also exhibit phase separation according to the AFM phase images; however, these composites exhibit smaller domains consistent with better mixing of the copolymer with the ionic salts. A comparison of AFM phase images of the composite films (Figure 4.3e, f) with the pure RgP**34** and RgP**69** copolymers (Figure 4.1b, c) shows that loading the copolymers with ionic salts changes how the materials self-assemble during film formation. The domains in the composite films are larger than the nanoscale domains of both RgP**34** and RgP**69**

copolymers alone, a consequence of the incorporation of ionic salts. Comparing AFM phase images of the RgP**34**/LiCF$_3$SO$_3$/Ir and RgP**69**/LiCF$_3$SO$_3$/Ir composite films indicates that mixing is the most effective when RgP**34** is the host copolymer: RgP**34**/LiCF$_3$SO$_3$/Ir composite films form nanoscale domains, whereas RgP**69**/LiCF$_3$SO$_3$/Ir composite films comprise a combination of nanoscale and microscale domains. Furthermore, the domains of RgP**34**/LiCF$_3$SO$_3$/Ir composite films show a smaller variation in the phase angle compared to RgP**69**/LiCF$_3$SO$_3$/Ir composite films, suggesting that RgP**34**/LiCF$_3$SO$_3$/Ir forms domains containing a mixture of materials rather than segregation into pure components. The AFM topographical images of the three composite films reveal that the RMS roughness increases as the PEO content increases, similar to films of the RgP copolymers alone and attributed to the crystallinity of PEO. RMS roughness values are 6.5 ± 0.4 nm, 9.0 ± 0.3 nm, and 18.2 ± 0.9 nm for RgP**16**/LiCF$_3$SO$_3$/Ir, RgP**34**/LiCF$_3$SO$_3$/Ir and RgP**69**/LiCF$_3$SO$_3$/Ir composite films, respectively. These values are higher than the RMS roughness of RgP copolymers alone, which can be attributed to the additional ionic salts present in the composite films.
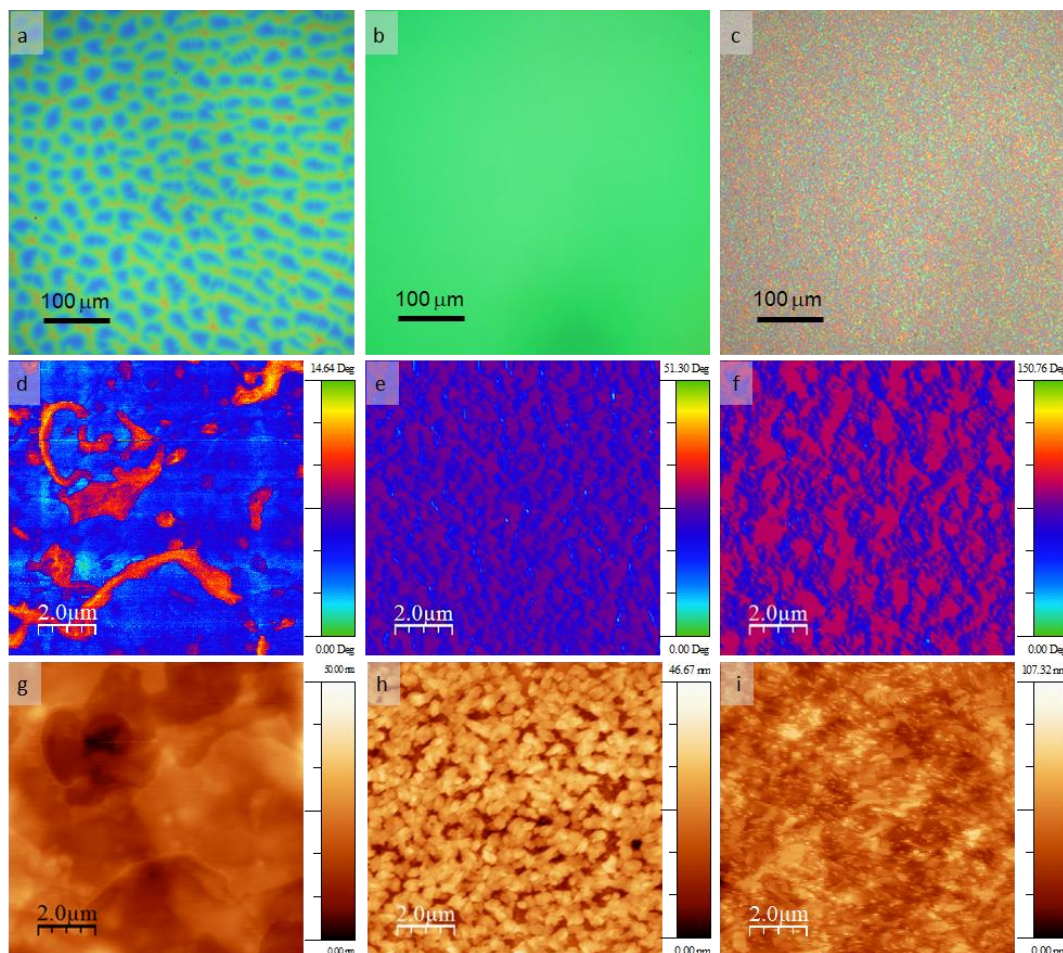
Figure 4.3. *Optical micrographs of (a) RgP**16**/LiCF₃SO₃/Ir, (b) RgP**34**/LiCF₃SO₃/Ir, and (c) RgP**69**/LiCF₃SO₃/Ir films on ITO/glass. AFM phase images of (d) RgP**16**/LiCF₃SO₃/Ir, (e) RgP**34**/LiCF₃SO₃/Ir, and (f) RgP**69**/LiCF₃SO₃/Ir films on ITO/glass. AFM height images of (g) RgP**16**/LiCF₃SO₃/Ir, (h) RgP**34**/LiCF₃SO₃/Ir, and (i) RgP**69**/LiCF₃SO₃/Ir films on ITO/glass.*

4.2.2. LEECs Incorporating RgP/LiCF₃SO₃/Ir Emissive Films

We assessed the performance of LEECs fabricated using RgP/LiCF₃SO₃/Ir composite films against two benchmark devices: LEECs fabricated from the pristine Ir complex alone, without polymer or ionic additives to reduce t_{on}, and LEECs fabricated from PEO/LiCF₃SO₃/Ir to maximize the reduction in t_{on} due to the high PEO content. We fabricated these LEECs in a non-stretchable device test structure by spin-coating the

120

emissive film onto ITO-coated glass (the device anode), and then applying a drop of the liquid metal EGaIn as the cathode (Figure S4.1 in the supporting information). LEECs fabricated using a pristine film of $[Ir(ppy)_2(dtb-bpy)]^+[PF_6^-]$ and operated at 6 V DC in an inert atmosphere show a slow onset of light emission consistent with the reported low ionic mobility in the film. We define the turn-on time of our devices according to the detection limit of radiance of ~10 nW. The radiance of the pristine Ir devices exceeded this lower limit at ~1500 s and continued to increase to a maximum radiance of 85 ± 6.8 μW at 3600 s (Table 4.1, Figure S4.2). In contrast, LEECs fabricated from PEO/LiCF$_3$SO$_3$/Ir composites begin to emit light at a t_{on} of <1 s, with a t_{max} of 9.5 ± 0.7 s and maximum radiance of 76 ± 12 μW (Figure S4.3), consistent with the high ionic mobility supported by the PEO/LiCF$_3$SO$_3$ solid electrolyte. However, the consequence of using the PEO/LiCF$_3$SO$_3$ solid electrolyte is a reduction in the device lifetime. For PEO/LiCF$_3$SO$_3$/Ir LEECs, the time at which the radiance decays to half the maximum value ($t_{1/2}$) is 129 ± 12 s. A similar effect has been reported in other iTMC devices and can be attributed to quenching of phosphorescence from long-living triplet excitons by electrochemical doping. Increasing the ion conductivity results in a faster propagation of the doped zones of LEECs, causing faster quenching of the long-living triplet.[36,37]

Table 4.1. *Summary of figures of merit for LEECs fabricated from RgP/LiF$_3$CSO$_3$/Ir composites on ITO/glass operated at 6 V DC in inert conditions*

Emissive Material	t_{on} (s)	t_{max} (s)	Max Rad (μW)	$t_{1/2}$ (s)	Max EQE (%)
Pristine Ir	~1500	>3600	85 ± 6.8	>3600	0.87 ± 0.12
Ir/RgP**16**/LiF$_3$CSO$_3$	~2400	>10800	0.61 ± 0.32	>10800	0.27 ± 0.11
Ir/RgP**34**/LiF$_3$CSO$_3$	12 ± 3	915 ± 179	10 ± 2.1	>10800	0.33 ± 0.04
Ir/RgP**69**/LiF$_3$CSO$_3$	<1	31 ± 7.5	26 ± 6.4	336 ± 82	0.54 ± 0.23
Ir/PEO/LiF$_3$CSO$_3$	<1	9.5 ± 0.7	76 ± 12	129 ± 12	0.38 ± 0.01

LEECs prepared from RgP**16**/LiCF$_3$SO$_3$/Ir, RgP**34**/LiCF$_3$SO$_3$/Ir, and RgP**69**/LiCF$_3$SO$_3$/Ir composite films exhibit device properties that correlate to the PEO content of the graft copolymer. Devices fabricated using RgP**16**/LiCF$_3$SO$_3$/Ir composites, with the lowest PEO content, exhibited device properties consistent with the poor solubilization of the ionic components indicated by the AFM analysis in Figure 4.3. The turn-on time of these devices was ~2400 s, and the radiance increased until the end of the testing time of 10800 s (3 h) to reach a maximum radiance of 0.61 ± 0.32 μW (Figure 4.4). Despite the inclusion of the PEO/LiCF$_3$SO$_3$ solid electrolyte into RgP**16**/LiCF$_3$SO$_3$/Ir LEECs, comparison of these device properties to those of benchmark devices fabricated from pristine [Ir(ppy)$_2$(dtb-bpy)]$^+$[PF6$^-$] is not favourable. The slower t_{on} of RgP**16**/LiCF$_3$SO$_3$/Ir LEECs indicates that the ion conductivity has not been improved, likely because the low PEO content of the copolymer limits the number of sites for LiCF$_3$SO$_3$ coordination necessary to facilitate ion conductivity and the presence of the non-polar, insulating IIR copolymer backbone. RgP**16**/LiCF$_3$SO$_3$/Ir LEECs also peaked at lower radiance than [Ir(ppy)$_2$(dtb-bpy)]$^+$[PF6$^-$] devices, even with a testing window that was three times longer. These device characteristics are consistent with the

detrimental effects of phase separation of RgP**16**/LiCF$_3$SO$_3$/Ir composites, which is known to slow electrochemical doping at the electrodes and also generate inhomogeneous electric fields across the device that diminish the device stability.[30,31]
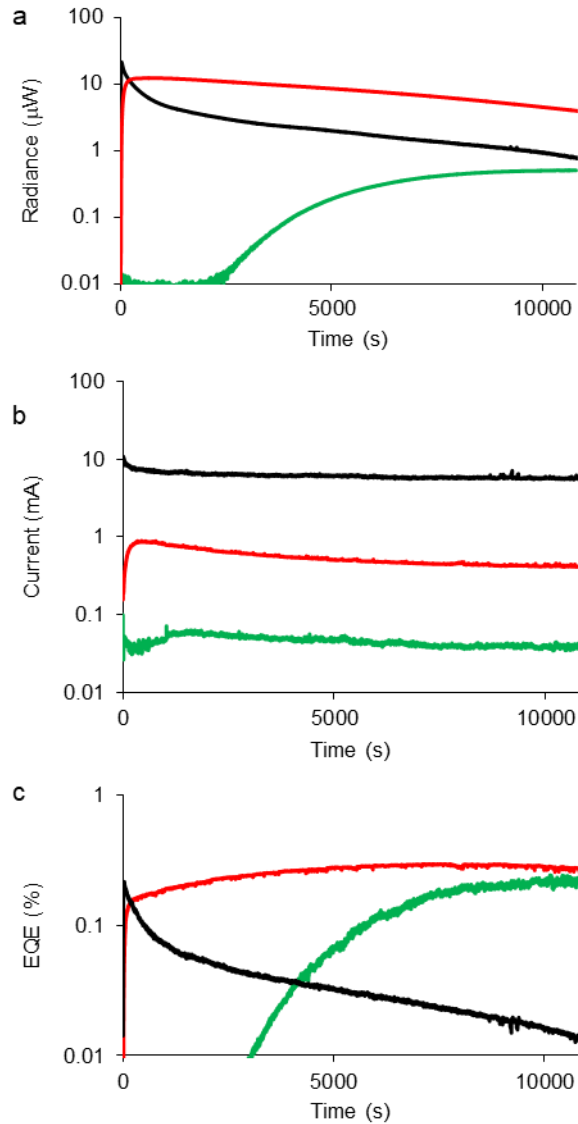

Figure 4.4. *Temporal evolution of (a) radiance, (b) current, and (c) EQE of a typical rigid LEEC fabricated from RgP**16**/LiCF$_3$SO$_3$/Ir (green), RgP**34**/LiCF$_3$SO$_3$/Ir (red), and RgP**69**/LiCF$_3$SO$_3$/Ir (black) operated at 6 V DC in inert conditions.*

In contrast, the properties of RgP**34**/LiCF$_3$SO$_3$/Ir and RgP**69**/LiCF$_3$SO$_3$/Ir LEECs indicate that the PEO content of these copolymers is sufficient to support a high ionic mobility and short turn-on times. These devices furthermore benefit from better mixing between the ionic components and copolymer according to the nanoscale phase separation shown in Figure 4.3. Application of 6 V DC to RgP**34**/LiCF$_3$SO$_3$/Ir and RgP**69**/LiCF$_3$SO$_3$/Ir LEECs resulted in light emission with t$_{on}$ values of 12 ± 3 s and <1 s, respectively (Figure 4.4). The very short turn-on times indicate a higher ionic mobility compared to pristine [Ir(ppy)$_2$(dtb-bpy)]$^+$[PF$_6$$^-$] devices. Consequently, PEO/LiCF$_3$SO$_3$/Ir LEECs, with a turn-on time of <1 s, are an appropriate benchmark for comparison. Although all three of these PEO-containing devices turn on within a few seconds, the time it takes for each device to reach the maximum radiance correlates with the PEO content of the film: t$_{max}$ values of RgP**34**/LiCF$_3$SO$_3$/Ir, RgP**69**/LiCF$_3$SO$_3$/Ir, and PEO/LiCF$_3$SO$_3$/Ir LEECs are 915 ± 179 s, 31 ± 7.5 s, and 9.5 ± 0.7 s, respectively, with maximum radiance values of 10 ± 2.1 μW, 26 ± 6.4 μW, and 76 ± 12 μW, respectively. Although the higher PEO content produces devices that turn on faster and are initially brighter, the trade-off between t$_{on}$ and device lifetime causes the radiance of these devices to diminish more quickly. Thus, PEO/LiCF$_3$SO$_3$/Ir LEECs exhibit the lowest t$_{1/2}$ value of 129 ± 12 s, whereas for RgP**69**/LiCF$_3$SO$_3$/Ir LEECs this value is 336 ± 82 s. The radiance of RgP**34**/LiCF$_3$SO$_3$/Ir LEECs does not decline to half the maximum value, instead reaching 60% of the maximum radiance at the end of 3 h of continuous device operation, corresponding to t$_{1/2}$ >10800 s.

Overall, the correlation of device properties of RgP**16**/LiCF$_3$SO$_3$/Ir, RgP**34**/LiCF$_3$SO$_3$/Ir, and RgP**69**/LiCF$_3$SO$_3$/Ir LEECs with PEO content indicates that

graft copolymers are an effective way to meter PEO content into the emissive layer of LEECs. This control over the dielectric properties of the emissive composite is a way to manipulate device properties as well as manage the trade-off between turn-on time and device lifetime. At the same time, each of these LEECs contains the soft IIR component designed to make these new composites suitable for use in intrinsically stretchable light-emitting devices.

4.2.3. Stretchable LEECs Using RgP34/LiCF$_3$SO$_3$/Ir and RgP69/LiCF$_3$SO$_3$/Ir Composites

We have used PEO in our LEECs to provide the dielectric constant necessary for reasonable turn-on times; however, PEO alone is a brittle material that is incompatible with intrinsically stretchable devices, exhibiting a small elastic range of < 5%. As expected, the emissive composite PEO/LiCF$_3$SO$_3$/Ir deposited on a PDMS substrate forms numerous cracks with stretching at low (5%) strains (Figure S4.4a). Combining PEO with IIR into RgP graft copolymers changes the mechanical properties of the emissive composite materials due to the low Young's modulus of the IIR backbone. Previous studies have demonstrated that as the amount of PEO in RgP copolymers is decreased from 34 wt% to 16 wt%, the Young's modulus decreases from 9.0 ± 1.9 MPa to 0.3 ± 0.1 MPa and the elongation at break increases.[33] Consistent with this study, optical micrographs at 5% tensile strain show that films of RgP**16**/LiCF$_3$SO$_3$/Ir do not exhibit cracks (Figure S4.4b); films of RgP**34**/LiCF$_3$SO$_3$/Ir exhibit fine, almost imperceptible cracks (Figure S4.4c); and films of RgP**69**/LiCF$_3$SO$_3$/Ir exhibit prominent, jagged cracks (Figure S4.4d). Therefore, high PEO content not only reduces turn-on times at the expense of device lifetime, but also device stretchability. This trade-off

indicates that metering PEO into emissive films is critical to balance the three properties of turn-on time, device lifetime, and stretchability

We fabricated intrinsically stretchable LEECs using RgP**34**/LiCF$_3$SO$_3$/Ir and RgP**69**/LiCF$_3$SO$_3$/Ir composites (omitting RgP**16**/LiCF$_3$SO$_3$/Ir due to the slow device response) by replacing the rigid ITO/glass electrode with a stretchable semitransparent gold film deposited on PDMS (Au/PDMS). Thin gold films on PDMS have a transmission of 37% at 558 nm (the peak wavelength of the electroluminescence spectrum of [Ir(ppy)$_2$(dtb-bpy)][PF6$^-$]) and have been used previously to fabricate intrinsically stretchable Ru-based LEECs.[13] These gold anodes remain conductive to tensile strains of ~20% and are convenient for preliminary investigations of device stretchability. After spin-coating RgP**34**/LiCF$_3$SO$_3$/Ir and RgP**69**/LiCF$_3$SO$_3$/Ir films on Au/PDMS, we applied a drop of EGaIn (5 mm diameter) as the cathode. In the initial, unstretched state, the radiance of RgP**34**/LiCF$_3$SO$_3$/Ir and RgP**69**/LiCF$_3$SO$_3$/Ir LEECs is ~40% lower than analogous devices fabricated using ITO/glass anodes due the lower transparency of Au/PDMS compared to ITO/glass, which reduces the light output (Figure 4.5, Table S4.1). We subjected RgP**34**/LiCF$_3$SO$_3$/Ir and RgP**69**/LiCF$_3$SO$_3$/Ir films on Au/PDMS to repetitive cycles of 15% strain and after a set number of cycles, we relaxed the device, deposited an EGaIn cathode, and operated the devices for 30 min. The radiance of RgP**34**/LiCF$_3$SO$_3$/Ir LEECs was negligibly affected by 30 strain cycles. At 50 strain cycles, the maximum radiance decreased to 36% of the initial (unstrained) value, due to cracking of the RgP**34**/LiCF$_3$SO$_3$/Ir layer, the gold anode, or a combination of the two. In contrast, cracking due to the higher PEO content of RgP**69**/LiCF$_3$SO$_3$/Ir

LEECs resulted in degradation of the device properties after only 10 strain cycles, with sporadic measurement of signal in the nW range making it indistinguishable from noise.

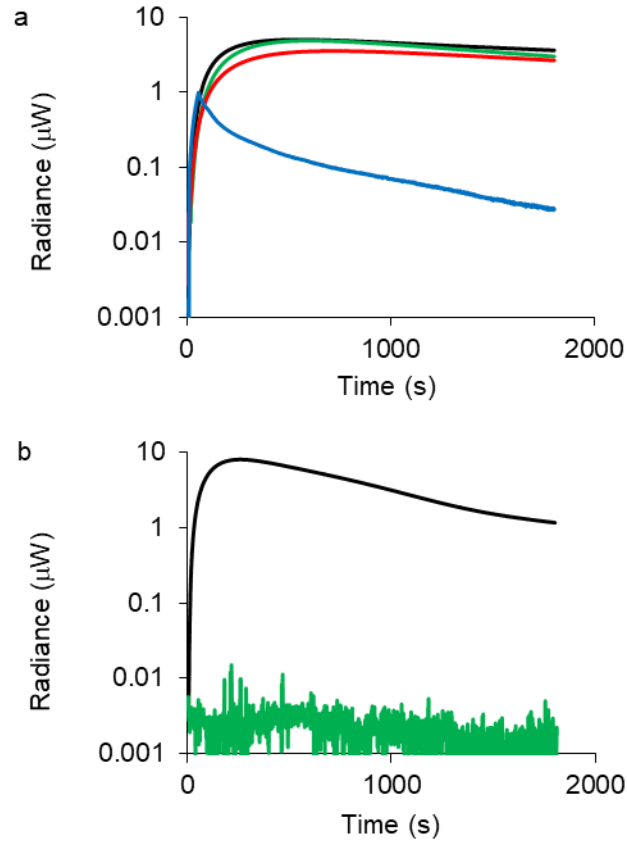**Figure 4.5.** *Temporal evolution of radiance of (a) RgP34/LiCF$_3$SO$_3$/Ir LEECs and (b) RgP69/LiCF3SO$_3$/Ir LEECs after 0 cycle (black), 10 cycles (green), 30 cycles (red) and 50 cycles (blue) of 15% strain.*

4.3. Conclusions

In conclusion, we have shown that combining PEO and IIR in a graft copolymer is an appealing way to manage the trade-off between device turn-on times, lifetime, and

stretchability. The ability to meter PEO content into the emissive composite by altering the molecular weight of PEO sidechains provides a convenient way to adjust the dielectric properties of the emissive composite and permit the incorporation of the soft IIR backbone, necessary for stretchability, while managing phase separation in the film. Further exploration of this copolymer-based approach to manage device properties and trade-offs is currently underway.

4.4. Experimental

$[Ir(ppy)_2(dtb-bpy)]^+[PF_6^-]$ was synthesized according to Slinker et al.[38] RgP graft copolymers were prepared according to Bonduelle et al.[34] PEO (M_w = 120000) and $LiCF_3SO_3$ salt were purchased from Sigma Aldrich and used as received.

Emissive Layer Fabrication. All the solutions were passed through 0.2 μm pore size PTFE syringe filters and then spin-coated onto the anode at a speed of 1000 rpm for 30 s per sample in a nitrogen glovebox. Thin films of pristine $[Ir(ppy)_2(dtb-bpy)]^+[PF_6^-]$ were prepared by spin-coating from a solution containing 24 mg/mL $[Ir(ppy)_2(dtb-bpy)]^+[PF_6^-]$ dissolved in dichloromethane. Thin films of RgP were prepared by spin-coating from a solution containing 50 mg/mL RgP dissolved in dichloromethane. Thin films of PEO/$LiCF_3SO_3$/Ir were prepared by spin-coating from a solution containing PEO, $LiCF_3SO_3$, and $[Ir(ppy)_2(dtb-bpy)]^+[PF_6^-]$ (24 mg/mL) in a molar ratio of 1: 10: 0.2 dissolved in dichloromethane. Thin films of IIR/Ir were prepared by spin-coating a solution containing IIR and $[Ir(ppy)_2(dtb-bpy)]^+[PF_6^-]$ (24 mg/mL) in a molar ratio of 10:1 in dichloromethane. Thin films of RgP/$LiCF_3SO_3$/Ir were prepared by spin-coating a solution containing RgP, $LiCF_3SO_3$, and $[Ir(ppy)_2(dtb-bpy)]^+[PF_6^-]$ (24 mg/mL) in a molar ratio of 10: 0.2: 1 (the molar ratio of PEO repeated unit in RgP to $LiCF_3SO_3$ was

10: 0.2). One edge of the spin-coated film was swabbed away using dichloromethane. The films were then annealed in vacuum oven at 80 °C overnight for 24 h.

Anode Preparation. ITO-coated glass substrates (15-25 Ω/sq, Delta Technologies) were employed for rigid devices; Au/PDMS substrates were employed for stretchable devices. ITO-coated glass substrates were sonicated in deionized water for 15 min and isopropyl alcohol for 15 min, dried under a stream of nitrogen, and then treated with UV-ozone for 5 min. Stretchable Au/PDMS anode was prepared by depositing a 15 Å titanium adhesion layer followed by 200 Å of gold onto an oxidized PDMS substrate in an e-beam evaporator at 10^{-6} mbar at a rate of 1 Å/s. PDMS substrates were prepared by casting PDMS prepolymer (Sylgard 184, Dow Chemical) against polystyrene Petri dishes and curing at 60 °C overnight. The PDMS surface were then exposed to an air plasma (Harrick Plasma) for 30 s to generate oxidized PDMS substrate.

Cathode Preparation. A 50 μL drop of EGaIn was deposited on the surface of emissive layer as the cathode. Devices fabricated on ITO anodes had a copper wire contact inserted into the EGaIn drop, which was then sealed with an epoxy resin.

Device Characterization. Optical characterization of the thin films was performed using an Olympus BX51 microscope equipped with an Olympus Q-Color3 digital camera. The measurement of phase and height information of the emissive layer were carried out on the tapping mode of a Digital Instruments Multimode AFM using a Veeco type FESP-V2 cantilever with a nominal tip radius of 8 nm and a nominal force constant of 2.8 N/m. LEECs were tested in a dry glove box using a Keithley 2601 source-measure unit to apply a voltage of 6 V DC and measure the current. Radiance was measured with a calibrated UDT S470 optometer using an integrating sphere.

129

Stretchability Measurements: Stretchable LEECs fabricated from RgP**34**/LiCF$_3$SO$_3$/Ir and RgP**69**/LiCF$_3$SO$_3$/Ir were subjected to repetitive cycles of 15% strain using a microvice stretching apparatus. Device performance was determined by first measuring the current and radiance of the unstretched device for 30 min. After applying 10, 30 and 50 cycles of 15% strain, an EGaIn cathode was deposited on to a new device and the devices were then encapsulated by epoxy. The current and radiance were measured at 6 V over 30 min in a dry glove box.

4.5. References

(1)   Wang, C.; Hwang, D.; Yu, Z.; Takei, K.; Park, J.; Chen, T.; Ma, B.; Javey, A. *Nat. Mater.* **2013**, *12*, 899.

(2)   Yang, C. H.; Chen, B. H.; Zhou, J. X.; Chen, Y. M.; Suo, Z. G. *Adv. Mater.* **2016**, *28*, 4480.

(3)   Park, S.-I.; Xiong, Y.; Kim, R.-H.; Elvikis, P.; Meitl, M.; Kim, D.-H.; Wu, J.; Yoon, J.; Yu, C.-J.; Liu, Z. *Science* **2009**, *325*, 977.

(4)   Wu, Y.; Mechael, S. S.; Chen, Y.; Carmichael, T. B. *Adv. Mater. Technol.* **2018**, *3*, 1700292.

(5)   Follmer, S.; Leithinger, D.; Olwal, A.; Hogge, A.; Ishii, H. *26th annual ACM symposium on User interface software and technology* (UIST '13) **2013**, 417

(6)   Whelan, H. T.; Smits, R. L.; Buchman, E. V.; Whelan, N. T.; Turner, S. G.; Margolis, D. A.; Cevenini, V.; Stinson, H.; Ignatius, R.; Martin, T.; Cwiklinski, J.; Philippi, A. F.; Graf, W. R.; Hodgson, B.; Gould, L.; Kane, M.; Chen, G.; Caviness, J. *J. Cli. Laser Med. Surg.* **2001**, *19*, 305.

(7)   Bayley, H.; Gasparro, F.; Edelson, R. *Trends Pharmacol. Sci.* **1987**, *8*, 138.

(8)   Hawkins, D.; Abrahamse, H. *Afr. J. Biomed. Res.* **2007**, *10*, 99.

(9)   Kim, R. H.; Kim, D. H.; Xiao, J. L.; Kim, B. H.; Park, S. I.; Panilaitis, B.; Ghaffari, R.; Yao, J. M.; Li, M.; Liu, Z. J.; Malyarchuk, V.; Kim, D. G.; Le, A. P.; Nuzzo, R. G.; Kaplan, D. L.; Omenetto, F. G.; Huang, Y. G.; Kang, Z.; Rogers, J. A. *Nat. Mater.* **2010**, *9*, 929.

(10)   Hu, X. L.; Krull, P.; Graff, B.; Dowling, K.; Rogers, J. A.; Arora, W. J. *Adv. Mater.* **2011**, *23*, 2933.

(11)   Sekitani, T.; Nakajima, H.; Maeda, H.; Fukushima, T.; Aida, T.; Hata, K.; Someya, T. *Nat. Mater.* **2009**, *8*, 494.

(12)   Wang, J.; Yan, C.; Cai, G.; Cui, M.; Eh, A.; Lee, P. S. *Adv. Mater.* **2015**, *28*, 4490.

(13)   Filiatrault, H. L.; Porteous, G. C.; Carmichael, R. S.; Davidson, G. J. E.; Carmichael, T. B. *Adv. Mater.* **2012**, *24*, 2673.

(14)   Wang, J. X.; Yan, C. Y.; Chee, K. J.; Lee, P. S. *Adv. Mater.* **2015**, *27*, 2876.

(15)   Costa, R. D.; Orti, E.; Bolink, H. J.; Monti, F.; Accorsi, G.; Armaroli, N. *Ang. Chem. Int. Ed.* **2012**, *51*, 8178.

(16)   Sun, Q.; Li, Y.; Pei, Q. *J. Display Technol.* **2007**, *3*, 211.

(17)   Meier, S. B.; Tordera, D.; Pertegas, A.; Roldan-Carmona, C.; Orti, E.; Bolink, H. J. *Mater. Today* **2014**, *17*, 217.

(18)   Liang, J.; Li, L.; Niu, X.; Yu, Z.; Pei, Q. *Nat. Photonics* **2013**, *7*, 817.

(19)   He, L.; Duan, L.; Qiao, J.; Dong, G.; Wang, L.; Qiu, Y. *Chem. Mater.* **2010**, *22*, 3535.

(20)   He, L.; Qiao, J.; Duan, L.; Dong, G.; Zhang, D.; Wang, L.; Qiu, Y. *Adv. Funct. Mater.* **2009**, *19*, 2950.

(21)   Tang, S.; Pan, J.; Buchholz, H.; Edman, L. *ACS Appl. Mater. Interfaces* **2011**, *3*, 3384.

(22)   Tang, S.; Pan, J.; Buchholz, H. A.; Edman, L. *J. Am. Chem. Soc.* **2013**, *135*, 3647.

(23)   Lowry, M. S.; Bernhard, S. *Chem. Eur. J.* **2006**, *12*, 7970.

(24)   Lyons, C. H.; Abbas, E. D.; Lee, J. K.; Rubner, M. F. *J. Am. Chem. Soc.* **1998**, *120*, 12100.

(25)   Pei, Q.; Yu, G.; Zhang, C.; Yang, Y.; Heeger, A. J. *Science* **1995**, *269*, 1086.

(26)   Kosilkin, I. V.; Martens, M. S.; Murphy, M. P.; Leger, J. M. *Chem. Mater.* **2010**, *22*, 4838.

(27)   Mindemark, J.; Tang, S.; Wang, J.; Kaihovirta, N.; Brandell, D.; Edman, L. *Chem. Mater.* **2016**, *28*, 2618.

(28)   Parker, S. T.; Slinker, J. D.; Lowry, M. S.; Cox, M. P.; Bernhard, S.; Malliaras, G. G. *Chem. Mater.* **2005**, *17*, 3187.

(29)   Costa, R. D.; Pertegas, A.; Orti, E.; Bolink, H. J. *Chem. Mater.* **2010**, *22*, 1288.

(30)   Wenzl, F.; Polt, P.; Haase, A.; Patil, S.; Scherf, U.; Leising, G. *Solid State Ionics* **2005**, *176*, 1747.

(31)   Ettedgui, E.; Davis, G. T.; Hu, B.; Karasz, F. E. *Synth. Met.* **1997**, *90*, 73.

(32)   Yu, Z.; Niu, X.; Liu, Z.; Pei, Q. *Adv. Mater.* **2011**, *23*, 3989.

(33)   Karamdoust, S.; Crewdson, P.; Ingratta, M.; Gillies, E. R. *Polymer Int.* **2015**, *64*, 611.

(34)   Bonduelle, C. V.; Karamdoust, S.; Gillies, E. R. *Macromolecules* **2011**, *44*, 6405.

(35)   Bonduelle, C. V.; Gillies, E. R. *Macromolecules* **2010**, *43*, 9230.

(36)   Slinker, J.; Bernards, D.; Houston, P. L.; Abruña, H. D.; Bernhard, S.; Malliaras, G. G. *Chem. Commun.* **2003**, *0*, 2392.

(37)   Kalyuzhny, G.; Buda, M.; McNeill, J.; Barbara, P.; Bard, A. *J. Am. Chem. Soc.* **2002**, *125*, 6272.

(38)   Slinker, J. D.; Gorodetsky, A. A.; Lowry, M., S.; Wang, J.; Parker, S.; Rohl, R.; Bernhard, S.; Malliaras, G. G. *J. Am. Chem. Soc.* **2004**, *126*, 2763.
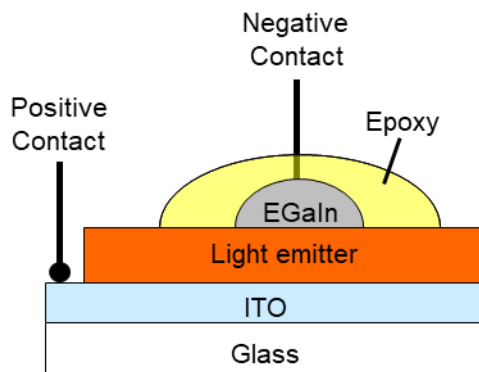
4.6. Supporting Information

Figure S4.1. *Diagram of the rigid LEEC test structure fabricated with an ITO-coated glass anode, Ir based emissive material, and liquid EGaIn as the cathode.*
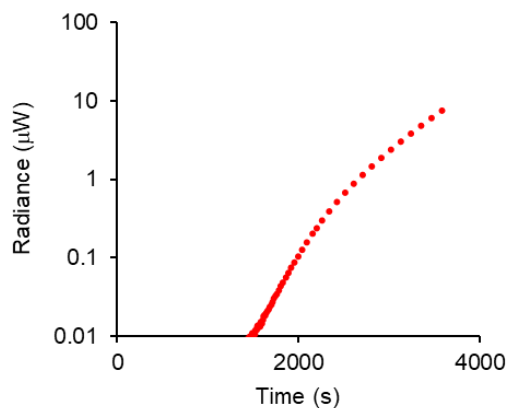

Figure S4.2. *Temporal evolution of radiance of a typical rigid LEEC fabricated from pristine film of [Ir(ppy)$_2$(dtb-bpy)]$^+$[PF$_6^-$] operated at a 6 V DC in inert conditions.*
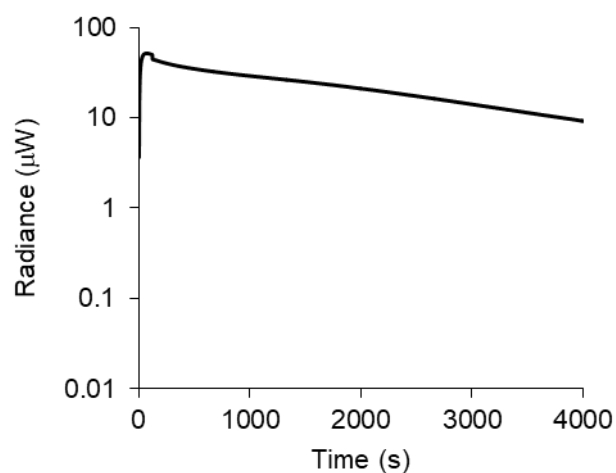
Figure S4.3. Temporal evolution of radiance of a typical rigid LEEC fabricated from film of PEO/LiCF$_3$SO$_3$/Ir composite operated at 6 V DC in inert conditions.
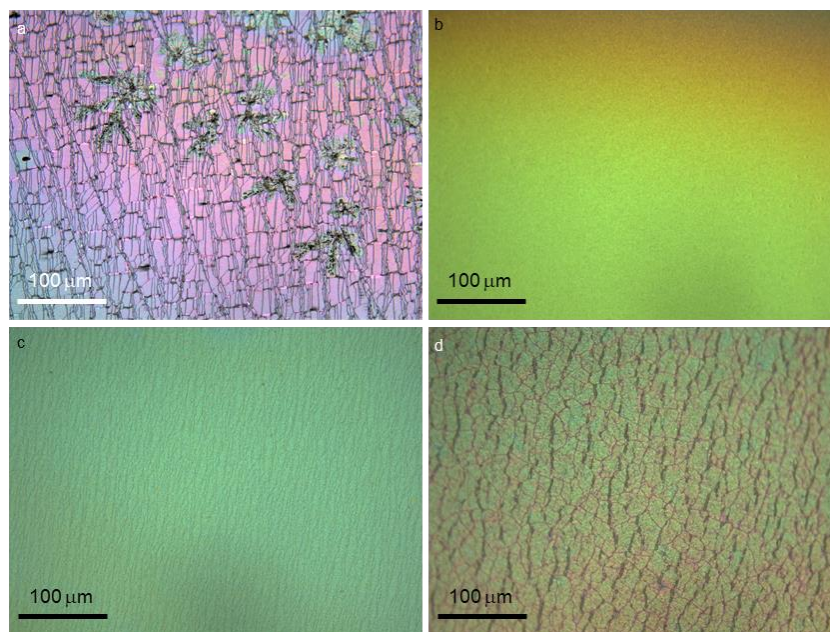
Figure S4.4. Optical micrographs of films of (a) PEO/LiCF$_3$SO$_3$/Ir composite, (b) RgP**16**/LiCF$_3$SO$_3$/Ir composite, (c) RgP**34**/LiCF$_3$SO$_3$/Ir composite, and (d) RgP**69**/LiCF$_3$SO$_3$/Ir composite on a PDMS substrate with stretching at 5 % strain. The samples were stretched in the horizontal direction.

.

Table S4.1. *Summary of figures of merit for LEECs fabricated from RgP34/LiCF₃SO₃/Ir composite and RgP69/LiCF₃SO₃/Ir composite on Au/PDMS operated at 6 V DC in inert conditions*

Emissive Material	t_{on} (s)	t_{max} (s)	Max Rad (μW)	$t_{1/2}$ (s)	Max EQE (%)
RgP**34**/LiF₃CSO₃/Ir	12 ± 3	570 ± 60	5.8 ± 2.1	> 1800	$0.012. \pm 0.003$
RgP**69**/LiF₃CSO₃/Ir	< 1	208 ± 41	8.9 ± 1.4	847 ± 50	0.026 ± 0.009

Figure S4.5. *Temporal evolution of current of a typical rigid LEEC fabricated from film of (a) RgP**34**/LiCF₃SO₃/Ir and (b) RgP**69**/LiCF₃SO₃/Ir composites operated at 6 V DC in inert condition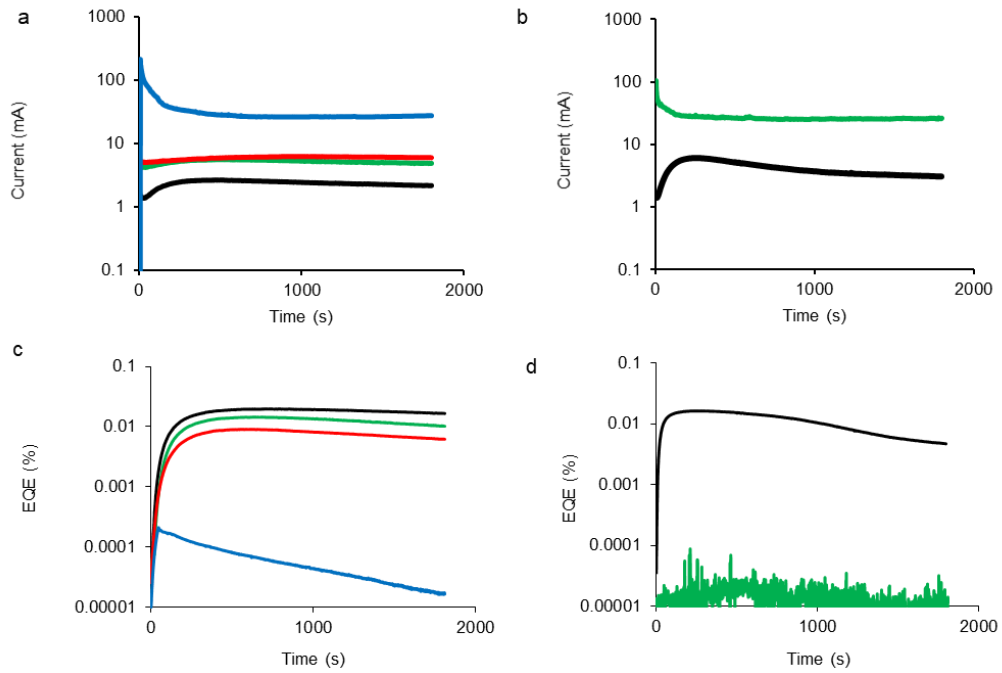s. Temporal evolution of EQE of a typical rigid LEEC fabricated from film of (c) RgP**34**/LiCF₃SO₃/Ir and (d) RgP**69**/LiCF₃SO₃/Ir composites operated at 6 V DC in inert conditions.*

5. Chapter 5

Exploiting the Formation of Nanocracks in Solution-Deposited Gold

Films on PDMS for Stretchable Electronics

5.1. Introduction

Electronic devices cannot exist without conductive materials to form circuit elements, such as electrodes, contacts, and interconnects. Stretchable conductors that are highly conductive, and remain so under high mechanical strain, make a variety of new applications possible, such as stretchable and wearable displays,[1,2] conformable strain sensors,[3,4] stretchable solar cells and batteries,[5,6] and implantable bioelectronics.[7,8] Highly conductive electrodes are particularly important in large-area devices such as intrinsically stretchable light-emitting devices to minimize Ohmic losses and prevent problematic voltage drop across the device, which produces non-uniform light emission. Metals are the materials of choice due to their low resistivities ($\sim 10^{-8}$ Ωm),[9] but the mechanical mismatch of hard metals with soft elastomers results in cracking of the metal film with stretching, which increases the resistance and limits the use of these structures in devices.[10-12] Although alternative materials , such as carbon nanotubes,[13] graphene,[14] and conductive polymers,[15] may provide more compatible mechanical properties, none of these possess conductivities that rival those of metals.

Extensive studies of gold films deposited on PDMS by PVD have demonstrated that the cracks that form in the gold film with stretching increase the resistance and eventually break the conductive pathway through the film.[11,12,20] At low elongations (< 5%), the strain localizes at defect sites in the gold film, resulting in the formation of incipient cracks. Further elongation of the structure causes the cracks to lengthen and widen, which increases the resistance of the gold films. Eventually, crack propagation completely breaks the conductive pathway through the film, typically at elongations of $\sim$20-30%.[11] Adding topographical features to the PDMS surface can prolong the

persistence of conductivity with strain by creating numerous sites for strain localization. Stretching these structures increases the number of incipient cracks compared to gold films on flat PDMS; interactions between the cracks limit long-range propagation to produce an array of short microcracks that preserve the conduction pathway to high strains (65%).[21-24] The rough topographies used in this approach, however, make these gold-coated PDMS surfaces unsuitable as electrodes for large-area light-emitting devices due to variation in the electric field generated over the rough electrode surface. Other strategies to improve the ability of metal films on elastomers to retain their conductivity with stretching involve configuring the metal films on the elastomer surface into in-plane serpentine[16,17] structures using photolithographic patterning[16,25] or out-of-plane sinusoidal[18,19] structures using compressive strain to cause buckling instabilities in the gold film.[19,26] Although these structures make excellent device interconnects, they are less applicable as electrodes due to the limited surface area of serpentines and considerable topography of out-of-plane structures. Furthermore, these methods rely on physical vapor deposition (PVD) of metals and photolithography, which bear high capital expense; require multiple steps of deposition, masking, resist patterning, and etching; and suffer from the dimensional instability of the elastomer with the organic solvents used in photolithography.

Despite real progress toward fabricating metal films on PDMS that retain conductivity to high elongations, two important goals remain: First, there is a need for flat metal films that remain highly conductive with stretching and possess sufficient surface area to be used as electrodes in thin-film, stretchable devices. Second, it is necessary to develop low-cost, simple procedures to accomplish the fabrication.

Researchers have responded to the latter need by replacing PVD and photolithography with solution-based electroless deposition (ELD)[27-30] and low-cost patterning methods, such as dip-pen nanolithography,[31] inkjet printing,[32] screen printing,[33] and microcontact printing.[34] ELD is a solution-based metal deposition method widely used in the microelectronics industry to form patterned conducting lines, inter-level connections, and through holes on printed circuit boards.[35] In the ELD process, metal ions in the plating bath are chemically reduced to metal by a palladium catalyst adsorbed on the surface of a PDMS substrate. The initial layer of deposited metal autocatalyzes further metal deposition as a reducing agent in the plating bath is oxidized.[35] One approach to ELD on PDMS involves attaching a functionalized polymer layer to the PDMS surface by surface-initiated polymerization or surface-grafted free radical polymerization. The polymer layer immobilizes the catalytic species, which catalyzes the deposition of a metal film in the ELD solution.[36] Patterned metal films can be produced by either patterning the polymer film using shadow masking or patterning the catalyst deposition using dip-pen nanolithography, inkjet printing, or screen printing.[37] Another approach uses a shadow mask to selectively treat the PDMS surface with UV radiation, thus defining the pattern for metal deposition.[38] Although these methods are low cost and relatively simple, the resulting metal films rely on the standard methods of in-plane patterning into serpentines[37] or out-of-plane buckling deformation[39] to produce metal films that retain high conductivity at high elongations.

We previously reported a process for the selective ELD of copper films on PDMS that uses microcontact printing to pattern a polymeric resist on a chemically-modified PDMS surface to direct the deposition of the copper.[27] The resulting copper films remain

conductive to 52% elongation, without the use of in-plane serpentine patterning or out-of-plane deformation. Here, we apply this methodology to produce patterned gold films on PDMS using electroless nickel and immersion gold (ENIG) solutions. The resulting ENIG films on PDMS possess planar topography and remain remarkably conductive to 95% tensile strain. The ability of these films to retain high conductivity under extreme strain is due to the unusual formation of nano-sized cracks in the gold film with stretching that originate from the highly polycrystalline nature of the ENIG films. We demonstrate that these films are effective as electrodes in large-area stretchable thin-film light-emitting devices.

5.2. Results and Discussion

5.2.1. Fabrication of ENIG films on PDMS substrate

We deposited gold films on PDMS using the ENIG process, which is widely used as a surface finish for microelectronic packaging technology.[40,41] The ENIG process avoids the problems associated with the direct ELD of gold, which suffers from short plating bath lifetimes, high sensitivity to contamination, and a low plating rates. The ENIG process instead uses two solution-based plating steps, beginning with the ELD of a nickel film from a stable plating solution followed by an immersion gold (IG) process in which a solution of potassium gold cyanide deposits a gold film by galvanic displacement. Ni atoms in the film reduce Au^+ ions from solution, releasing Ni^{2+} ions into the solution and depositing a gold film on the surface through molecular exchange.[35,42]

The process for selective ENIG on PDMS uses our previously reported method for the selective activation of the PDMS surface to prepare patterned copper films using ELD. This process first activates the PDMS surface to ELD, and then deactivates selected regions using microcontact printing of a polymeric resist (Scheme 5.1a). Native PDMS is inert to ELD due to the methyl groups at the surface. Plasma oxidation creates a thin silica layer on the PDMS surface with Si-OH groups,[43] which subsequently react with 3-aminopropyltriethoxysilane (APTES) via the formation of Si-O-Si bonds.[27] The resulting amino-terminated surface can be activated for ELD by simply protonating the amine groups to form a positively charged surface, which binds a palladium-tin colloidal catalyst commonly used to initiate metal ELD. Pd/Sn colloids consist of a Pd-rich core protected from oxidation by a hydrolyzed Sn^{2+}/Sn^{4+} shell; associated chloride ions give the colloids a negatively charged surface to inhibit aggregation and allow the colloids to be electrostatically bound to the activated PDMS surface.[35] A subsequent acceleration step etches away the Sn^{2+}/Sn^{4+} shell to expose the Pd core, thus priming the surface for ELD. To deactivate selected regions of the surface, we prevent the amine groups from becoming protonated and binding Pd/Sn colloids by microcontact printing a polymeric resist, poly(octadecenyl-alt-maleic anhydride) (POMA). The anhydride groups of POMA rapidly react with the amine groups on the PDMS surface during the microcontact printing process to form amide groups that cannot easily be converted to a cationic form (Scheme 5.1b). The hydrophobicity of the bound POMA film (water contact angle of 98.3°)[27] also repels the aqueous Pd/Sn solution to provide a barrier to Pd/Sn colloid adsorption. Thus, immersing amine-terminated PDMS substrates printed with the POMA resist into the Pd/Sn colloidal solution results in catalyst binding only in POMA-free

areas. The bound Pd catalyst subsequently initiates nickel ELD by catalyzing the reduction of Ni^{2+} ions in the ELD plating solution to nickel metal. The initial layer of deposited nickel autocatalyzes further nickel deposition as the dimethylamine borane reducing agent is oxidized in the plating solution. Galvanic displacement of nickel for gold in the potassium gold cyanide solution results in the formation of a gold film on the surface.[44]
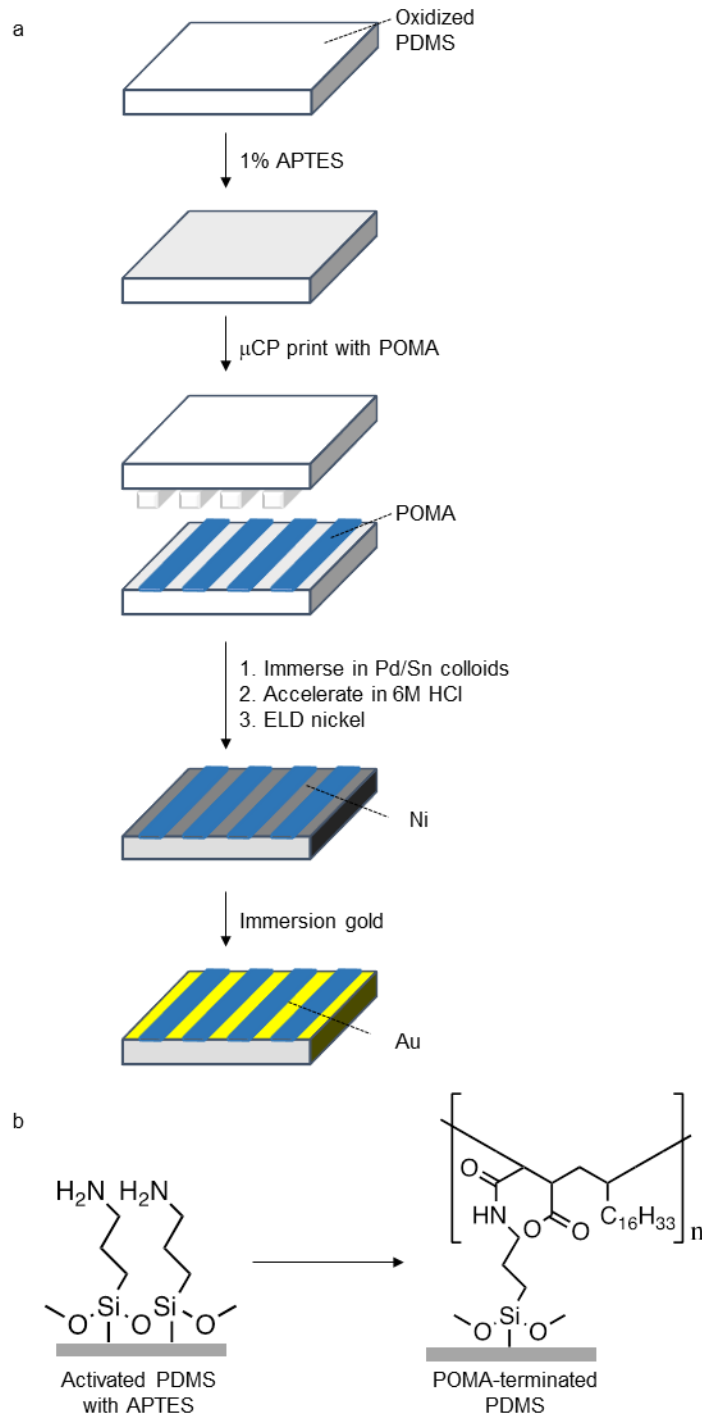
Scheme 5.1. *(a) Illustrated process of patterning ENIG wires on PDMS substrate. (b) μCP print with POMA*

5.2.2. Resolution of Patterned ENIG Films

The resolution of the microcontact printing process enables the fabrication of patterned ENIG films on PDMS with features as small as 10 μm. We used a microcontact printing stamp to create ENIG features consisting of straight and square-wave lines with line widths ranging from 10 μm to 20 μm and square shapes with side lengths of 50 μm to 100 μm. An optical micrograph of the patterned ENIG film on PDMS (Figure 5.1a) shows the clean deposition of gold within the printed pattern, indicating that the POMA resist prevents Pd/Sn colloids from binding to the PDMS surface to deactivate these areas to ENIG. Scanning electron microscopy (SEM) micrograph of the patterned ENIG films reveals a ~1.5-μm-wide zone at the edge composed of fine structures (Figure 5.1b).
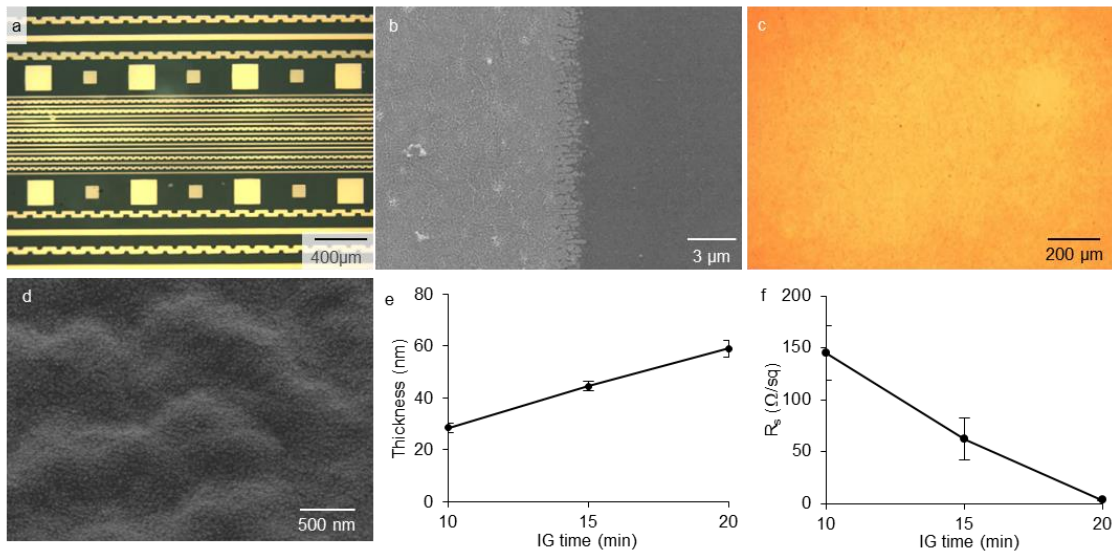

Figure 5.1. (a) Optical and (b) SEM micrographs of patterned ENIG$_{20}$ films on PDMS substrate. (c) Optical and (d) SEM micrographs of an unpatterned ENIG$_{20}$ film on PDMS substrate. (e) Thickness as a function of IG time. (f) R_s as a function of IG time.

5.2.3. Optimization of ENIG Deposition Parameters

The electrical properties, morphology, and adhesion of ENIG films to PDMS depend on the thickness of the nickel film and extent of galvanic displacement with gold. Both of these variables are governed by the immersion time in the ELD Ni and IG solutions. We tested deposition times of 5, 10, 15, and 20 minutes for the ELD of nickel films on PDMS. Nickel ELD for 5 minutes at 28 °C results in a nickel layer with a thickness of 19.2 ± 1.5 nm and a sheet resistance (R_s) of 26.2 ± 3.7 kΩ/sq (Figure S5.1a in supporting information). Increasing the ELD time to 10 min produces nickel films with a substantially lower R_s of 908.5 ± 286.0 Ω/sq (Figure S5.1b), consistent with the deposition of a thicker (26.5 ± 0.9 nm) nickel film. Further increasing the nickel ELD time to 15 min or 20 min causes cracking and delamination of the nickel film (Figure S5.1c, d) due to the detrimental accumulation of hydrogen in the ELD nickel layer, which causes the well-known problem of blistering, cracking, and delamination.[35] We therefore used nickel films made using an immersion time of 10 min in the nickel ELD solution to study three different immersion times (10, 15, and 20 min) in the IG solution. We designate the films resulting from these immersion times as $ENIG_{10}$, $ENIG_{15}$, and $ENIG_{20}$. Optical micrographs reveal that each immersion time produces uniform gold surfaces without cracks or delamination (Figure 5.1c, S5.2a-b). SEM images show that each of these films exhibit nodular surfaces are composed of granular, nanoscale gold particles, which is typical for ENIG films (Figure 5.1d, S5.2c-d).[44-47] We furthermore did not detect visible gold on adhesive tape after conducting a tape test on these ENIG films (Figure S5.3a-c), indicating a strong adhesion between PDMS, nickel, and gold layers.

Increasing the immersion time in the IG solution results in expected increases in the gold content and film thickness, as well as a reduction in the sheet resistance. Energy dispersive X-ray spectroscopy (EDX) of $ENIG_{10}$, $ENIG_{15}$, and $ENIG_{20}$ films deposited on a silicon wafer – a mechanically rigid model for the oxidized PDMS surface – showed an increase in the atomic weight percentage of gold atoms as the immersion time in the IG bath increases from $ENIG_{10}$ to $ENIG_{15}$ to $ENIG_{20}$ films, with values of 38.05%, 48.53%, and 54.79%, respectively (Figure S5.4a-c). The increasing trend in gold content with immersion time in the IG solution is accompanied by an increase in the thickness of ENIG films. We measured the thickness of ENIG films using tapping mode atomic force microscopy (AFM) at the edge of patterned ENIG films on silicon wafer, which showed film thicknesses of 28.4 ± 1.9 nm, 44.5 ± 1.7 nm, and 59.0 ± 3.2 nm for $ENIG_{10}$, $ENIG_{15}$, and $ENIG_{20}$, respectively (Figure 5.1e). We also used cross-sectional SEM to confirm the thickness of ~60 nm for $ENIG_{20}$ films on a silicon wafer (Figure S5.5). The thickness of $ENIG_{10}$, $ENIG_{15}$, and $ENIG_{20}$ films increased by 2 nm, 18 nm, and 32 nm, respectively, compared to the thickness of the initial ELD nickel films. The increasing trend in thickness for $ENIG_{10}$, $ENIG_{15}$, and $ENIG_{20}$ films is due to two factors: First, there is a doubling of the number of metal atoms that occurs during the IG process because two Au^+ ions from the IG solution are reduced at the surface for each nickel atom that is oxidized to Ni^{2+} and subsequently displaced. Second, displacing nickel atoms with an atomic radius of 149 pm with larger gold atoms (atomic radius of 174 pm) also increases the film thickness.

As the time in the IG solution increases, the sheet resistance of $ENIG_{10}$, $ENIG_{15}$, and $ENIG_{20}$ films decreased from 145 ± 26 Ω/sq to 62 ± 20 Ω/sq to 3 ± 1 Ω/sq, respectively (Figure 5.1f). This decrease in R_s is consistent with equation 5.1

$$R_s = \frac{\rho}{t} \qquad (5.1)$$

where ρ represents the resistivity and t represents the thickness. Since R_s is proportional to the resistivity of the metal, displacing nickel ($\rho = 6.99 \times 10^{-8}$ Ωm) with lower resistivity gold ($\rho = 2.44 \times 10^{-8}$ Ωm) decreases R_s.[9] At the same time, R_s is inversely proportional to thickness. Longer IG times form thicker ENIG films with a higher gold content, leading to lower resistivity.

We used $ENIG_{20}$ films for the rest of the study due to the low R_s value (3 ± 1 Ω/sq), and also fabricated a comparison system of gold on PDMS with a similar film thickness as $ENIG_{20}$ using e-beam evaporation. This comparison system, termed EBAu, consisted of 3 nm of Ti deposited as an adhesion layer followed by 57 nm Au. Optical microscope and SEM images of EBAu films reveal a consistent, uniform surface without cracks, comprising nanoscale gold grains similar to the surface of $ENIG_{20}$ films (Figure S5.6a, b). EBAu films exhibit excellent adhesion to PDMS (Figure S5.6c) and an R_s of 2.9 ± 0.1 Ω/sq, also similar to that of $ENIG_{20}$. Topographical analysis using AFM revealed that $ENIG_{20}$ and EBAu films on PDMS both consist of columnar grains, with a root-mean-square roughness (R_{RMS}) values of 3.2 ± 0.5 nm and 5.0 ± 0.8 nm, respectively (Figure S5.7a, b), similar grain heights (~6 nm and ~9 nm, respectively), and a similar grain diameter of for both film types (62.5 ± 12.1 nm for $ENIG_{20}$ films and 67.0 ± 8.2 nm for EBAu films) (Figure S5.7c, d).

5.2.4. Stretchability of ENIG Films on PDMS

Electrical conductivity that persists during mechanical deformation is essential for the fabrication of soft electronic devices. We measured the change in electrical resistance of 3.0 cm $\times$ 1.5 cm $ENIG_{20}$ films on PDMS substrates at 5% strain intervals until the PDMS substrate fractured (Figure 5.2a). $ENIG_{20}$ films on PDMS substrate remained conductive to a remarkable 95% elongation with a normalized resistance (R/R_0) increase of only 18.7 $\pm$ 3.4. The PDMS substrate fractured after 95% linear strain. To the best of our knowledge, this is the first report of continuous, large-area, planar gold films that remain highly conductive with stretching without the use of serpentine designs, wavy features fabricated using compressive strain, or high surface roughness. The conductivity with stretching of $ENIG_{20}$ films far surpasses that of EBAu films on PDMS with the same thickness which undergoes electrical failure $(R/R_0 > 10^6)$ at only 5% elongation, and is better than that of thicker EBAu films.[45] After releasing the tensile strain, the R/R_0 of the $ENIG_{20}$ films recovered back to 1.9 $\pm$ 0.4.
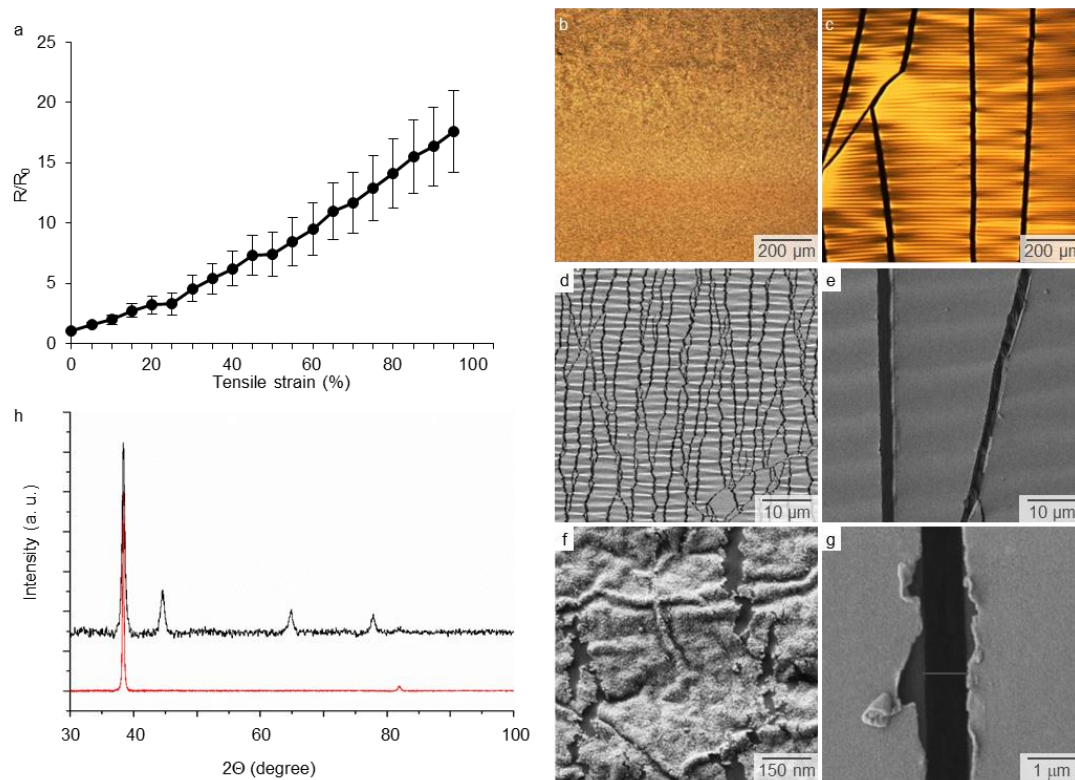
Figure 5.2. (a) Change in resistance of $ENIG_{20}$ films as a function of tensile strain. Optical micrographs of (b) $ENIG_{20}$ film and (c) EBAu film on PDMS substrates at 10% tensile strain. SEM micrographs of (d) $ENIG_{20}$ films and (e) EBAu films on PDMS substrates at 30% tensile strain. Higher magnification SEM micrographs of (f) $ENIG_{20}$ film and (g) EBAu films on PDMS substrates at 30% elongation. Samples were stretched in the horizontal direction. (h) XRD spectra of $ENIG_{20}$ (black line) and EBAu films (red line) on glass substrates.

The dramatic difference in conductivity with elongation of $ENIG_{20}$ and EBAu films can be attributed to how cracks in these metal layers evolve with stretching. Optical micrographs of $ENIG_{20}$ films under strain show that the effect of elongation on $ENIG_{20}$ films at both low (10%) and high (80%) strains are nearly imperceptible using optical microscopy (Figure 5.2b, S5.8a). In contrast, stretching EBAu films on PDMS to 10%

149

strain generates long channel cracks that propagate through the width of the film and break the conduction pathway (Figure 5.2c). Further elongation results in the formation of additional channel cracks as well as widening of the cracks from $10 - 12$ μm at 10% strain to $10 - 30$ μm at 80% strain (Figure S5.8b). SEM images reveal that stretching $ENIG_{20}$ films to 30% tensile strain causes the formation of numerous jagged nanocracks roughly perpendicular to the stretching direction (Figure 5.2d), consistent with strain localization occurring at numerous sites on the surface. These non-linear cracks, ~10 nm to 65 nm in width, intercept one another to prevent crack propagation, limiting the maximum crack length to < 45 μm. Higher magnification SEM images (Figure 5.2f) show the presence of narrow (~30-70 nm) bridges of $ENIG_{20}$ spanning the cracks, which preserve tortuous conductive pathways and thus keep the film conductive under strain. In contrast, at 30% tensile strain, EBAu films exhibit notably straighter, longer, and wider cracks (~1-2 μm) without gold bridges (Figure 5.2e), indicating a clean break in the conductive pathway. The EBAu film lifts slightly at the crack edges (Figure 5.2g), which can be attributed to traction at the EBAu/PDMS interface that arises due to the localization of strain at defect sites in the film with stretching. The processes of strain localization and traction cause film delamination and crack formation, and then these two processes coevolve leading to the propagation of the channel cracks observed for EBAu films on PDMS.[10]

5.2.5. Crystallographic Analysis of $ENIG_{20}$ and EBAu Films

Despite the similarities in thickness, uniformity, adhesion, and surface roughness, the differences in how cracks initiate and propagate in $ENIG_{20}$ and EBAu films on PDMS suggest that there are fundamental differences between these two films not detected by

SEM or AFM analysis. We investigated the crystallinity of ENIG$_{20}$ and EBAu gold films deposited on glass substrates using powder X-ray diffraction (XRD) (Figure 5.2h). EBAu gold films are polycrystalline films with a dominant (111) texture with corresponding peaks at 38.3°, which is typical for face-centered cubic (fcc) metal films deposited using PVD processes. A small (222) phase with corresponding peaks at 82° also appears. In contrast, the surface orientation of the polycrystalline ENIG$_{20}$ film is more heterogeneous than films prepared using PVD. Along with the primary (111) crystalline texture, XRD pattern also included peaks at 44.6°, 64.8°, 77.8°, corresponding to (200), (220), and (311) orientations, respectively. The difference in crystallization can be attributed to the different metal growth mechanism of these two deposition processes. In EBAu, the high energy of vaporized gold atoms deposited on the substrate rearrange and grow to expose the more thermodynamically favorable (111) plane at the surface.[48] In contrast, the ELD process is known to generate heterogeneously oriented crystals because the relatively low deposition temperature does not provide the metal atoms with enough energy to rearrange, resulting in the formation of various orientations.[49-51]

The heterogeneous crystallographic textures in ENIG$_{20}$ films than EBAu films likely cause the formation of the numerous nanocracks during stretching. Shear stress beyond the critical resolved shear stress causes grains with a favorable slip system ((111) orientation for fcc metal) to slip starting from the defect sites in crystals.[52] Slip of grains results in plastic deformation and metal fracture. Compared to EBAu films with a (111) slip plane, grains in ENIG$_{20}$ films with (200), (211), and (311) phases are less easy or impossible to slip.[53-55] This effect impedes the propagation of cracks, leading to the formation of numerous small cracks in the ENIG$_{20}$ films.

5.2.6. ENIG$_{20}$ as Stretchable Interconnects and Electrodes

The ability of ENIG$_{20}$ films to remain highly conductive under strain makes these films useful as stretchable interconnects in circuits to connect rigid devices, such as LEDs (Figure S5.9). Metal films configured into serpentine interconnect or out-of-plane buckles have been similarly used due to the low resistance change with strain. The most significant features of ENIG$_{20}$, however, are its planar topography and the nanoscale cracks that relieve strain. These attributes make ENIG$_{20}$ applicable as electrodes in thin-film light-emitting devices by providing key advantages over other metal films on PDMS: EBAu films on PDMS fail electrically at significantly lower strains due to channel cracking; metal films structured into in-plane serpentines do not provide sufficient surface area for large-area light emission; and metal films with high topographical features such as out-of-plane wavy structures or metal films fabricated using an intentionally rough topography to engineer cracks are not compatible with thin film devices due to variation in the electric field generated over the rough electrode surface. We demonstrated the use of ENIG$_{20}$ films as electrodes in alternating current electroluminescent (ACEL) devices, which consist of phosphor microparticles deposited between two electrodes. Stretchable ACEL devices have previously been fabricated by blending ZnS:Cu phosphor microparticles with the elastomer polydimethylsiloxane (PDMS), and using stretchable PDMS-based electrodes. We fabricated stretchable ACEL devices according to Figure 5.3a by depositing a film of ZnS:Cu microparticles blended with PDMS onto an ENIG$_{20}$ film on PDMS substrate, and then depositing a film of the conductive polymer PEDOT:PSS plasticized with the surfactant Triton X-100 as the transparent electrode.[56] Operating the ACEL device at a voltage of 150 V AC and a

frequency of 30 kHz generates uniform blue light emission. ACEL devices fabricated using 3 cm x 3 cm $ENIG_{20}$ films as electrodes continued to emit light with bending to 15% and 40% strain (Figure 5.3b, c). Furthermore, the uniform light emission of ACEL devices fabricated using 1.5 cm x 3 cm $ENIG_{20}$ films persisted from 0% to 40% elongation (Figure 5.3d). Figure 5.3e shows that the normalized emission radiance varied slightly by <10% during stretching to 40% strain. The change in intensity can be attributed to the change in electrical field strength. Stretching the device decreases the thickness of the emission layer, which results in a larger applied electrical field on the emissive particles, and thus, an increased intensity.[57] The stable performance of the ACEL devices could be due to the good compliance of the device structure and the unique electroluminescent mechanism of ACEL devices. Stretching beyond 40% elongation causes the top PEDOT:PSS electrode to crack, leading to the loss of conductivity of this electrode at > 40% strain.
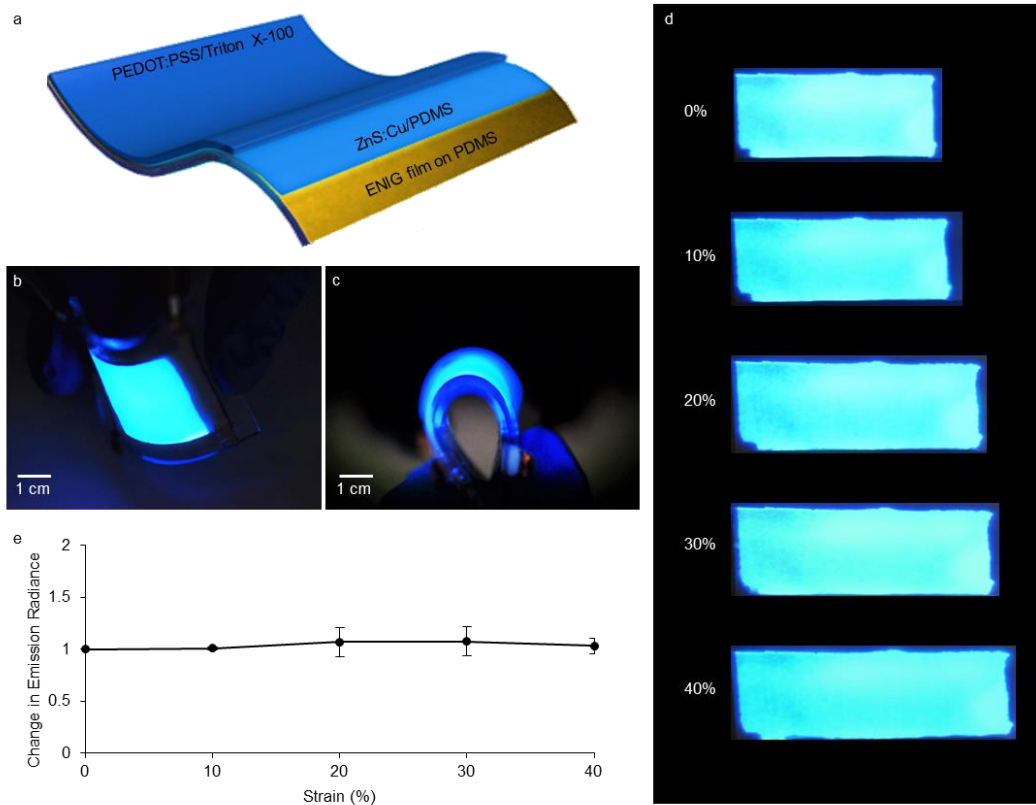
Figure 5.3. (a) Structure of ACEL device. Photographs of ACEL devices (3 cm x 3 cm) bent to (b) 15% and (c) 40% strain. (d) Photographs of ACEL devices (1.5 cm x 3 cm) stretched to 0%, 10%, 20%, 30% and 40% strain. (e) Change in emission radiance of the ACEL devices under various stretching strains during three minutes of operation in ambient conditions.

We also tested the durability of the stretchable ACEL devices to repetitive strain within the operating strain limit defined by the PEDOT:PSS electrode. We subjected the same device to a total of 100 cycles of 40% tensile strain. After every 20 strain cycles, we recorded the radiance of the device during three minutes of operation in ambient conditions. Six samples were tested, and the resulting maximum radiances were averaged. Compared to the maximum radiance of the device at 0% strain, the maximum radiance of the device decreased to 0.83 ± 0.01, 0.72 ± 0.02, and 0.67 ± 0.01 times after

20, 40, and 60 cycles of 40% tensile strain, and remained stable through 40 additional stretching cycles thereafter (Figure S5.10a). A previous report showed that the emission intensity of a stretchable ACEL device made from AgNW electrodes and ZnS:Cu emissive material decreased to ~0.86, ~0.77, and ~0.70 times the initial value after subjected to 20, 40, and 60 cycles of repetitive 80% strain and remained stable with more cycles.[57] The authors attributed this observation to the degradation of the electrode conductivity, which can also explain our observation. Although the electrical conductivity of $ENIG_{20}$ film is not significantly altered during stretching, the large increase in resistance of the PEDOT: PSS/Triton X-100 transparent electrode after the first 60 cycles of repeated 40% strain cycles (Figure S5.10b) likely lowers the applied voltage on the emissive layer, which consequently causes the decline in radiance. The insignificant resistance increase of PEDOT:PSS/Triton X-100 electrode after 60 cycles of 40% strain can also explain the more stable emission radiance in this regime.

5.3. Conclusions

We have developed a solution-based method to fabricate patterned ENIG films with dimensions as small as 1 μm. The resulting ENIG films are smooth and exhibit remarkable conductivity with stretching that significantly exceeds that of EBAu films prepared using PVD. The high stretchability of these ENIG films likely originates from the heterogeneous orientations of the crystallites, which impede crack propagation and lead to a fine nanocracking that distributes strain relief. The large-scale, conductive, and smooth surface of ENIG films make them particularly well-suited as electrodes in thin film devices. We demonstrated patterned ENIG films as stretchable interconnects for conductive circuits and stretchable electrodes for ACEL devices. The stretchability of the

155

ACEL devices may be further improved by using a transparent electrode with higher conductivity and stretchability. We believe that our method provides an inexpensive and reliable approach for future deformable devices that range from wearable sensors, actuators, to conformable light-emitting panels.

5.4. Experimental

All chemicals were purchased commercially and used as received. PDMS stamps and flat substrates were prepared by casting PDMS prepolymer against patterned photolithographic masters or polystyrene Petri dishes.

Activation of PDMS Substrates: Flat PDMS substrates were oxidized for 40 s in an air plasma (Harrick Plasma, Ithaca NY), immersed in a 1% v/v APTES solution in deionized water for 10 min, rinsed with deionized water and dried under a stream of N_2

Selective Deactivation of PDMS Substrates: The surface of a PDMS stamp was flooded with a solution of POMA in acetone (2 mg/mL). After 10 s, a stream of dry N_2 was used to blow off the excess solution and dry the stamp. The stamp was then placed on the surface of the activated PDMS substrate for 1 min and then removed.

Electroless Nickel/Immersion Gold Deposition: PDMS substrates were immersed in a Pd/Sn solution prepared as directed by the manufacturer (Cataposit 44 and Cataprep 404, Shipley) for 2 min, then immersed in an accelerator solution (6 M HCl) for 1 min. The substrate was then metalized in the nickel plating solution (0.08 M nickel (II) sulfate hexahydrate, 0.14 M sodium pyrophosphate decahydrate, and 0.07 M dimethylamine borane; pH adjusted to 8) at room temperature (25-30°C) for 10 min with sonication. After rinsing with water and drying using a stream of nitrogen, nickel coated PDMS

substrates were immediately immersed in the IG solution (Uyemura Gobright TAM-55 Neutral Immersion Gold Bath) for 10 – 20 min at 60 °C.

E-beam Evaporated Gold Films: PDMS and glass substrates were oxidized for 40 s in air plasma with an air pressure of 10 psig (flow rate of 32 mL/min), and then e-beam evaporation was employed to deposit a 3-nm-thick titanium adhesion layer, followed by a 57-nm-thick gold layer.

Stretchable Interconnect Fabrication: A stretchable conductor was prepared by patterning three $ENIG_{20}$ wires (2 cm x 0.25 cm) on a PDMS substrate. The conductor was loaded onto a micro-vice holder, and coper tapes were used to contact between the surface of $ENIG_{20}$ wires and the alligators attached to the Arduino. The LEDs and resistors were also built on the breadboard following the instructions provided by Arduino. The circuit was driven by the Arduino at 5V.

ACEL Device Fabrication: ZnS: Cu microparticles (Shanghai KPT Company) were mixed with PDMS prepolymers (weight ratio of base to curing agent = 10: 1) in the weight ratio of 1:1 to produce a phosphor paste. The prepared ZnS: Cu/PDMS paste was then spin coated onto the $ENIG_{20}$ films at 500 rpm for 1 min. The composite was then cured in an oven at 60 °C overnight. The emissive layer was oxidized with air plasma for 1 min, and then a mixture of PEDOT:PSS aqueous dispersion with 2 wt% Triton X-100 was spin-coated on the emissive layer at 2000 rpm for 1 min.

Characterization: Optical characterization was performed using an Olympus BX51 microscope equipped with an Olympus Q-Color3 digital camera. A micro-vice stretcher (S. T. Japan, USA, Inc.) was mounted to the microscope stage and samples were

secured in the stretcher to obtain microscopy images of stretched samples. SEM images were taken by a Hitachi S-4500 scanning electron microscopy (Surface Science Western, London, ON, Canada). XPS spectra were obtained using a Kratos Axis Ultra Spectrometer (Surface Science Western, London, ON, Canada). AFM images were obtained using a Nanoscope VI Digital Instrument Multimode atomic force microscope with a silicon high-aspect-ratio tip (10 nm radius) in the tapping mode. 1.0 mm areas were scanned at a rate of 0.8 Hz. Powder XRD spectra were determined using a Proto AXRD benchtop instrument with Cu αK radiation. Electrical characterization was performed using a Keithley 2601A source meter. Gallium-indium eutectic (EGaIn) (~5 μL) was first deposited by syringe to the corners (for R_s measurements) or ends (for resistance measurements) of the ENIG surface to facilitate the electrical contact. R_s measurements were carried our using a four-point probe setup. Data sets consisted of a minimum of three samples, and the average was reported. For electrical measurements under strain, samples (1.5 cm x 3 cm) were camped at both ends in a micro-vice stretcher, and we manually stretched the films by moving the mobile clamps. EGaIn was applied to the two ends of the sample to reduce the contact resistance. The resistance was measured at 5 % increments of strain.

5.5. References

(1)   Sekitani, T.; Nakajima, H.; Maeda, H.; Fukushima, T.; Aida, T.; Hata, K.; Someya, T. *Nat. Mater.* **2009**, *8*, 494.

(2)   Liang, J. J.; Li, L.; Niu, X. F.; Yu, Z. B.; Pei, Q. B. *Nat. Photonics* **2013**, *7*, 817.

(3)   Amjadi, M.; Pichitpajongkit, A.; Lee, S.; Ryu, S.; Park, I. *ACS Nano* **2014**, *8*, 5154.

(4)   Yamada, T.; Hayamizu, Y.; Yamamoto, Y.; Yomogida, Y.; Izadi-Najafabadi, A.; Futaba, D. N.; Hata, K. *Nat. Nanotechnol.* **2011**, *6*, 296.

(5)   Lipomi, D. J.; Tee, B. C. K.; Vosgueritchian, M.; Bao, Z. N. *Adv. Mater.* **2011**, *23*, 1771.

(6)   Liu, W.; Chen, J.; Chen, Z.; Liu, K.; Zhou, G.; Sun, Y. M.; Song, M.-S.; Bao, Z.; Cui, Y. *Adv. Energy Mater.* **2017**, *7*, 1701076.

(7)   Vitale, F.; Summerson, S. R.; Aazhang, B.; Kemere, C.; Pasquali, M. *ACS Nano* **2015**, *9*, 4465.

(8)   Kim, S. J.; Cho, H. R.; Cho, K. W.; Qiao, S. T.; Rhim, J. S.; Soh, M.; Kim, T.; Choi, M. K.; Choi, C.; Park, I.; Hwang, N. S.; Hyeon, T.; Choi, S. H.; Lu, N. S.; Kim, D. H. *ACS Nano* **2015**, *9*, 2677.

(9)   Cutnell, J. D.; Johnson, K. W. *Physics, 9th ed.*; John Wiley & Sons: New York, 2012.

(10)   Xiang, Y.; Li, T.; Suo, Z. G.; Vlassak, J. J. *Appl. Phys. Lett.* **2005,** *87*, 161910.

(11)   Lacour, S. P.; Wagner, S.; Huang, Z. Y.; Suo, Z. *Appl. Phys. Lett.* **2003**, *82*, 2404.

(12)   Li, T.; Huang, Z. Y.; Suo, Z.; Lacour, S. P.; Wagner, S. *Appl. Phys. Lett.* **2004**, *85*, 3435.

(13)   Cao, Q.; Rogers, J. A. *Adv. Mater.* **2009**, *21*, 29.

(14)   Liu, N.; Chortos, A.; Lei, T.; Jin, L. H.; Kim, T. R.; Bae, W. G.; Zhu, C. X.; Wang, S. H.; Pfattner, R.; Chen, X. Y.; Sinclair, R.; Bao, Z. A. *Sci. Adv.* **2017**, *3*. 1700159

(15)   Lipomi, D. J.; Lee, J. A.; Vosgueritchian, M.; Tee, B. C. K.; Bolander, J. A.; Bao, Z. A. *Chem. Mater.* **2012**, *24*, 373.

(16)   Gray, D. S.; Tien, J.; Chen, C. S. *Adv. Mater.* **2004**, *16*, 393.

(17)   Kim, D.-H.; Song, J.; Choi, W. M.; Kim, H.-S.; Kim, R.-H.; Liu, Z.; Huang, Y. Y.; Hwang, K.-C.; Zhang, Y.-W.; Rogers, J. A. *Proc. Natl. Acad. Sci. USA.* **2008**, *105*, 18675.

(18)   Kim, D.-H. *Proc. Matl. Acad. Sci. USA* **2008**, *105*, 18675.

(19)   Lacour, S. P.; Jones, J.; Wagner, S.; Li, T.; Suo, Z. *Proc. IEEE* **2005**, *93*, 1459.

(20)   Lacour, S. P.; Chan, D.; Wagner, S.; Li, T.; Suo, Z. *Appl. Phys. Lett.* **2006**, *88*, 204103.

(21)   Robinson, A. P.; Minev, I.; Graz, I. M.; Lacour, S. P. *Langmuir* **2011**, *27*, 4279.

(22)   Lambricht, N.; Pardoen, T.; Yunus, S. *Acta Mater.* **2013**, *61*, 540.

(23)   Filiatrault, H. L.; Carmichael, R. S.; Boutette, R. A.; Carmichael, T. B. *ACS Appl. Mater. Interfaces* **2015**, *7*, 20745.

(24)   Mandlik, P.; Lacour, S. P.; Li, J. W.; Chou, S. Y.; Wagner, S. *IEEE Electr. Device L* **2006**, *27*, 650.

(25)   Brosteaux, D.; Axisa, F.; Gonzalez, M.; Vanfleteren, J. *IEEE Electron Device Lett.* **2007**, *28*, 552.

(26)   Gorrn, P.; Cao, W.; Wagner, S. *Soft Matter* **2011**, *7*, 7177.

(27)   Miller, M. S.; Davidson, G. J. E.; Sahli, B. J.; Mailloux, C. M.; Carmichael, T. B. *Adv. Mater.* **2008**, *20*, 59.

(28)   Miller, M. S.; Filiatrault, H. L.; Davidson, G. J. E.; Luo, M.; Carmichael, T. B. *J. Am. Chem. Soc.* **2010**, *132*, 765.

(29)   Yu, Y.; Zeng, J.; Chen, C. S.; Xie, Z.; Guo, R.; Liu, Z.; Zhou, X.; Yang, Y.; Zheng, Z. *Adv. Mater.* **2013**, *26*, 810.

(30)   Yu, Y.; Zhang, Y.; Li, K.; Yan, C.; Zheng, Z. *Small* **2015**, *11*, 3444.

(31)   Salaita, K.; Wang, Y. H.; Mirkin, C. A. *Nat. Nanotechnol.* **2007**, *2*, 145.

(32)   Sirringhaus, H.; Kawase, T.; Friend, R. H.; Shimoda, T.; Inbasekaran, M.; Wu, W.; Woo, E. P. *Science* **2000**, *290*, 2123.

(33)   Pardo, D. A.; Jabbour, G. E.; Peyghambarian, N. *Adv. Mater.* **2000**, *12*, 1249.

(34)   Carmichael, T. B.; Vella, S. J.; Afzali, A. *Langmuir* **2004**, *20*, 5593.

(35)   Mallory, G. O.; Hajdum, J. B., Eds.; *Electroless Plating: Fundamentals and Applications*; American Electroplaters and Surface Finishers Society: Orlando, FL, 1990.

(36)   Azzaroni, O.; Zheng, Z. J.; Yang, Z. Q.; Huck, W. T. S. *Langmuir* **2006**, *22*, 6730.

(37)   Guo, R.; Yu, Y.; Xie, Z.; Liu, X.; Zhou, X.; Gao, Y.; Liu, Z.; Zhou, F.; Yang, Y.; Zheng, Z. *Adv. Mater.* **2013**, *25*, 3343.

(38)   Polywka, A.; Jakob, T.; Stegers, L.; Riedl, T.; Görrn, P. *Adv. Mater.* **2015**, *27*, 3755.

(39)   Wang, X. L.; Hu, H.; Shen, Y. D.; Zhou, X. C.; Zheng, Z. J. *Adv. Mater.* **2011**, *23*, 3090.

(40)   Meng, C. K.; Selvamuniandy, T. S.; Gurumurthy, C.; *11th International Symposium on the Physical & Failure Analysis of Integrated Circuits* **2004**, 229.

(41)   Snugovsky, P.; Arrowsmith, P.; Romansky, M. *J. Electron. Mater.* **2001**, *30*, 1262.

(42)   Schlesinger, M.; Paunovic, M., Eds.; *Modern Electroplating, Fifth Edition*; John Wiley & Sons, Inc.: Hoboken, NJ, USA, 2010.

(43)   Hillborg, H.; Ankner, J. F.; Gedde, U. W.; Smith, G. D.; Yasuda, H. K.; Wikstrom, K. *Polymer* **2000**, *41*, 6851.

(44)   Liu, H. P.; Li, N.; Bi, S.; Li, D. *J. Electrochem. Soc.* **2007**, *154*, 662.

(45)   Walton, R. F. *J. Electrochem. Soc.* **1961**, *108*, 767.

(46)   Venables, J. A.; Spiller, G. D. T.; Hanbucken , M. *Rep. Prog. Phys.* **1984**, *47*, 399.

(47)   Graudejus, O.; Görrn, P.; Wagner, S. *ACS Appl. Mater. Interfaces* **2010**, *2*, 1927.

(48)   Schwoebel, R. L. *J. Appl. Phys.* **1967**, *38*, 672.

(49)   Hou, Z. Z.; Abbott, N. L.; Stroeve, P. *Langmuir* **1998**, *14*, 3287.

(50)   Dubrovsky, T. B.; Hou, Z. Z.; Stroeve, P.; Abbott, N. L. *Anal. Chem.* **1999**, *71*, 327.

(51)   Hou, Z. Z.; Dante, S.; Abbott, N. L.; Stroeve, P. *Langmuir* **1999**, *15*, 3011.

(52)   Bronkhorst, C. A.; Kalidindi, S. R.; Anand, L. *Philos. Trans. Royal Soc. A* **1992**, *341*, 443.

(53)   Anand, L.; Kalidindi, S. R. *Mech. Mater.* **1994**, *17*, 223.

(54)   Shi, J.; Zikry, M. A. Int. J. *Solids Struct.* **2009**, *46*, 3914.

(55)   Cheong, K. S.; Busso, E. P. *J. Mech. Phys. Solids* **2006**, *54*, 671.

(56)   Oh, J. Y.; Shin, M.; Lee, J. B.; Ahn, J. H.; Baik, H. K.; Jeong, U. *ACS Appl. Mater. & Interfaces* **2014**, *6*, 6954.

(57)   Wang, J.; Yan, C.; Chee, K. J.; Lee, P. S. *Adv. Mater.* **2015**, *27*, 2876.

5.6. Supporting Information
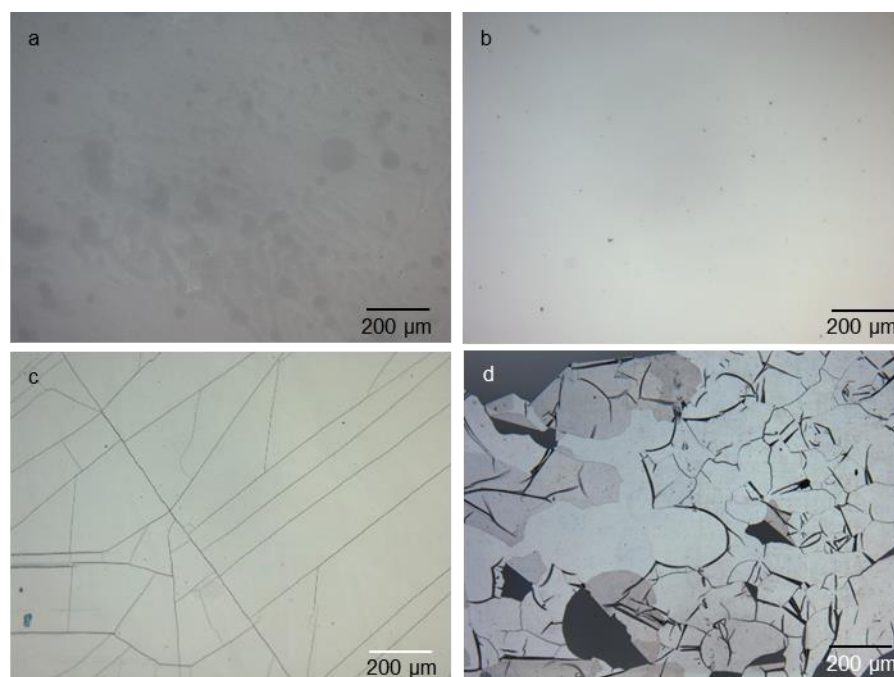
Figure S5.1. *Optical micrographs of (a) 5 min, (b)10 min, (c)15 min, and (d) 20 min ELD of nickel film on PDMS substrate.*
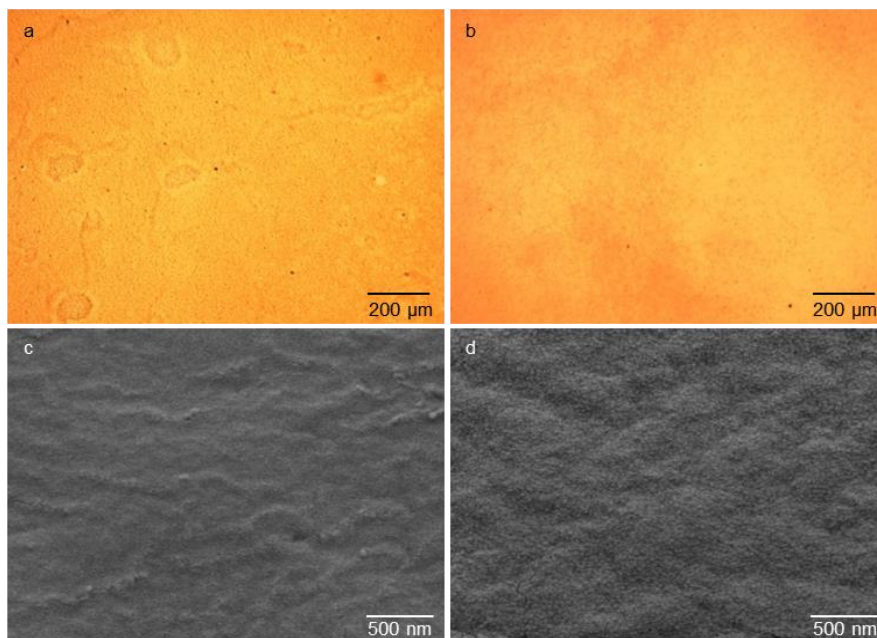
Figure S5.2. Optical micrographs of (a) $ENIG_{10}$ and (b) $ENIG_{15}$ on PDMS substrate. SEM micrographs of (c) $ENIG_{10}$ and (d) $ENIG_{15}$ on PDMS substrate.
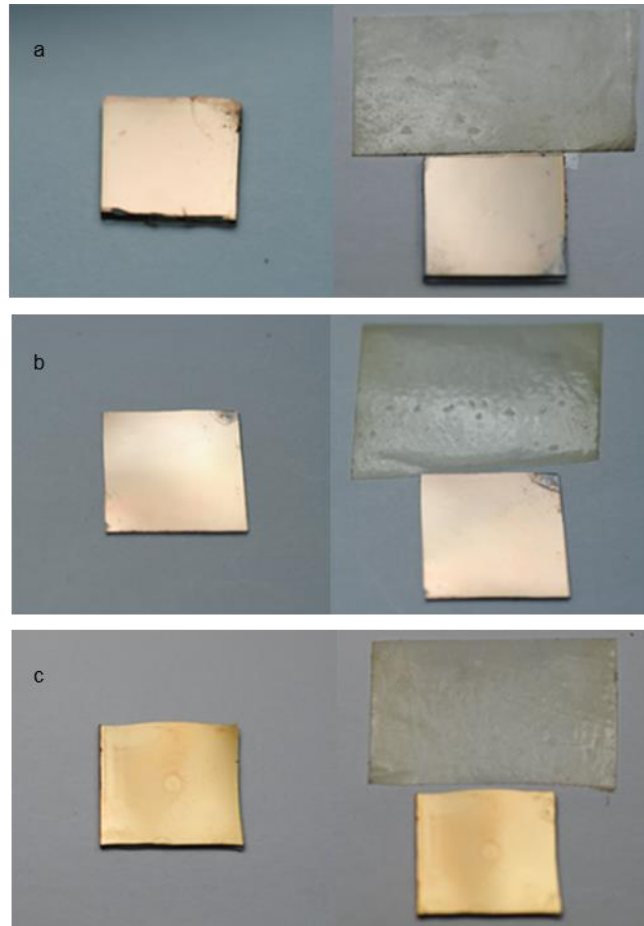
Figure S5.3. *Photographs of (a) ENIG$_{10}$, (b) ENIG$_{15}$, and (c) ENIG$_{20}$ films before (left column) and after (right column) tape test.*
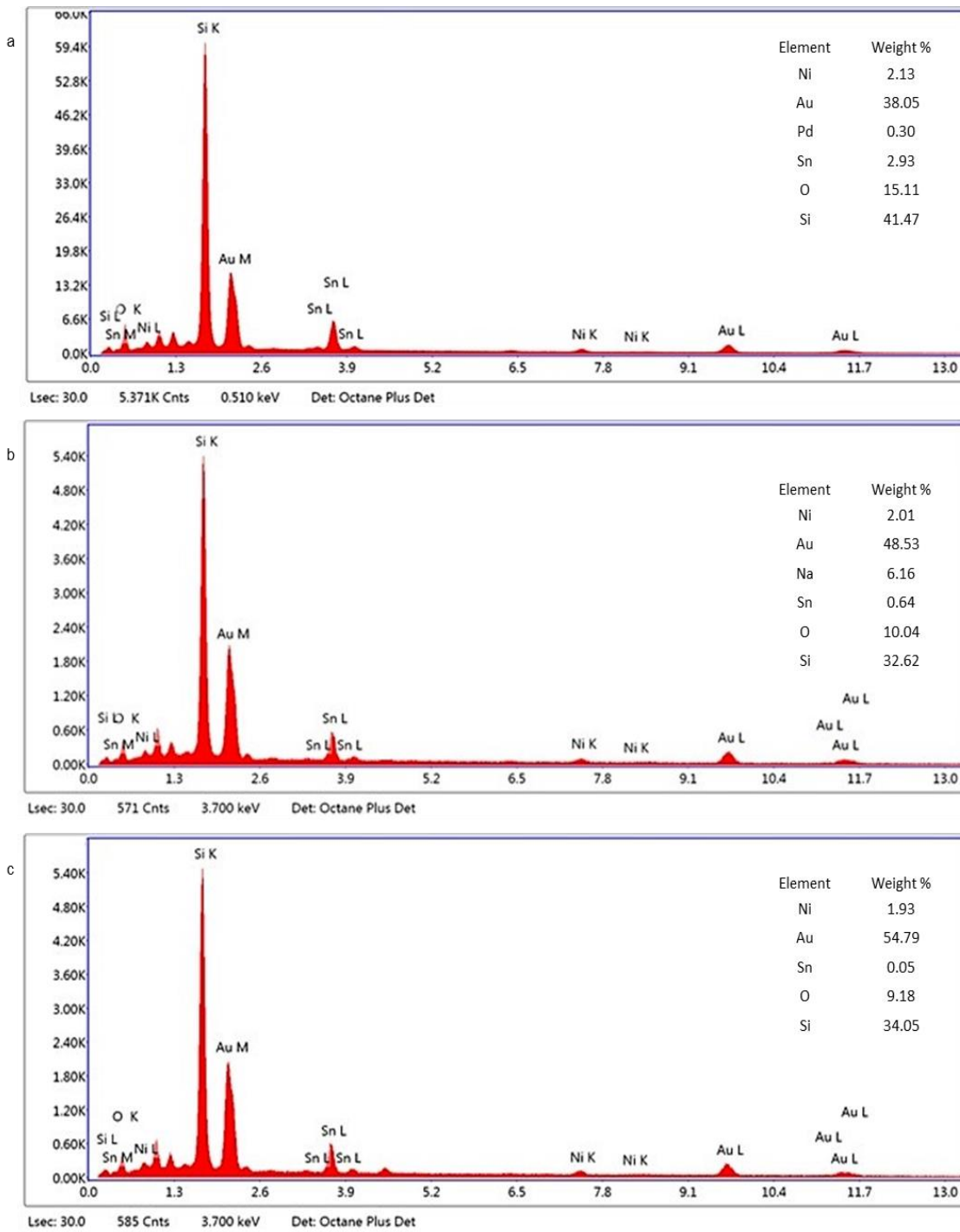
Figure S5.4. *EDX of (a) ENIG$_{10}$, (b) ENIG$_{15}$, and (c) ENIG$_{20}$ films on a silicon wafer.*
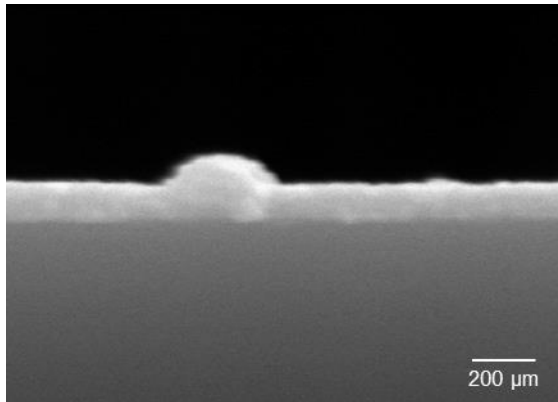
Figure S5.5. SEM cross-sectional image of ENIG$_{20}$ film on a silicon wafer.
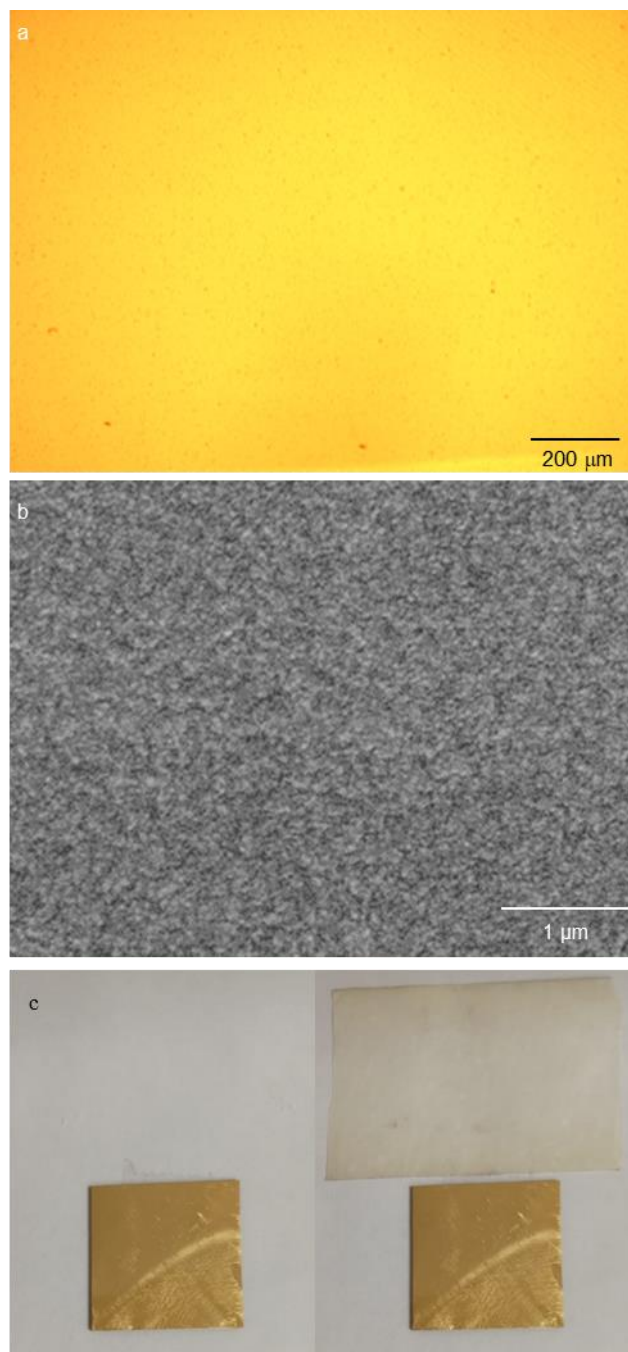
Figure S5.6. (a) Optical and (b) SEM micrographs of EBAu films on PDMS. (c) Photographs of EBAu film on PDMS substrate before (left) and after (right) tape test. The marks on the gold film were left when it was taken off from the sample holder.
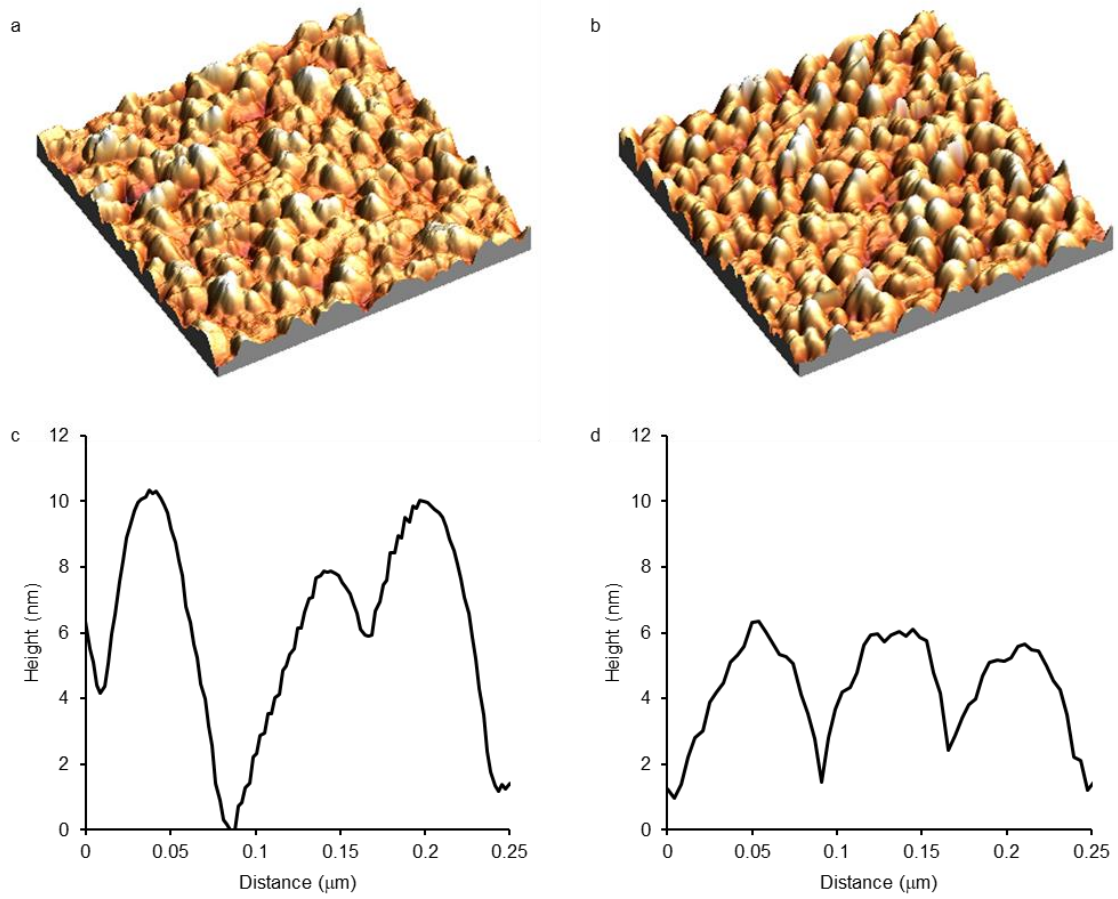
Figure S5.7. (a) AFM height image and (c) corresponding profile measurement of ENIG$_{20}$ film on a silicon wafer. (b) AFM height image and (d) corresponding profile measurement of EBAu film on a silicon wafer.
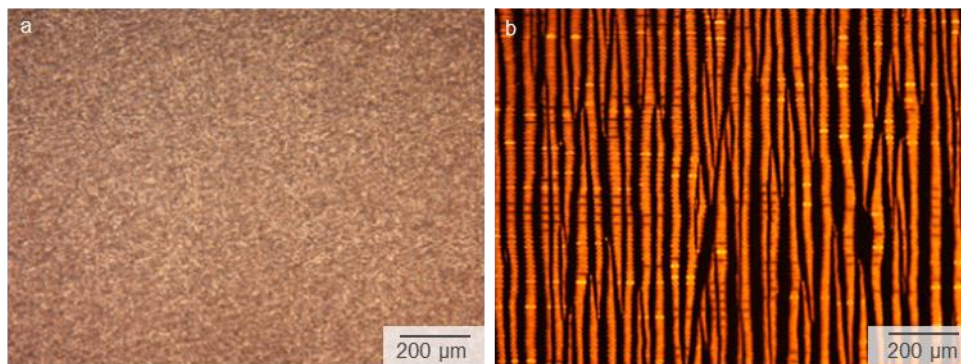
Figure S5.8. *Optical micrographs of (a) ENIG$_{20}$ film and (b) EBAu film on PDMS substrate at 80% tensile strain.*
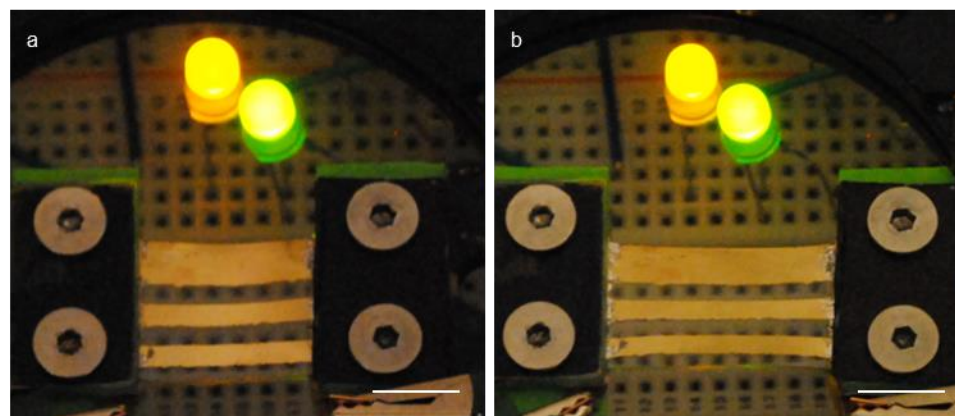
Figure S5.9. *Photographs of patterned ENIG$_{20}$ wires on PDMS substrate (scale = 1 cm) as stretchable interconnects for LED circuits at (a) 0% and (b) 40% tensile strain.*
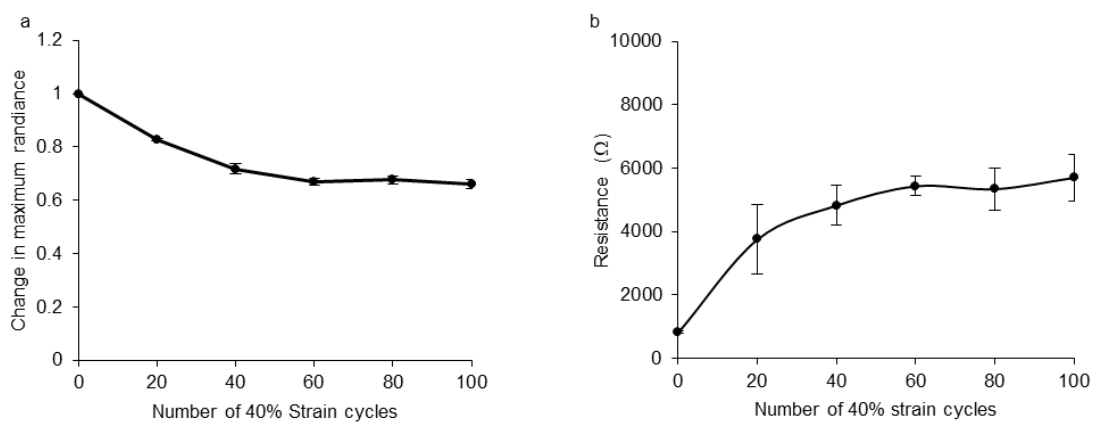
Figure S5.10. *(a) Change in maximum radiance of ACEL devices as a function of repeated 40% strain cycles. (b) Resistance of PEDOT:PSS/Triton X-100 film on PDMS substrate as a function of repeated 40% strain cycles.*

6. Chapter 6

Conclusions and Outlook

6.1. Conclusions

Stretchable optoelectronics provide opportunities for this envision-centered world. The research presented in this dissertation focused on developing a range of new elastomeric electronic components and methods for the fabrication of large-area mechanically flexible and stretchable light-emitting devices: how to fabricate patterned, deformable, and reliable top transparent conductive electrodes (TCEs), how to impart stretchability to brittle emissive materials while improving the optoelectronic performance, and how to directly produce highly stretchable metal electrodes on elastomeric substrates using a low-cost solution-based method. The following sections will summarize each chapter, pointing out the challenges faced over the due course of this research and the solutions to solve them.

Patterned and deformable TCEs are essential components in compliant optoelectronic devices. AgNW network provides high optical transparency, electrical conductivity and the ability to tolerate both bending and stretching strain, making it a promising candidate to fabricate flexible and stretchable TCEs. However, there are two problems with using AgNWs for patterned and deformable TCEs. First, AgNW network produces a rough surface with protrusions > 100 nm from the surface, potentially leading to an electrical shortage in thin film devices; Second, it is challenging to produce large-area patterned AgNW network with mechanical compliance using a simple, cost-effective and high-throughput method. We solved these two problems at the same time by first using a benchtop wet/dewet fabrication method to generate patterned AgNWs followed by embedding the AgNWs in a flexible or stretchable polymer matrix. We presented this work in Chapter 2 of this dissertation. By only using selective plasma exposure and drop-

casting, we obtained uniform and well-defined patterns of AgNWs with versatile features. We smoothed the surface of the AgNW network by embedding AgNWs into either flexible OA or stretchable CF polymer matrix on PDMS substrate, which also enhanced the flexibility or stretchability. The obtained patterned AgNW/polymer coatings on PDMS substrate possessed smooth surface, high optical transparency, high conductivity and high flexibility and stretchability with a low change in resistance, making these films an ideal option for compliant TCEs. We demonstrated a flexible ACEL device with the flexible AgNW/OA coating on PDMS as the TCE.

One obstacle for AgNWs to be used as stretchable and reliable TCEs is that their corrosion behavior in ambient conditions easily destroys AgNW network and subsequently alters the optical, electrical, and mechanical properties of the AgNW network. PDMS, the default substrate used in stretchable electronics, has a high permeability to water and oxygen and cannot effectively protect AgNWs from corrosion. Although various barrier layers have been investigated to protect the stability of AgNWs, this additional layer lowers the transmittance as well as increases the fabrication complexity. Furthermore, the change in optical and mechanical properties of AgNW network after exposure to harsh environments has not been fully investigated. We sought to improve the reliability of AgNW network while imparting stretchability to the AgNW network by replacing the permeable PDMS platform with the T-IIR platform, an elastomer possessing higher impermeability to moisture and gas. A shift to T-IIR platform combines oxygen and moisture barrier functionality with stretchability into one material. In Chapter 3, we used a similar method developed in Chapter 2 to produce a AgNW/CF coating on a T-IIR substrate with optical transparency, high electrical

conductivity, and mechanical stretchability. We have demonstrated that these properties of this AgNW/CF coating on T-IIR substrate negligibly changed under environmental stress, and significantly improved the reliability of the compliant AgNW coating.

Another goal of the dissertation was to impart stretchability into a brittle electroluminescent material. Filiatrault et al. used a stretchable electroluminescent material to fabricate a light-emitting electrochemical cell (LEEC) with intrinsic stretchability. They dispersed an emissive material, a ruthenium ionic transition-metal complex, in an elastomeric PDMS matrix to impart stretchability to the emissive layer itself. These large-area devices maintained orange light emission with bending, twisting, and stretching. To diversify the colors, researchers shift to iridium iTMC complexes as the electroluminescent materials, whose emission colors cover the whole visible spectrum from red to blue. However, two challenges hinder the employment of iridium iTMC as the emissive material: first, the long responding time due to its low ion conductivity is not suitable for devices that require an instant response; adding ionic species to the emissive material can reduce the responding time of LEECs as well as reducing the device lifetime. Second, its brittleness does not tolerate mechanical stretch. We aimed to solve these problems by dispersing the iridium iTMC in an amphiphilic graft copolymer matrix consisting of IIR backbone and PEO side chains (RgP). The IIR backbone provides stretchability to the emissive material while the PEO side chain not only solubilizes iridium iTMC to reduce phase separation but also forms a solid electrolyte with $LiCF_3SO_3$ to improve the ionic mobility. In Chapter 4, we reported that LEECs fabricated from emissive layers containing RgP with **34** wt% PEO (RgP**34**) started to emit bright yellow light within few seconds, and their intensity decayed to 60% of the

maximum radiance after three hours of operation at 6 V DC. This supported that incorporation of RgP in the emissive layer is beneficial to device turn-on time and stability. Stretchable LEECs fabricated from a stretchable semi-transparent gold film on PDMS as the anode, the developed iridium composites as the emissive material, and a liquid metal eutectic indium gallium as the cathode withstood 30 cycles of 15% strain with minimal influence on the radiance.

Stretchable metal films are suitable to act as the bottom electrode for compliant light-emitting devices due to the high conductivity. One method to improve the stretchability of gold films on PDMS substrate is to configure the metal films into stretchable designs such as out-of-plane buckles, pop-ups, or serpentine designs. Another method is to induce morphologies to the substrate to change the crack propagation behavior. Although these methods produce highly stretchable gold films, the non-planar topography, small conductive area, or the micro-scare surface roughness make the gold films produced using these methods not suitable to act as electrodes for large-area thin film device. In addition, all these methods use physical vapor deposition (PVD) to deposit the gold film, which is a high-cost fabrication process. Moreover, the typical method to generate patterned metal film uses photolithography, which is a multi-step process. We sought to improve the stretchability of gold films on PDMS by using a low-cost solution-based electroless nickel/immersion (ENIG) process to deposit gold on PDMS and produce pattered gold films using a single step micro-contact printing (μCP). In Chapter 5, we have demonstrated that the gold films fabricated using ENIG method were superior to the gold films fabricated using PVD in conductivity with stretching: The ENIG films remained conductive up to 95% elongation with the change in resistance less

than 19x the initial value, after which the PDMS substrate fractured. In contrast, gold films produced using PVD method, specifically electron beam evaporation, failed to be conductive at < 5% strain. This excellent stretchability of ENIG films was likely originated for its heterogeneous crystallographic orientations. The patterned ENIG films had a high resolution as small as 10 μm. We demonstrated these films as the bottom electrode in large-area stretchable ACEL devices and showed that the intensity of the device changed negligibly with stretching.

6.2. Outlook

6.2.1. Patterned, Compliant, and Durable AgNW Network as TCEs

In Chapter 2, we showed a simple method to produce patterned and durable AgNW/polymer coatings with mechanical compliance. These coatings functionalized well individually, however, integrating them into deformable light-emitting devices through lamination is challenging. Due to the weak adhesion between the top electrode and the emissive layer, the structure is easily destroyed when devices are bent or stretched. The next steps to improve the robustness of the integrated device structures require enhancing the adhesion between all the layers in the deformable device. The possible approach includes developing an ultrathin AgNW/polymer coating that can adhere better to the emissive layer due to the larger energy required to peel off the thin coating. One interesting phenomenon we observed in Chapter 3 is that the delamination of the elastic AgNW/CF coating from the T-IIR substrate with stretching might prolong the stretchability of the AgNW/CF coating on T-IIR. Further study needs to be conducted in order to fully understand the stretching mechanism of the bilayer structure, including

using SEM technique to provide insight on the delamination spots of the interface, testing the debond energy of the AgNW/CF coating on T-IIR substrate, and using computational stimulation to study the stress localization in the composite. This work will provide a new method to impart stretchability to bilayer structure.

6.2.2. Elastomeric Matrices in LEECs

In Chapter 4, we demonstrated that incorporating an amphiphilic graft copolymer into the emissive material not only improved device response time and lifetime, but also stretchability. In addition, we will focus on quantifying the ion conductivity of the copolymer based solid electrolyte and studying the effect of adding RgP copolymers to the active materials on the ionic mobility, stability, and stretchability of other types of devices such as batteries. These studies will open up a new method to fabricate stretchable electronics spanning from light-emitting devices and energy storage.

6.2.3. Stretchable Metal Films

The work described in Chapter 5 presents solutions to produce highly stretchable gold films on PDMS substrate using a low-cost solution-based method. These gold films possess low surface roughness, large-conductive area, and high conductivity with stretching likely due to the heterogeneous orientation of the ENIG films. Future work will examine the stress distribution in the ENIG film with stretching and provide an in-depth understanding of the stretching behavior of polycrystalline films on the elastomeric substrate. Since this solution-based deposition method is compatible with irregularly shaped surfaces, we will also apply this method to coat metal on a non-planar substrate such as textiles and fibers to achieve wearable electronics.

Appendices

Copyright Permission

Title: Luminescent Ionic Transition-Metal Complexes for Light-Emitting Electrochemical Cells

Author: Rubén D. Costa, Enrique Ortí, Henk J. Bolink, et al

Publication: Angewandte Chemie International Edition

Publisher: John Wiley and Sons

Date: Aug 6, 2012

Copyright © 2012, John Wiley and Sons

Order Completed

Thank you for your order.

This Agreement between university of windsor -- Yiting Chen ("You") and John Wiley and Sons ("John Wiley and Sons") consists of your license details and the terms and conditions provided by John Wiley and Sons and Copyright Clearance Center.

Your confirmation email will contain your order number for future reference.

printable details

License Number	4326561410889
License date	Apr 12, 2018
Licensed Content Publisher	John Wiley and Sons
Licensed Content Publication	Angewandte Chemie International Edition
Licensed Content Title	Luminescent Ionic Transition-Metal Complexes for Light-Emitting Electrochemical Cells
Licensed Content Author	Rubén D. Costa, Enrique Ortí, Henk J. Bolink, et al
Licensed Content Date	Aug 6, 2012
Licensed Content Volume	51
Licensed Content Issue	33
Licensed Content Pages	34
Type of use	Dissertation/Thesis
Requestor type	University/Academic
Format	Print and electronic
Portion	Figure/table
Number of figures/tables	2
Original Wiley figure/table number(s)	Figure 1.1 Figure 1.2 Figure1.3
Will you be translating?	No
Title of your thesis /	Development and Integration of Stretchable Electronic Components into Light-Emitting Devices
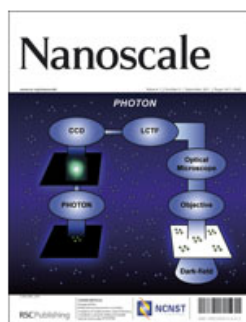
Title:	Metallic nanowire networks: effects of thermal annealing on electrical resistance
Author:	D. P. Langley,M. Lagrange,G. Giusti,C. Jiménez,Y. Bréchet,N. D. Nguyen,D. Bellet
Publication:	Nanoscale
Publisher:	Royal Society of Chemistry
Date:	Sep 19, 2014
	Copyright © 2014, Royal Society of Chemistry

Review Order

Please review the order details and the associated terms and conditions.

No royalties will be charged for this reuse request although you are required to obtain a license and comply with the license terms and conditions. To obtain the license, click the Accept button below.

Licensed Content Publisher	Royal Society of Chemistry
Licensed Content Publication	Nanoscale
Licensed Content Title	Metallic nanowire networks: effects of thermal annealing on electrical resistance
Licensed Content Author	D. P. Langley,M. Lagrange,G. Giusti,C. Jiménez,Y. Bréchet,N. D. Nguyen,D. Bellet
Licensed Content Date	Sep 19, 2014
Licensed Content Volume	6
Licensed Content Issue	22
Type of Use	Thesis/Dissertation
Requestor type	academic/educational
Portion	figures/tables/images
Number of figures/tables/images	1
Distribution quantity	1
Format	print and electronic
Will you be translating?	no
Order reference number	
Title of the thesis/dissertation	Development and Integration of Stretchable Electronic Components into Light-Emitting Devices
Expected completion date	May 2018
Estimated size	210
Attachment	
Requestor Location	university of windsor 401 Sunset Avenue

ACS Publications
Most Trusted. Most Cited. Most Read.

Title: Silver Nanowire/Optical Adhesive Coatings as Transparent Electrodes for Flexible Electronics

Author: Michael S. Miller, Jessica C. O'Kane, Adrian Niec, et al

Publication: Applied Materials

Publisher: American Chemical Society

Date: Oct 1, 2013

Copyright © 2013, American Chemical Society

PERMISSION/LICENSE IS GRANTED FOR YOUR ORDER AT NO CHARGE

This type of permission/license, instead of the standard Terms & Conditions, is sent to you because no fee is being charged for your order. Please note the following:

- Permission is granted for your request in both print and electronic formats, and translations.
- If figures and/or tables were requested, they may be adapted or used in part.
- Please print this page for your records and send a copy of it to your publisher/graduate school.
- Appropriate credit for the requested material should be given as follows: "Reprinted (adapted) with permission from (COMPLETE REFERENCE CITATION). Copyright (YEAR) American Chemical Society." Insert appropriate information in place of the capitalized words.
- One-time permission is granted only for the use specified in your request. No additional uses are granted (such as derivative works or other editions). For any other uses, please submit a new request.

If credit is given to another source for the material you requested, permission must be obtained from that source.

Review Order

Please review the order details and the associated terms and conditions.

No royalties will be charged for this reuse request although you are required to obtain a license and comply with the license terms and conditions. To obtain the license, click the Accept button below.

Licensed Content Publisher	Springer Nature
Licensed Content Publication	Nano Research
Licensed Content Title	Fabrication of silver nanowire transparent electrodes at room temperature
Licensed Content Author	Takehiro Tokuno, Masaya Nogi, Makoto Karakawa et al
Licensed Content Date	Jan 1, 2011
Licensed Content Volume	4
Licensed Content Issue	12
Type of Use	Thesis/Dissertation
Requestor type	non-commercial (non-profit)
Format	print and electronic
Portion	figures/tables/illustrations
Number of figures/tables/illustrations	1
Will you be translating?	no
Circulation/distribution	<501
Author of this Springer Nature content	no
Title	Development and Integration of Stretchable Electronic Components into Light-Emitting Devices
Instructor name	n/a
Institution name	n/a
Expected presentation date	May 2018
Portions	Figure 1.5
Attachment	
Requestor Location	university of windsor 401 Sunset Avenue

182

PERMISSION/LICENSE IS GRANTED FOR YOUR ORDER AT NO CHARGE

183

Title: The effect of light and humidity on the stability of silver nanowire transparent electrodes

Author: Jinting Jiu,Jun Wang,Tohru Sugahara,Shijio Nagao,Masaya Nogi,Hirotaka Koga,Katsuaki Suganuma,Masanao Hara,Eri Nakazawa,Hiroshi Uchida

Publication: RSC Advances

Publisher: Royal Society of Chemistry

Date: Mar 9, 2015

Copyright © 2015, Royal Society of Chemistry

Review Order

Please review the order details and the associated terms and conditions.

No royalties will be charged for this reuse request although you are required to obtain a license and comply with the license terms and conditions. To obtain the license, click the Accept button below.

Licensed Content Publisher	Royal Society of Chemistry
Licensed Content Publication	RSC Advances
Licensed Content Title	The effect of light and humidity on the stability of silver nanowire transparent electrodes
Licensed Content Author	Jinting Jiu,Jun Wang,Tohru Sugahara,Shijio Nagao,Masaya Nogi,Hirotaka Koga,Katsuaki Suganuma,Masanao Hara,Eri Nakazawa,Hiroshi Uchida
Licensed Content Date	Mar 9, 2015
Licensed Content Volume	5
Licensed Content Issue	35
Type of Use	Thesis/Dissertation
Requestor type	academic/educational
Portion	figures/tables/images
Number of figures/tables/images	1
Distribution quantity	1
Format	print and electronic
Will you be translating?	no
Order reference number	
Title of the thesis/dissertation	Development and Integration of Stretchable Electronic Components into Light-Emitting Devices
Expected completion date	May 2018
Estimated size	210
Attachment	
Requestor Location	university of windsor

PERMISSION/LICENSE IS GRANTED FOR YOUR ORDER AT NO CHARGE

This type of permission/license, instead of the standard Terms & Conditions, is sent to you because no fee is being charged for your order. Please note the following:
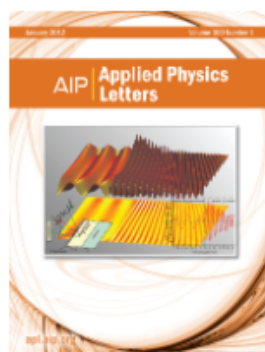
Review Order

Please review the order details and the associated terms and conditions.

No royalties will be charged for this reuse request although you are required to obtain a license and comply with the license terms and conditions. To obtain the license, click the Accept button below.

Licensed Content Publisher	Springer Nature
Licensed Content Publication	Nature Photonics
Licensed Content Title	Elastomeric polymer light-emitting devices and displays
Licensed Content Author	Jiajie Liang, Lu Li, Xiaofan Niu, Zhibin Yu, Qibing Pei
Licensed Content Date	Sep 22, 2013
Licensed Content Volume	7
Licensed Content Issue	10
Type of Use	Thesis/Dissertation
Requestor type	academic/university or research institute
Format	print and electronic
Portion	figures/tables/illustrations
Number of figures/tables/illustrations	1
High-res required	no
Will you be translating?	no
Circulation/distribution	<501
Author of this Springer Nature content	no
Title	Development and Integration of Stretchable Electronic Components into Light-Emitting Devices
Instructor name	n/a
Institution name	n/a
Expected presentation date	May 2018
Portions	Figure 1.7
Attachment	
Requestor Location	university of windsor 401 Sunset Avenue

187

RightsLink®

Home | Account Info | Help

Title: Stretchable Light-Emitting Electrochemical Cells Using an Elastomeric Emissive Material

Author: Heather L. Filiatrault, Gyllian C. Porteous, R. Stephen Carmichael, et al

Publication: Advanced Materials

Publisher: John Wiley and Sons
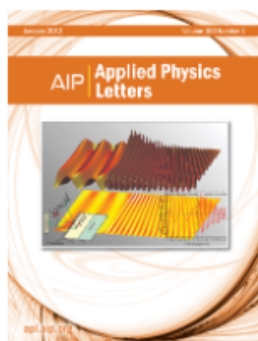
Date: Mar 26, 2012

Copyright © 2012, John Wiley and Sons

Review Order

Please review the order details and the associated terms and conditions.

No royalties will be charged for this reuse request although you are required to obtain a license and comply with the license terms and conditions. To obtain the license, click the Accept button below.

Licensed Content Publisher	John Wiley and Sons
Licensed Content Publication	Advanced Materials
Licensed Content Title	Stretchable Light-Emitting Electrochemical Cells Using an Elastomeric Emissive Material
Licensed Content Author	Heather L. Filiatrault, Gyllian C. Porteous, R. Stephen Carmichael, et al
Licensed Content Date	Mar 26, 2012
Licensed Content Volume	24
Licensed Content Issue	20
Licensed Content Pages	6
Type of use	Dissertation/Thesis
Requestor type	University/Academic
Format	Print and electronic
Portion	Figure/table
Number of figures/tables	2
Original Wiley figure/table number(s)	Figure 1.7
Will you be translating?	No
Title of your thesis / dissertation	Development and Integration of Stretchable Electronic Components into Light-Emitting Devices
Expected completion date	May 2018
Expected size (number of pages)	210
Attachment	
Requestor Location	university of windsor 401 Sunset Avenue

Title:	High ductility of a metal film adherent on a polymer substrate
Author:	Yong Xiang, Teng Li, Zhigang Suo, et al
Publication:	Applied Physics Letters
Volume/Issue	87/16
Publisher:	AIP Publishing
Date:	Oct 17, 2005
Page Count:	3

Rights managed by AIP Publishing.

Review Order

Please review the order details and the associated terms and conditions.

No royalties will be charged for this reuse request although you are required to obtain a license and comply with the license terms and conditions. To obtain the license, click the Accept button below.

Licensed Content Publisher	AIP Publishing
Licensed Content Publication	Applied Physics Letters
Licensed Content Title	High ductility of a metal film adherent on a polymer substrate
Licensed Content Author	Yong Xiang, Teng Li, Zhigang Suo, et al
Licensed Content Date	Oct 17, 2005
Licensed Content Volume	87
Licensed Content Issue	16
Requestor type	University or Educational Institution
Format	Print and electronic
Portion	Figure/Table
Number of figures/tables	1
Attachment	
Requestor Location	university of windsor 401 Sunset Avenue Windsor, ON N9B 3P4 Canada Attn: Yiting Chen
Total	0.00 USD

RightsLink®

Copyright Clearance Center

Title: Stretchable gold conductors on elastomeric substrates

Author: Stéphanie Périchon Lacour, Sigurd Wagner, Zhenyu Huang, et al

Publication: Applied Physics Letters

Volume/Issue 82/15

Publisher: AIP Publishing

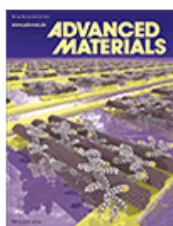**Date:** Apr 14, 2003

Page Count: 3

Rights managed by AIP Publishing.

Review Order

Please review the order details and the associated terms and conditions.

No royalties will be charged for this reuse request although you are required to obtain a license and comply with the license terms and conditions. To obtain the license, click the Accept button below.

Licensed Content Publisher	AIP Publishing
Licensed Content Publication	Applied Physics Letters
Licensed Content Title	Stretchable gold conductors on elastomeric substrates
Licensed Content Author	Stéphanie Périchon Lacour, Sigurd Wagner, Zhenyu Huang, et al
Licensed Content Date	Apr 14, 2003
Licensed Content Volume	82
Licensed Content Issue	15
Requestor type	University or Educational Institution
Format	Print and electronic
Portion	Figure/Table
Number of figures/tables	1
Attachment	
Requestor Location	university of windsor 401 Sunset Avenue Windsor, ON N9B 3P4 Canada Attn: Yiting Chen
Total	0.00 USD

Title:	Stretchable wavy metal interconnects
Author:	Joyelle Jones, Stéphanie P. Lacour, Sigurd Wagner, et al
Publication:	Journal of Vacuum Science & Technology A
Volume/Issue	22/4
Publisher:	AIP Publishing
Date:	Jul 1, 2004
Page Count:	3

Rights managed by AIP Publishing.

Review Order

Please review the order details and the associated terms and conditions.

No royalties will be charged for this reuse request although you are required to obtain a license and comply with the license terms and conditions. To obtain the license, click the Accept button below.

Licensed Content Publisher	AIP Publishing
Licensed Content Publication	Journal of Vacuum Science & Technology A
Licensed Content Title	Stretchable wavy metal interconnects
Licensed Content Author	Joyelle Jones, Stéphanie P. Lacour, Sigurd Wagner, et al
Licensed Content Date	Jul 1, 2004
Licensed Content Volume	22
Licensed Content Issue	4
Requestor type	University or Educational Institution
Format	Print and electronic
Portion	Figure/Table
Number of figures/tables	1
Attachment	
Requestor Location	university of windsor 401 Sunset Avenue Windsor, ON N9B 3P4 Canada Attn: Yiting Chen

192

Review Order

Please review the order details and the associated terms and conditions.

No royalties will be charged for this reuse request although you are required to obtain a license and comply with the license terms and conditions. To obtain the license, click the Accept button below.

Licensed Content Publisher	John Wiley and Sons
Licensed Content Publication	Advanced Materials
Licensed Content Title	High-Conductivity Elastomeric Electronics (Adv. Mater. 2004, 16, 393.)
Licensed Content Author	C. S. Chen, J. Tien, D. S. Gray
Licensed Content Date	Mar 22, 2004
Licensed Content Volume	16
Licensed Content Issue	6
Licensed Content Pages	1
Type of use	Dissertation/Thesis
Requestor type	University/Academic
Format	Print and electronic
Portion	Figure/table
Number of figures/tables	1
Original Wiley figure/table number(s)	Figure 1.9
Will you be translating?	No
Title of your thesis / dissertation	Development and Integration of Stretchable Electronic Components into Light-Emitting Devices
Expected completion date	May 2018
Expected size (number of pages)	210
Attachment	
Requestor Location	university of windsor 401 Sunset Avenue

Thesis / Dissertation Reuse

The IEEE does not require individuals working on a thesis to obtain a formal reuse license, however, you may print out this statement to be used as a permission grant:

Requirements to be followed when using any portion (e.g., figure, graph, table, or textual material) of an IEEE copyrighted paper in a thesis:

1) In the case of textual material (e.g., using short quotes or referring to the work within these papers) users must give full credit to the original source (author, paper, publication) followed by the IEEE copyright line © 2011 IEEE.
2) In the case of illustrations or tabular material, we require that the copyright line © [Year of original publication] IEEE appear prominently with each reprinted figure and/or table.
3) If a substantial portion of the original paper is to be used, and if you are not the senior author, also obtain the senior author's approval.

Requirements to be followed when using an entire IEEE copyrighted paper in a thesis:

1) The following IEEE copyright/ credit notice should be placed prominently in the references: © [year of original publication] IEEE. Reprinted, with permission, from [author names, paper title, IEEE publication title, and month/year of publication]
2) Only the accepted version of an IEEE copyrighted paper can be used when posting the paper or your thesis on-line.
3) In placing the thesis on the author's university website, please display the following message in a prominent place on the website: In reference to IEEE copyrighted material which is used with permission in this thesis, the IEEE does not endorse any of [university/educational entity's name goes here]'s products or services. Internal or personal use of this material is permitted. If interested in reprinting/republishing IEEE copyrighted material for advertising or promotional purposes or for creating new collective works for resale or redistribution, please go to http://www.ieee.org/publications_standards/publications/rights/rights_link.html to learn how to obtain a License from RightsLink.

If applicable, University Microfilms and/or ProQuest Library, or the Archives of Canada may supply single copies of the dissertation.
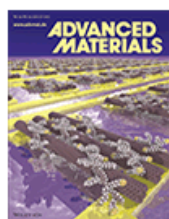
195

Review Order

Please review the order details and the associated terms and conditions.

No royalties will be charged for this reuse request although you are required to obtain a license and comply with the license terms and conditions. To obtain the license, click the Accept button below.

Licensed Content Publisher	John Wiley and Sons
Licensed Content Publication	Advanced Materials
Licensed Content Title	Fabrication of Elastomeric Wires by Selective Electroless Metallization of Poly(dimethylsiloxane)
Licensed Content Author	T. B. Carmichael, C. M. Mailloux, B. J. Sahli, et al
Licensed Content Date	Dec 7, 2007
Licensed Content Volume	20
Licensed Content Issue	1
Licensed Content Pages	6
Type of use	Dissertation/Thesis
Requestor type	University/Academic
Format	Print and electronic
Portion	Figure/table
Number of figures/tables	1
Original Wiley figure/table number(s)	Figure 1.12
Will you be translating?	No
Title of your thesis / dissertation	Development and Integration of Stretchable Electronic Components into Light-Emitting Devices
Expected completion date	May 2018
Expected size (number of pages)	210
Attachment	
Requestor Location	university of windsor

Title: Matrix-Assisted Catalytic Printing for the Fabrication of Multiscale, Flexible, Foldable, and Stretchable Metal Conductors

Author: Ruisheng Guo, You Yu, Zhuang Xie, et al

Publication: Advanced Materials

Publisher: John Wiley and Sons

Date: May 13, 2013

Copyright © 2013, John Wiley and Sons

Review Order

Please review the order details and the associated terms and conditions.

No royalties will be charged for this reuse request although you are required to obtain a license and comply with the license terms and conditions. To obtain the license, click the Accept button below.

Licensed Content Publisher	John Wiley and Sons
Licensed Content Publication	Advanced Materials
Licensed Content Title	Matrix-Assisted Catalytic Printing for the Fabrication of Multiscale, Flexible, Foldable, and Stretchable Metal Conductors
Licensed Content Author	Ruisheng Guo, You Yu, Zhuang Xie, et al
Licensed Content Date	May 13, 2013
Licensed Content Volume	25
Licensed Content Issue	24
Licensed Content Pages	8
Type of use	Dissertation/Thesis
Requestor type	University/Academic
Format	Print and electronic
Portion	Figure/table
Number of figures/tables	1
Original Wiley figure/table number(s)	Figure 1.12
Will you be translating?	No
Title of your thesis / dissertation	Development and Integration of Stretchable Electronic Components into Light-Emitting Devices
Expected completion date	May 2018
Expected size (number of pages)	210
Attachment	
Requestor Location	university of windsor

Vita Auctoris

NAME:	Yiting Chen
PLACE OF BIRTH:	Fuxin, Liaoning Province, China
YEAR OF BIRTH:	1989
EDUCATION:	Tianjin Polytechnic University, B.Sc., Tianjin, China, 2012
	University of Windsor, Ph. D., Windsor, ON, Canada, 2018